

NASA-CR-197195

NASw-4435

Project Number: DJO-93AA

Design and Construction of a Remote Piloted Flying Wing

NASA/USRA ADVANCED AERONAUTICS DESIGN PROGRAM

IN-05-CR

26177

A Major Qualifying Project
Submitted to the Faculty
of the

P-187

WORCESTER POLYTECHNIC INSTITUTE

in Partial Fulfillment of the Requirements
for the
Degree of Bachelor of Science
Submitted on May 2, 1994

N95-12695

Unclas

G3/05 0026177

Alfred J. Costa

Jaime Duquette

Fritz Koopman

Scott Krause

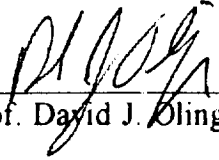
Craig Soboleski

David Susko

Thai-Ba Trieu

Thuyba Trieu

Approved by:



Prof. David J. Olinger

(NASA-CR-197195) DESIGN AND
CONSTRUCTION OF A REMOTE PILOTED
FLYING WING B.S. Thesis (Worcester
Polytechnic Inst.) 187 p

Abstract

Currently, there is a need for a high-speed, high-lift civilian transport. Although unconventional, a flying wing could fly at speeds in excess of Mach 2 and still retain the capacity of a 747. The design of the flying wing is inherently unstable since it lacks a fuselage and a horizontal tail. The project goal was to design, construct, fly, and test a remote-piloted scale model flying wing. The project was completed as part of the NASA/USRA Advanced Aeronautics Design Program.

These unique restrictions required us to implement several fundamental design changes from last year's Elang configuration including wing sweepback and wingtip endplates. Unique features such as a single ducted fan engine, composite structural materials, and an electrostatic stability system were incorporated. The result is the *Banshee '94*. Our efforts will aid future projects in design and construction techniques so that a viable flying wing can become an integral part of the aviation industry.

Acknowledgements

A project such as this requires assistance outside of the central project group. The members of this group would like to extend thanks for the guidance and technical support during all phases of this project:

Professor David J. Olinger

Paul Crivelli

NASA/USRA

Alesandro Cucci

O.S. Engines Inc.

Fiber Materials Inc.

Rob Cunningham of Monsanto Inc.

Wayne Chamberlin and Klegecell

Roy Costa of Costa's Auto Body

Scott Simmons

Maynard Hill

Master Hobbies

Henry's Hobby House

Cappy Cross of Futaba Corp. of America

Mark Spivey of RSM Inc.

Stephen Desrosiers

Robert Taylor

Table of Contents

Abstract	i
Acknowledgments	ii
Table of Contents	iii
List of Figures	v
List of Tables	vii
1. Introduction	1
1.1 The Flying Wing	1
1.2 The Oblique Flying Wing	3
1.3 The Flying Wing, <i>Elang</i>	4
1.4 The Flying Wing, <i>Banshee 94'</i>	7
2. Design Summary	9
2.1 Introduction	9
2.2 General Design Specifications	9
2.3 Specific Characteristics	9
2.3.1 The Wing	9
2.3.2 The Propulsion System	10
2.3.3 Electronic Components	11
2.4 The Cruise Condition	11
2.5 The <i>Banshee 94'</i> Versus The <i>Elang</i>	11
3. Aerodynamics	13
3.1 Introduction	13
3.2 Aircraft Configuration	14
3.3 Airfoil Selection	16
3.4 Calculations	18
3.4.1 Introduction	18
3.4.2 Assumptions	19
3.4.3 Calculations	20
3.5 Lift Calculations	23
3.5.1 Introduction	23
3.5.2 Calculations	23
3.6 Lift Versus Drag Calculations	24
3.6.1 Introduction	24
3.6.2 Calculations	24
3.7 Results and Conclusions	24
4. Stability and Controls	28
4.1 Introduction	28
4.2 Static Stability	29
4.3 Dynamic Stability	34
4.3.1 Results	35
4.4 Sweep-back	38
4.5 Electrostatic Stability System	38

4.6	Component Placement - Planform	42
4.7	Conclusions	44
5.	Propulsion	45
5.1	Objective	45
5.2.1	Engine Selection	45
5.2.2	Manufactures Data	46
5.3	Methods of Propulsion	47
5.3.1	Propellers	47
5.3.2	Ducted Fans	48
5.4	Single Engine	49
5.5	Location	50
5.6	Fuel System	50
5.7	Engine Type	51
5.8	Excess Power	54
5.9	Rate of Climb	55
5.10	Equations	56
5.11	Conclusions	58
6.	Structures	59
6.1	Introduction to Structures	59
6.2	Material Selection	60
6.2.1	Kevlar	61
6.2.2	Carbon Fiber	63
6.2.3	PVC Foam Core	64
6.3	Methods of Analysis	64
6.3.1	I-DEAS Code	65
6.3.2	NASTRAN Code	71
6.3.3	Experimental Analysis	72
6.3.4	Comparison of Hand-Calculation with MSC/NASTRAN	73
6.3.4.1	Weight / Strength	73
6.3.4.2	Check Shear Stress and Bending Moment	75
6.3.4.3	Section Properties of the Composite Materials	75
6.4	Construction Methods	78
7.	Conclusions and Recommendations	81
8.	References	83
9.	Appendix	84

List of Figures

	<u>page</u>
1 Introduction	
1.1 Northrop B-35 and B-49 Flying Wings	2
1.2 Northrop B-2 Stealth Bomber	2
1.3 The Oblique Wing Demonstrator, the NASA AD-1	3
1.4 The Conceptual Oblique Flying Wing	5
1.5 The Flying Wing, <i>Elang</i>	6
1.6 The HPRS 33 and SD 8020 Airfoils	7
1.7 The Flying Wing, <i>Banshee '94</i>	8
2 Design Review	
2.1 The <i>Banshee '94</i> Four View CAD Drawing	10
3 Aerodynamics	
3.1 The <i>Banshee '94</i>	14
3.2 The <i>Elang</i> and <i>Banshee '94</i> with Quarter Chord Line	14
3.3 Lift Distribution on Wing With and Without an Endplate	17
3.4 The Eppler 325 Series	17
3.5 Airfoil Placement Along the Wing	19
3.6 C_l vs. C_m from Airfoil Design and Data, Richard Eppler	19
3.7 Lift vs. Velocity	25
3.8 Drag vs. Velocity	26
3.9 Thrust and Drag vs. Velocity	27
4 Stability	
4.1 Moment Arm Analysis	30
4.2 Static Stability Curve	32
4.3 C_m vs. C_l	33
4.4 Angular Acceleration, The Pitch Axis	35
4.5 Angular Acceleration, The Roll Axis	36
4.6 Angular Acceleration, The Yaw Axis	37
4.7 The Effect of Sweepback	39
4.8 Static Master Placement for ESS	40
4.9 Electric Component Flowchart	41
4.10 Color Coded Placement of Various Components	43
5 Propulsion	
5.1 O.S. Max 91 VR-DF Engine	45
5.2 Ramtec Ducted Fan Assembly	48
5.3 Thrust and Drag vs. Velocity Curve	54
5.4 Climb Rate vs. Velocity Curve	56

	<u>page</u>
6 Structures	
6.1a Specific Tensile Modulus	62
6.1b Stress vs. Strain Curve	62
6.2 Lift and Weight Loading	66
6.3 Drag Loading	66
6.4 Load Applied to the Wing in I-DEAS	67
6.5 Stresses in the X-Y Plane	68
6.6 Stresses on the Wing , Von Mises and Maximum Principle Stresses	69
6.7 Wing Deflection	70
6.8 Test Beam Deflection	73
6.9 Comparison of Test and I-DEAS Data	73
6.10 Wing Twist Angle Caused by Swept	76
6.11 Wing Chordwise Deflection	78

List of Tables

	<u>page</u>
4 Stability	
Table 4.1 Experimental Airfoil Data	30
Table 4.2 Control Surfaces Sizes	37
Table 4.3 Component Weights and Sizes	42

1. Introduction

Currently, there is a need for a high-speed, high-lift civilian transport. Although unconventional, an oblique flying wing could fly at speeds in excess of Mach 2 and retain the capacity of a 747. The long term goal of this project is to produce a scale model of such an aircraft. This project, sponsored by NASA/USRA, dealt with the design, construction, flight, and testing of a remote-piloted scale model conventional flying wing. It is hoped that design and construction techniques learned from this project will aid in the future construction of a scale model remote-piloted oblique flying wing.

1.1 The Flying Wing

The flying wing was first developed in the 1940's by Northrop Aircraft Inc. . During the World War II, military planners wanted a bomber that would be able to fly from the East Coast of the US to Germany, round trip, with payload. This goal was defined as "10000 pounds for 10000 miles"⁶. Jack Northrop believed that a flying wing would be able to attain this goal. He believed that the lack of a fuselage and tail would reduce weight and, therefore, produce a higher cruise lift to drag ratio. Also, the lower weight would make it possible for the wing to carry more fuel. These design considerations would give the flying wing the range necessary for an intercontinental bomber. The two bombers constructed, the B-35 propeller driven and the B-49 jet propelled flying wings (see Figure 1.1), were inherently unstable due to the lack of a tail. Aerodynamic forces produced unfavorable pitching moments in the flying wing. To correct this,

the flying wing is swept back with its control surfaces behind the center of gravity, producing some stability. A damping system was also added to account for the pitching moment of the wing.

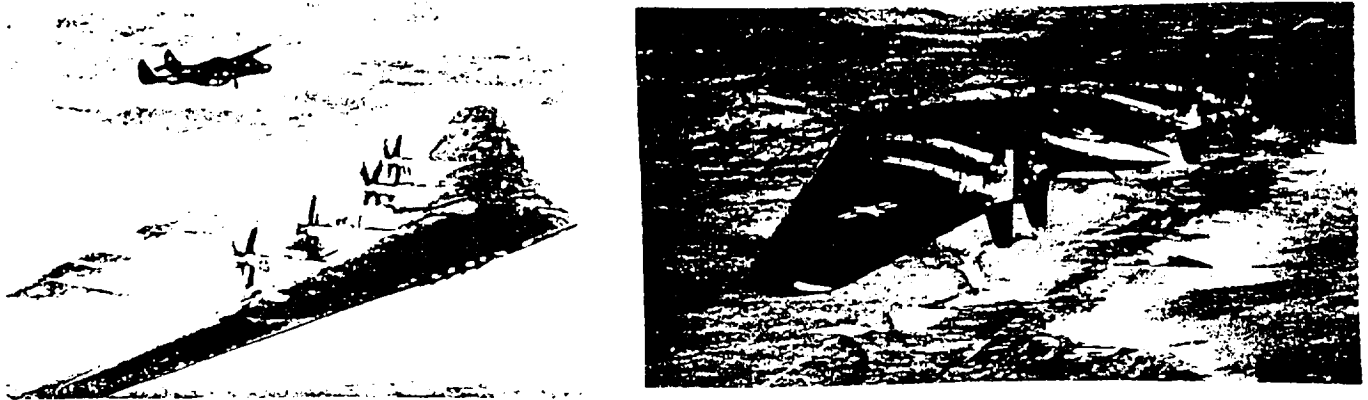


Figure 1.1 The Northrop B-35 and B-49 Flying Wings ¹⁶

In the end the Convair B-36 and not the Northrop B-49 that was chosen as the next intercontinental bomber. In November 1949, the existing B-35's and B-49's were destroyed. Derivatives of the Flying Wing design can be seen today in the Northrop B-2 Stealth Bomber (see Figure 1.2) and the recently cancelled McDonnell Douglas A-12.

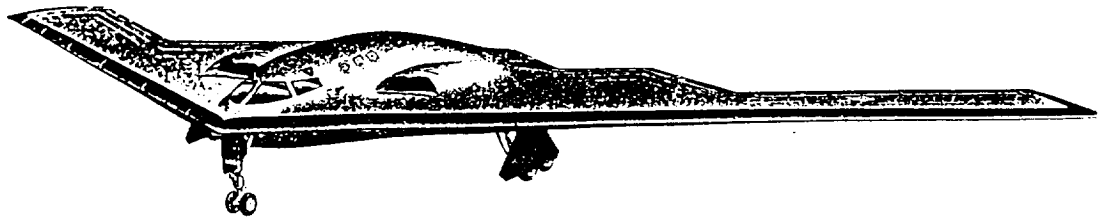


Figure 1.2 The Northrop B-2 Stealth Bomber¹⁶

1.2 The Oblique Flying Wing

An oblique flying wing differs from a conventional wing, like the B-35 and B-49, since it, flies with one wing tip ahead of the other, relative to the direction of flight. The concept of the oblique wing was first developed after World War II by NASA aerodynamicist, Robert T. Jones. This design, due to the orientation of the wing, would reduce drag increasing the lift to drag ratio at any speed. The high lift to drag ratio of the oblique wing aircraft would improve low speed performance for an aircraft designed to fly at high speeds¹⁷.

The first oblique wing demonstrator aircraft was the NASA AD-1 (see Figure 1.3). This design placed a high aspect ratio wing on a pivot atop a conventional fuselage. The wing itself could be swept up to 60 degrees. The AD-1 was first built in 1978 but work was halted soon after due to the fuel crisis. The 50 test flights of the AD-1 proved highly successful and showed that such technology could be adapted for a flying wing configuration⁹.

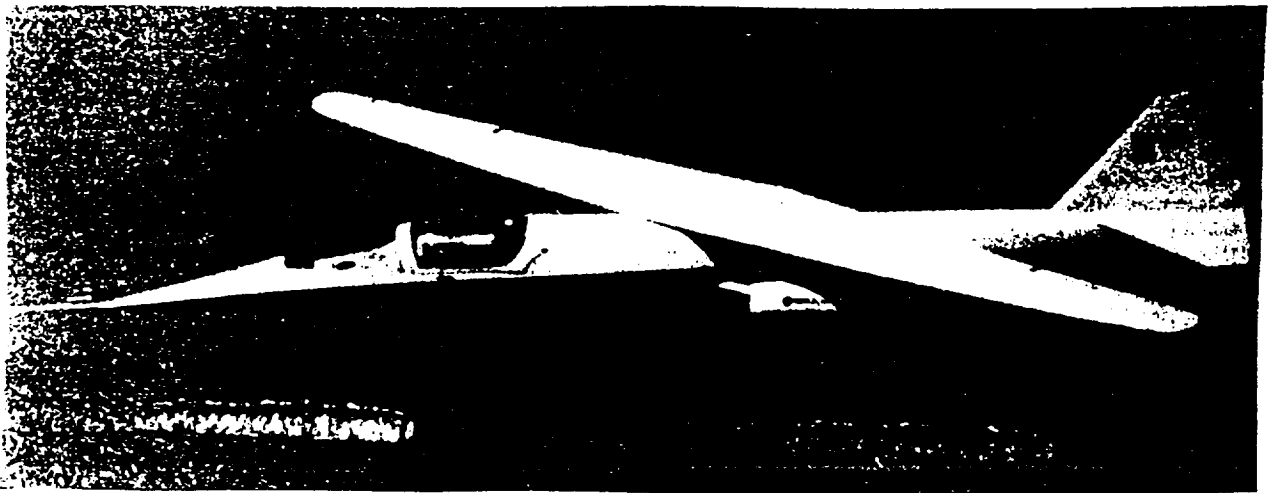


Figure 1.3 The Oblique Wing demonstrator, the NASA AD-1⁹

Airlines and aircraft manufacturers are showing serious interest in the oblique flying wing

as a high speed, high capacity commercial transport. The conceptual oblique flying wing (see Figure 1.4) could carry 500+ passengers, more than a conventional Boeing 747, and fly at speeds in excess of Mach 2. It is believed that an oblique flying wing would be 16-30% cheaper to fly than the Boeing 747. Travelling twice the speed of a 747, the oblique flying wing would use slightly more fuel while carrying more passengers.

The obliqueness of the wing would be changed by the rudders. Orientation of the wing would determine the speed of the aircraft; the lower the angle, the lower the speed. Overland flights could be made just below the speed of sound with high efficiency just by changing the angle of the wing.

The eventual goal of these NASA/USRA sponsored projects in WPI's Advanced Aeronautics Design Program is to construct a scale model oblique flying wing. For the last two years, the scope included designing and constructing a conventional scale model flying wing. The results are the *Elang* and the *Banshee '94*. The current, the *Banshee '94*, design improved upon and corrected the mistakes made in the design of the *Elang*. Also, the *Banshee '94* used base numbers of the *Elang* for calculation and scale of the aircraft.

1.3 The Flying Wing, *Elang*

Last year's design resulted in the *Elang* (see Figure 1.5). The *Elang* used the custom HPRS 33 airfoil (see Figure 1.6). To ensure minimum induced drag (elliptical distribution), the *Elang* used an elliptical planform. The flying wing had a root chord of 45.5cm, a span of 2.5m, and an aspect ratio of 7. To provide yaw control, two SD 8020 symmetrical airfoil (Figure 1.6)

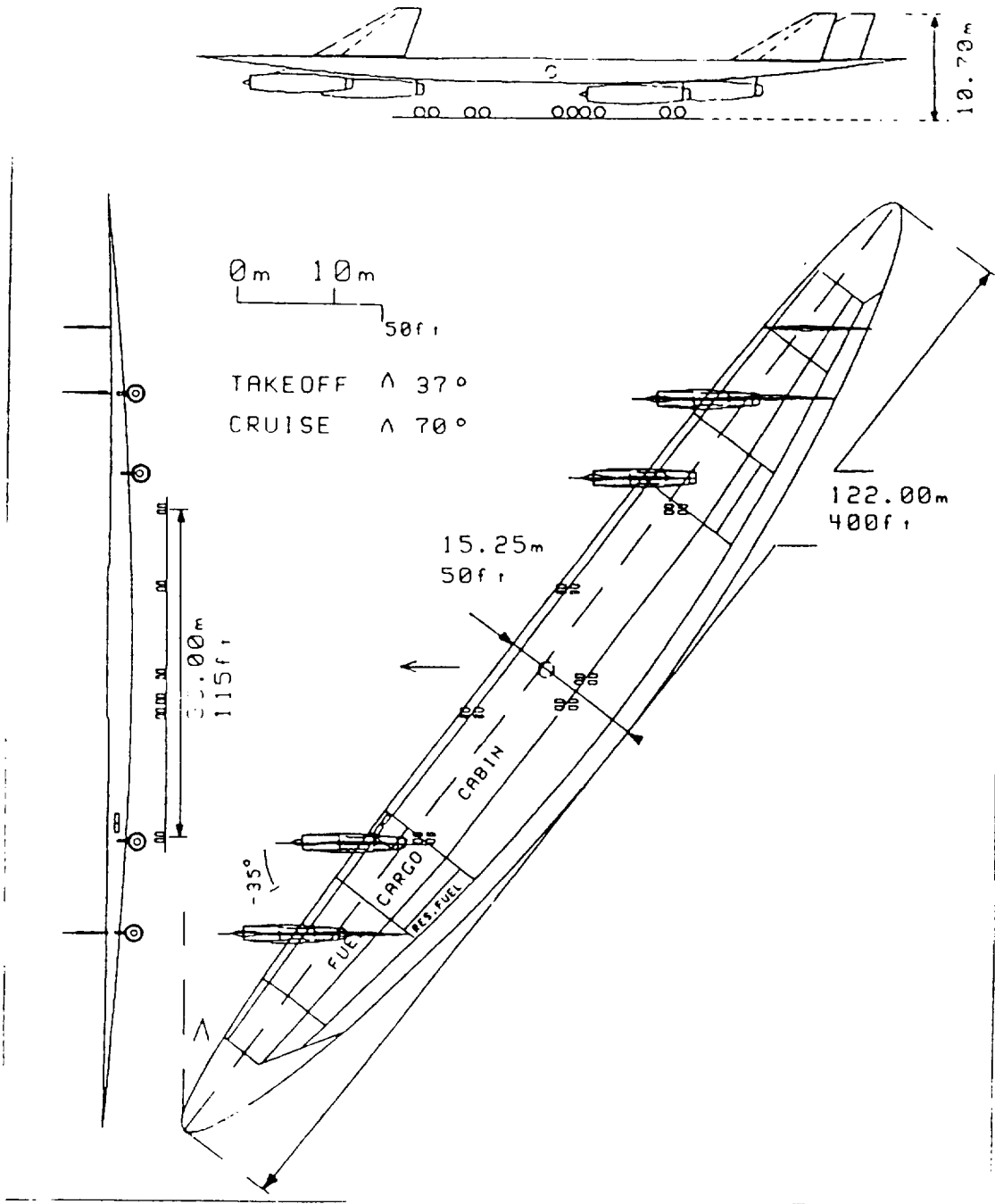


Figure 1.4 The conceptual Oblique Flying Wing transport¹⁷

were used as vertical stabilizers.

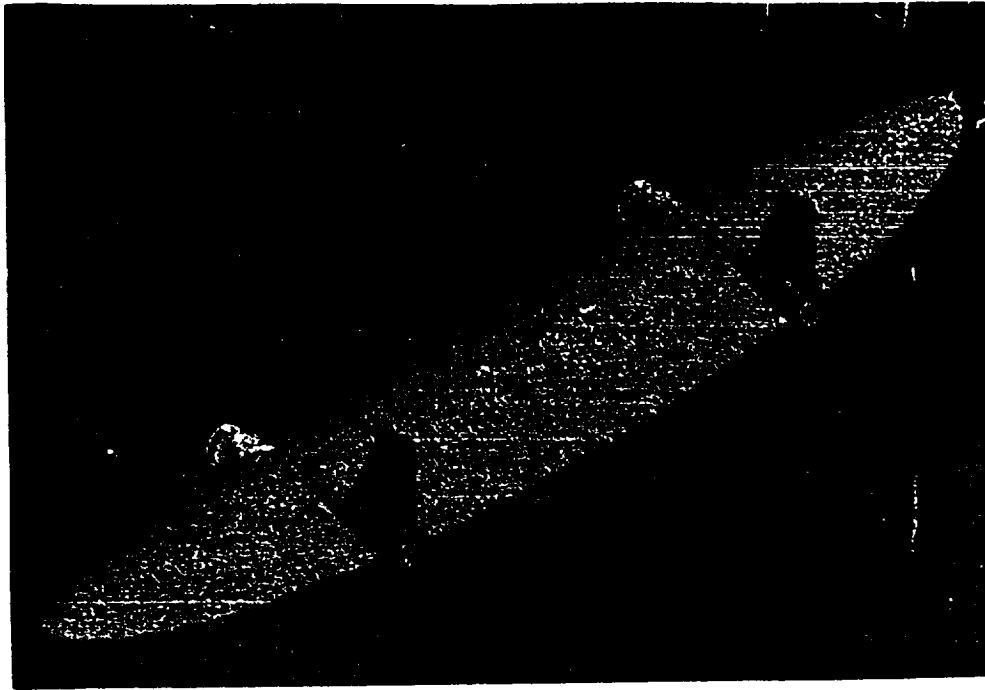


Figure 1.5 The Flying Wing, *Elang*

The propulsion system for the *Elang* consisted of two ducted fan engines. Ducted fans were chosen over propeller driven engines because of the ducted fan's clean aerodynamics. Propellers tend to produce undesirable turbulence over the wing and control surfaces, adding to the instability of the aircraft. Each of these ducted fan engines operated at 22000rpm and produces 15.6N of thrust. Due to their small size and high complexity, the ducted fan engines were reluctantly replaced with standard propeller driven engines late in last year's design. Propeller engines are highly accepted in the remote control aircraft world and are easier to operate and maintain.

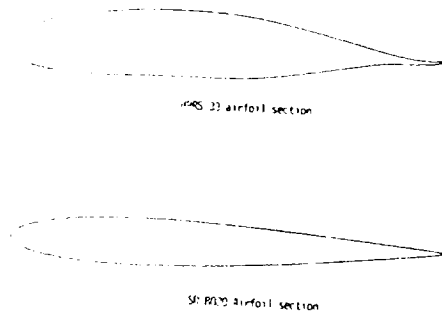


Figure 1.6 The HPRS 33 and SD 8020 airfoils

The materials used in the construction of the *Elang* needed to be strong enough to withstand "accidents" and have a low weight. The *Elang* used a styrofoam core with a skin of carbon fiber. The carbon fiber skin proved to be strong enough for the testing stage of the *Elang*.

The testing stage for the *Elang* was very brief. The *Elang's* lack of an automatic stability system proved to be fatal to the aircraft. The *Elang* was fitted with a standard R/C gyroscope system, but it was unclear whether it was used during test flights. Without some form of automatic stability system, a flying wing, on any scale, will not fly.

1.4 The Flying Wing, *Banshee '94*

The purpose of this project was to design, construct, fly, and test a scale model remote piloted flying wing. As in industry, an emphasis was put on design teams. The project group was split into four separate sub-groups, each dealing in a different aspect of design, working together towards the final goal. The result, the *Banshee '94* (see Figure 1.7), named after the spirit of Celtic lore, was designed to solve the problems involved with the stability of flying

wings. The Aerodynamics group dealt with calculation of lift and drag, also with airfoil selection. The Controls and Stability sub-group was responsible for design and analysis of control surfaces for the *Banshee '94* and also the installation and construction of an automatic stability system which will control the inherently unstable design. The Propulsion group dealt with the selection and testing of an engine with suitable power for the flying wing. The Structures and Construction group dealt with material selection, finite element modeling of that material, and the actual construction of the flying wing.

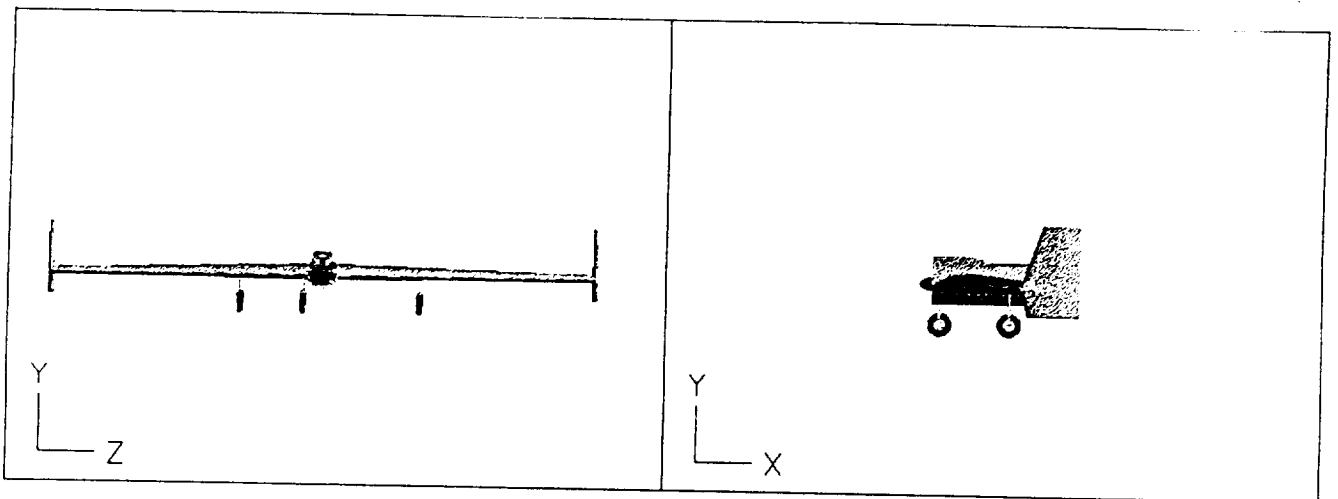
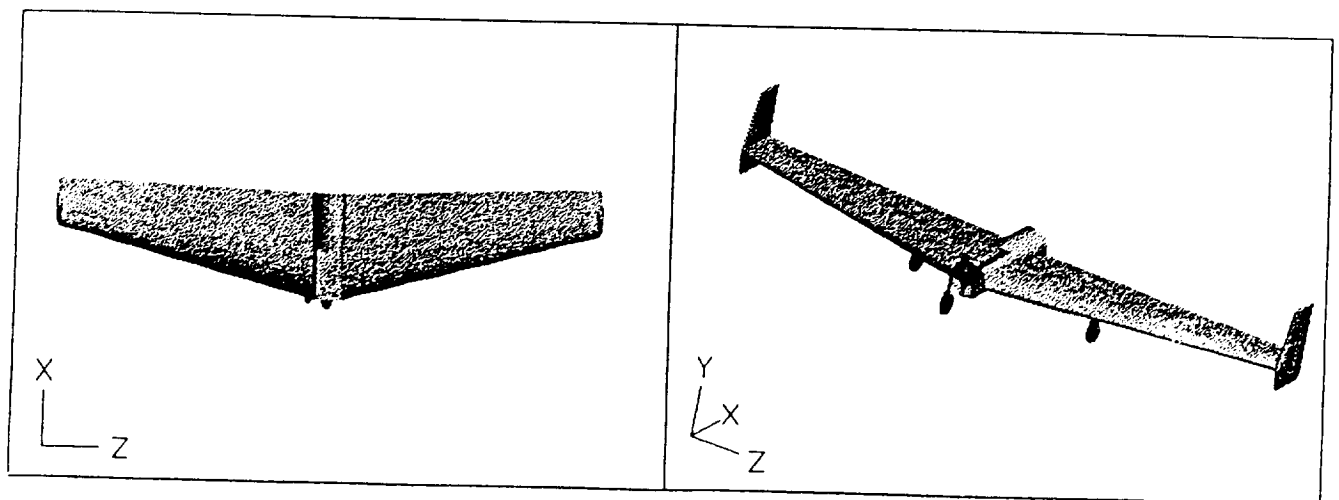


Figure 1.7 The Flying Wing, *Banshee '94*



2. Design Summary

2.1 Introduction

Before the detailed calculations and methods are discussed, a basic summary of the aircraft's design will be given. In this section, the general design parameters for *the Banshee '94* will be discussed. A table comparing the design parameters of the 1992-1993 Flying Wing, *the Elang*, to *the Banshee '94* is given.

2.2 General Design Specifications

The Banshee '94 is a tapered, swept flying wing. This differs from *the Elang*, in that *the Elang* was an elliptical flying wing. *The Banshee '94* was designed with a straight wing for ease of construction and a tapered, swept wing for increased stability. A four view computer aided design (CAD) drawing of *the Banshee '94* is shown in Figure 2.1. The aircraft is powered by a single ducted fan engine located in the center of the wing. *The Elang* was designed with two ducted fan engines, which promoted stability problems due to the difficulty in equalizing the two engine's thrust. Each wing tip on *the Banshee '94* has an endplate to act as a vertical stabilizer. For control surfaces, each wing has an aileron and a elevator and each endplate has a rudder. These will enable control in all three axes; roll, pitch, and yaw.

2.3 Specific Characteristics

2.3.1 The Wing

The total wingspan is 92.0 inches. The root chord is 18.0 inches and the tip chord is 8.0

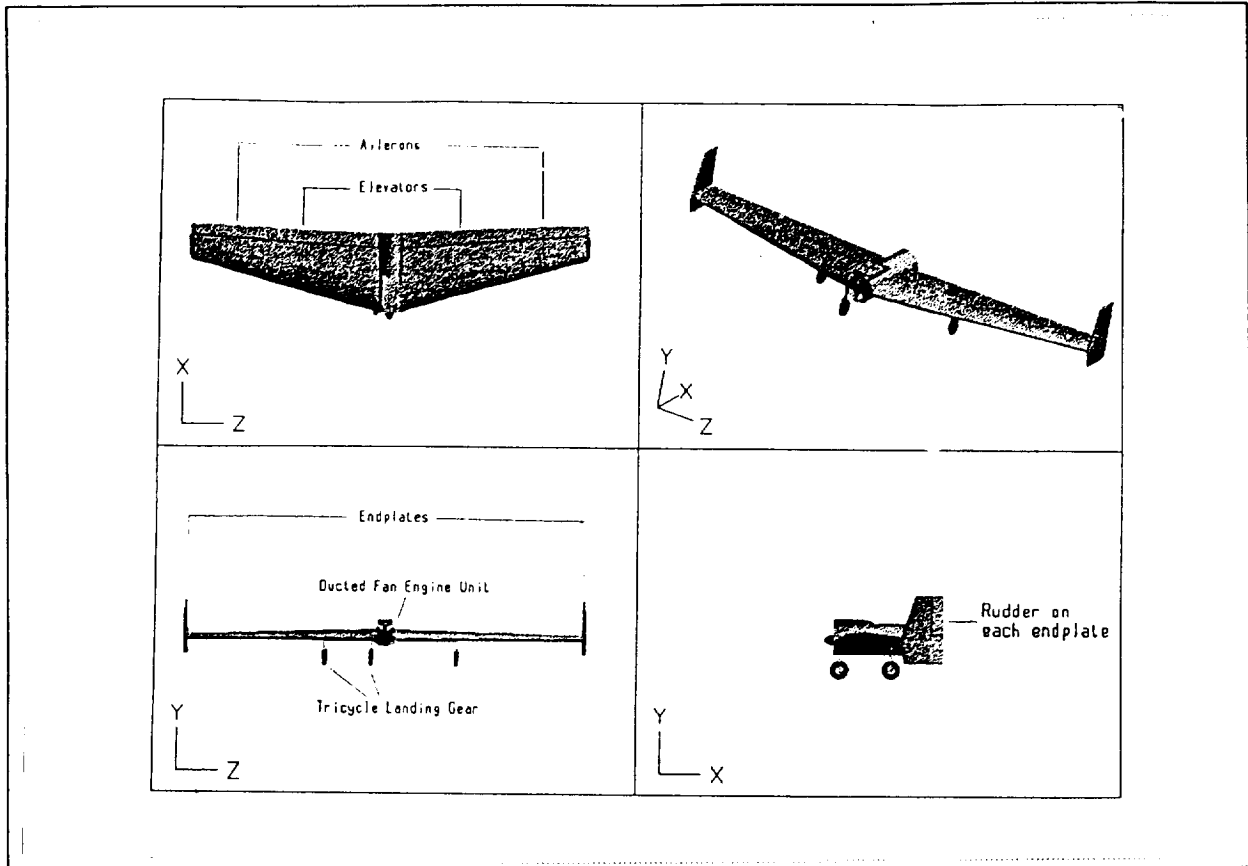


Figure 2.1 *The Banshee '94* 4-view CAD drawing

inches. The leading edge is swept back 15 degrees from the horizontal. This provides an aspect ratio of 6.689, a taper ratio of 0.444, and a total planform area, including the duct, of approximately 8.5 square feet. From the analysis, the lift to drag ratio for *the Banshee '94* is 19.44.

2.3.2 The Propulsion System

The Banshee '94 is powered by a 4.6 horse-powered OS Max 91 scaled-aircraft engine. The engine has a thrust of 11.0 to 14.0 pounds-force from manufacturer's data and a thrust to weight ratio of 4.67. The engine powers a nine-bladed ducted fan unit which propels the

aircraft. The engine is fueled by two fuel tanks enclosed inside the wing on either side of the duct.

2.3.3 Electronic Components

The engine and control surfaces in *the Banshee '94* are controlled by electronic servos. These servos are controlled by wireless remote. To insure stability, an electro-static stability system was built and installed inside the aircraft. All of the components are housed within the wing and accessible through removable panels.

2.4 The Cruise Condition

This report details the analyses performed which led to the final design of *the Banshee '94*. These analyses resulted in cruise conditions for the aircraft. The aircraft will fly with the wing at an angle of attack of four degrees to insure stability. The aircraft will have a cruise velocity of thirty-three miles per hour to insure enough lift to remain in level flight.

2.5 *The Banshee '94* Versus *The Elang*

	<u><i>The Banshee '94</i></u>	<u><i>The Elang</i></u>
Wingspan	92.5 inches	98.4 inches
Root chord length	18 inches	18 inches
Wing sweep	15 degrees	0 degrees
Aspect Ratio	6.689	7
Total planform area	8.5 square feet	9.6 square feet

Lift to drag ratio	19.44	19.69
# of engines	1	2
Total thrust from engines	14 lbs-f	7 lbs-f
Angle of attack	4 degrees	4 degrees
Cruise velocity	33 miles per hour	34 miles per hour

3. Aerodynamics

3.1 Introduction

Each individual design group is responsible for designing and analyzing specific aspects of the *Banshee '94*. The Aerodynamics group is responsible for determining the aircraft's lift and drag after determining the aircraft's configuration and airfoils. In addition to building and calibrating the electro-static stability system, the Controls/Stability group must determine the stable angle of attack and effect of control surface deflections. The Propulsion group chooses the engine and analyzes its thrust at various flight and throttle conditions. They must also calculate take-off and landing parameters including take-off speed and take-off distance. The Structures group is responsible for structural analysis, material selection, and fabrication of the aircraft.

Although each group possesses significantly different responsibilities, each group must perform its design and analysis in cooperation with the other groups. To obtain cruise conditions, the Aerodynamics, Propulsion, and Stability groups need to perform a combined analysis. With the chosen airfoils, the correct statically stable angle of attack may be determined by the Stability group. Once the angle of attack is determined, the Aerodynamics group determines the velocity, lift, and drag at cruise conditions. With the drag known, the Propulsion group can determine the correct engine throttle setting to produce the necessary thrust at cruise conditions.

For structural analysis, all groups needed to provide information to the Structures group. The Controls and Propulsion group provided component weights while the Aerodynamics group

provided the lift and drag distribution. This information allowed for the use of a finite element analysis of the flying wing.

Also, every group needed to work in cooperation while determining the lofting and construction. The Aerodynamics group needed to a configuration that would prove easy to manufacture and an airfoil with the proper thickness for component placement. The Stability and Controls group needed to provide control surface and component sizes to allow the Structures group to construct the wing. The Propulsion group needed to provide engine size so that a properly dimensioned duct could be manufactured. With this general overview, further discussion of the design process is discussed below.

3.2 Aircraft Configuration

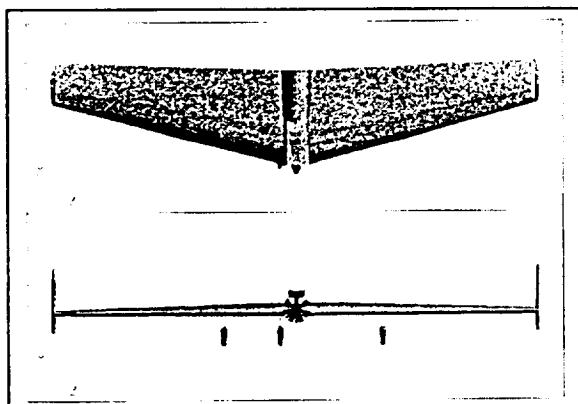


Figure 3.1 *The Banshee '94*

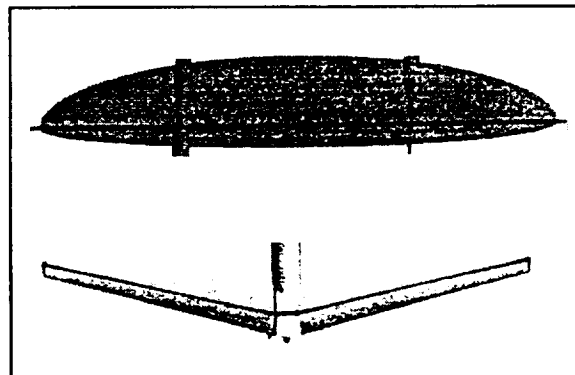


Figure 3.2 *The Elang and the Banshee '94* with quarter chordlines

The configuration of the *Banshee '94* incorporates a twisted swept wing with endplates. Wing sweep creates two major effects: decreased drag and additional stability. Decreased drag improves an aircraft's performance. The stability effects are created by the airfoil's aerodynamic centers acting along the length of the root chord axis rather than a single point

(quarter chord), as is the case with an unswept wing (see Figure 3.2). The specific stability calculations will be discussed in another section.

The *Banshee '94* incorporates aerodynamic wing twist in its design. Twist varies the sectional lift coefficient along the wingspan allowing for increased stability. Two types of wing twist can be utilized: geometric, where the wing itself is physically twisted to change the sectional angle of attack; and aerodynamic, where the airfoil section changes along the wing. The *Banshee '94* flying wing uses the latter.

Another feature of the *Banshee's* configuration are endplates at the end of both wing tips. Being the largest wing tip device, this particular wing tip device is rarely used due to their excess skin friction drag produced by the considerably large surface area. However, on a flying wing, endplates may be used as vertical stabilizers. On conventional aircraft, (with tail and fuselage) the vertical stabilizer is usually placed on the tail. On such an aircraft, wing endplates would only serve as a lift to drag improvement device. By allowing the endplates to serve a dual purpose, little additional drag is created. This placement allows the best performance of the vertical stabilizer. On conventional aircraft, the vertical stabilizer is placed on the tail. On an aircraft without a tail or fuselage, the tips of a swept wing are the rear-most locations on the aircraft.

In addition to acting as a control surface, the endplates also increase the lift to drag ratio. The endplates allow for a non-zero lift distribution at the wing tip (see Figure 3.3). In addition to increased lift, the endplates also reduce drag. Large plates placed at the end of the tips of the aircraft inhibit the trailing vortices which create induced drag. The aerodynamic effects influenced by the endplates increases overall performance.

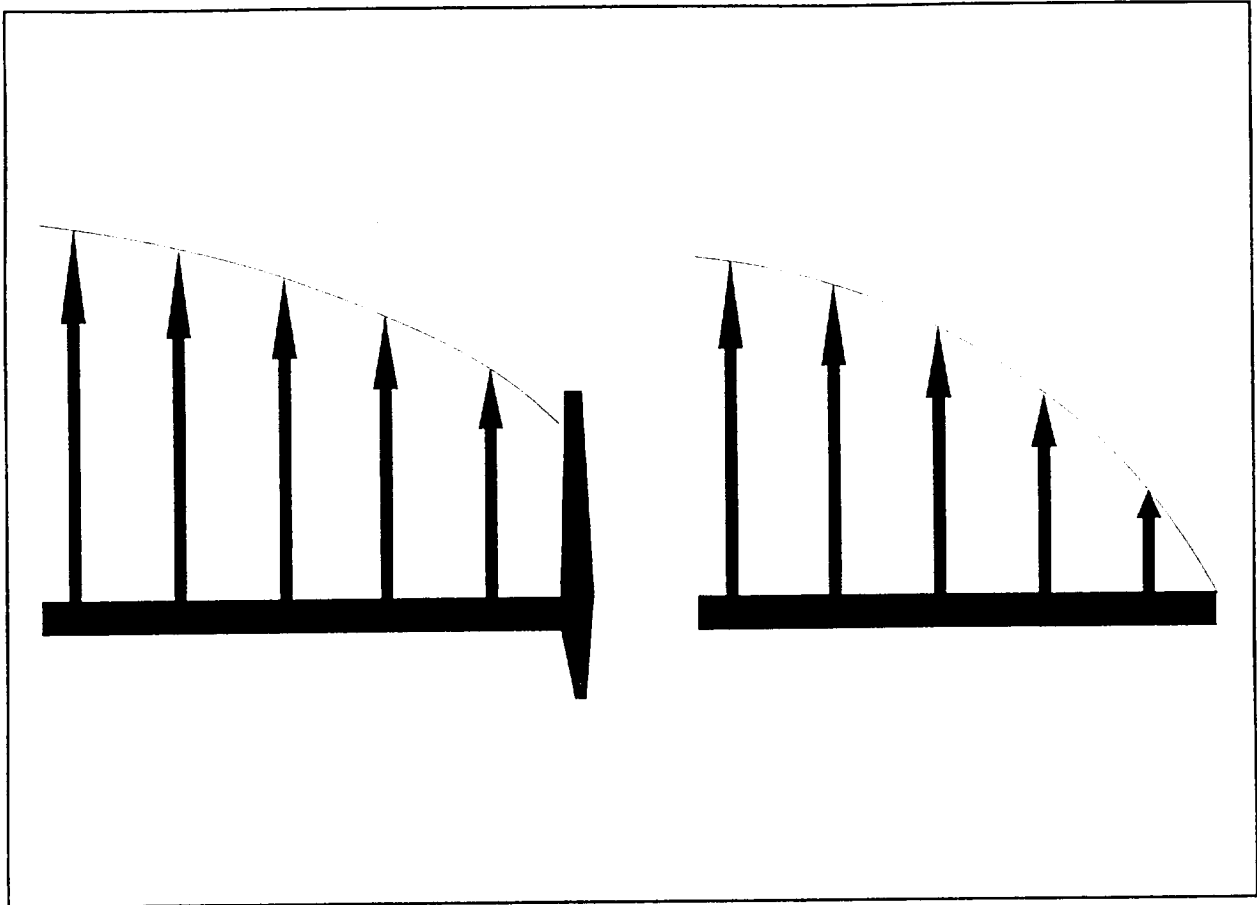


Figure 3.3 Lift distribution on wing with and without an endplate

3.3 Airfoil Selection

Due to the use of aerodynamic twist, a number of airfoils are necessary. The *Banshee* '94 uses a series of five airfoils, the Eppler 325 series⁵. The E325, E326, E327, E328, and E329 airfoils are pictured in Figure 3.4. The airfoil sections are placed on the wing as illustrated in Figure 3.5. The aerodynamic data for the E325, E327, and E329 is listed in Appendix A1.

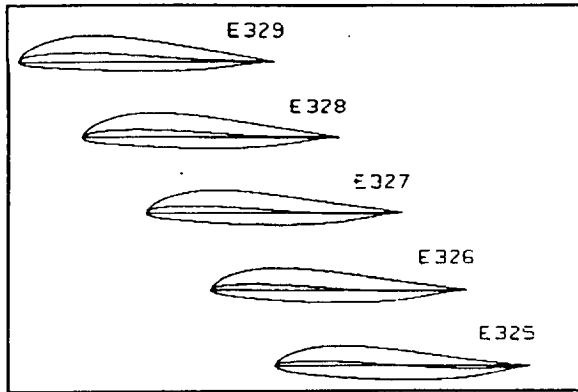


Figure 3.4 The Eppler E325 series

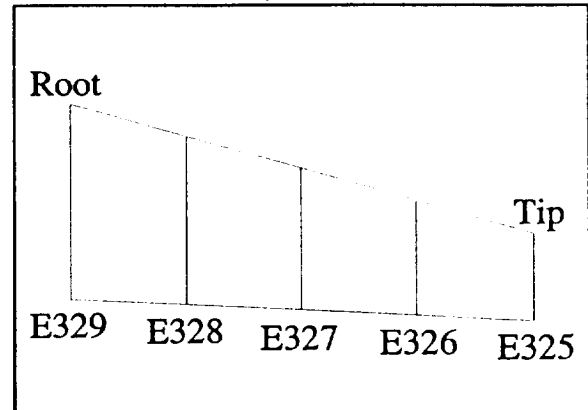


Figure 3.5 Airfoil placement along the wing

For a flying wing, certain considerations require additional attention during design, such as stability and component placement. The chosen airfoils must have certain characteristics including necessary moments, thickness, and similarity of shape. The E325 series satisfies these requirements.

With the absence of a tail, a horizontal stabilizer cannot be incorporated in the design. Without such a device, an aircraft could not achieve pitch stability with a conventional airfoil. Most airfoils have a negative moment about the aerodynamic center. With the horizontal stabilizer absent, it becomes necessary to use a set of airfoils which produces a positive pitching moment about the wing. To obtain a positive moment, an airfoil with a reflexed camber is needed. For a swept wing, the reflex of the camber increases along the wingspan toward the tip, as illustrated in Figure 3.4. This change in the reflex of the camber creates aerodynamic twist along the wing promoting pitch stability. The airfoils near the root, the E329 and E328, have significant negative pitching moments. However, with proper placement of the airfoils, the lift produced by the airfoils creates a positive moment about the aircraft's center of gravity. The calculation of center of gravity is discussed in depth in the controls and stability section.

In addition to the absence of a tail, a flying wing has no fuselage. This poses an additional problem with component placement since all components must now be placed within the wing. There must be adequate space for the components. The E325 series has one of the largest thicknesses of all available airfoil series for tailless aircraft.

A series of airfoils implies a similarity in shape. In fact, the mid- and semi-span airfoils are geometrically linear extrapolations of the tip and root airfoils. This similarity allows for additional benefits during analysis and construction. The aerodynamic data varies linearly among airfoils, as illustrated in Figure 3.6. This linear relationship allows for certain assumptions to be made about averaging the airfoils aerodynamic characteristics. This will be discussed in detail in the aerodynamic and stability analysis sections. Another benefit occurs with construction. The hotwiring technique used allows the form of each half of the wing to be cut swiftly and accurately. The similarity of shape allowed the wing to be fabricated using only two templates at the root and tip. This construction method will be discussed further in the structures section.

3.4 Drag Calculations

3.4.1 Introduction

The main purpose of this section is to describe in detail the calculations performed to predict the drag on *the Banshee '94*. The first section describes the different assumptions used for the analysis. The second section gives a detailed description of the calculations; citing all of the required equations and constants.

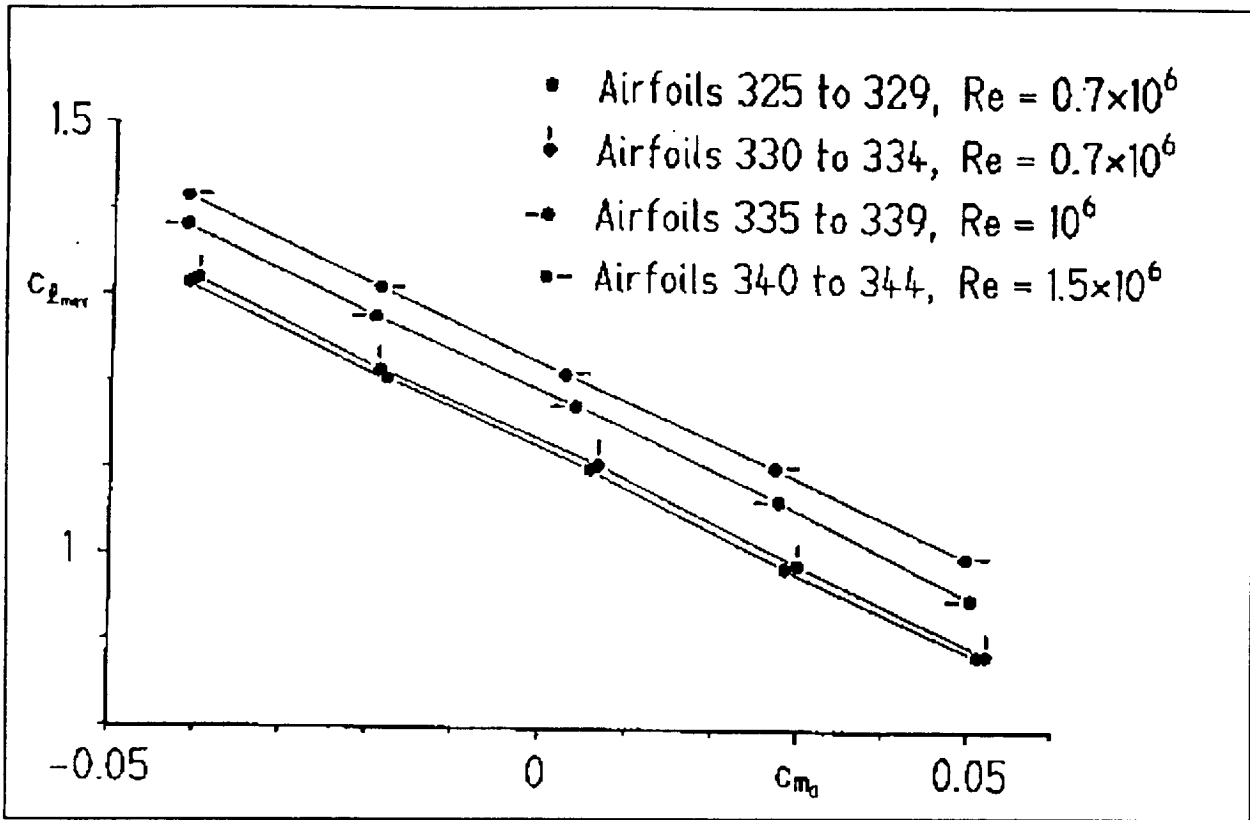


Figure 3.6 C_l vs. C_m from *Airfoil Design and Data*, Richard Eppler

3.4.2 Assumptions

As with any calculations, certain assumptions needed to be made in order to analytically determine the drag exerted on *the Banshee '94*. These assumptions are summarized as follows:

1. Incompressible Flow: Since *the Banshee '94* will fly at a cruise velocity well below the speed of sound, compressibility effects are negligible.
2. Turbulent Flow: The historical trends of the cruise velocity of similar aircraft demonstrate a low velocity profile. However, the characteristic length of *the Banshee '94* is large enough to raise the value of the Reynold's number to about 700,000. This value is well above the 500,000 transition Reynold's number. This is important to the skin friction calculations.

3. Flat-Plate Theory: All of the major components of the aircraft including the landing gear and endplates were treated as flat-plates with the same cross-sectional area. The landing gear were assumed to be one inch thick and three inches tall. The wing was not treated in this matter. Experimental data from the airfoil reference provided the drag coefficients.
4. The Wing Sizes: The wing was "divided" into different sections representing the different airfoils. The chord length was held constant at an average of the chord lengths associated with each section.
5. Constant Properties of Air: Since *the Banshee '94* will be flying at low altitudes, the properties of air remain constant with slight changes in altitude. Sea level values were assumed.
6. Approximate Pressure Drag: Since the only way to accurately account for pressure drag is through a lengthy Computational Fluid Dynamics procedure, an approximation was used as a more efficient method. This was only implemented in the calculations for the endplates.

3.4.3 Calculations

The following constants were used in the analysis:

density of air	ρ	0.076474 lbm/ft ³
viscosity coefficient of air	μ	1.2024 x 10 ⁻⁵ lbm/s ft
Oswald Efficiency Factor	e	0.98

A component method was used to calculate the drag exerted on *the Banshee '94*. The first component that will be considered is the actual wing itself excluding the landing gear, duct, and endplates. The wing was sectioned analytically to represent the three airfoils that data was available for; E325, E327, and E329 (see Figure 3.5). The drag was calculated for each section and then summed.

By definition, the drag is calculated as follows:

$$Drag = C_D \frac{1}{2} \rho V^2 S$$

For the wing, the parasitic drag was calculated for each portion of the wing using the different drag coefficients for each airfoil (see Appendix A1). These values were then summed to provide a total parasitic drag for each wing. The induced drag is the drag due to the lift. It is calculated using the following equations:

$$D_i = C_{D_i} \frac{1}{2} \rho V^2 S$$

$$C_{D_i} = k C_L^2$$

$$k = \frac{1}{\pi A e}$$

As with the parasitic drag, each induced drag component was calculated for each section of the wing and then summed for a total induced drag for each wing.

Thin-plate theory was used to calculate the drag on each of the endplates. The coefficient of drag for one endplate is calculated using the following equations:

$$C_{D_E} = C_{D_{oE}} \approx 1.25 C_{D_{FE}}$$

$$C_{D_{FE}} = C_{F_E} \frac{S_{WET}}{S_{REF}}$$

where S_{WET} is the surface area of the endplate and S_{REF} is the reference area (planform area) of the endplate. Using the previous equations, the drag was calculated for each endplate.

The drag for the duct was calculated in a similar manner. The coefficient of drag for the duct was calculated as follows, neglecting pressure effects:

$$C_{D_D} = C_{D_{oD}} = C_{D_{FD}}$$

$$C_{D_{FD}} = C_{F_D} \frac{S_{WET}}{S_{REF}}$$

where S_{WET} is the surface area of the duct, S_{REF} is the reference area (planform area) of the duct, and C_F is calculated the same way as for the endplate.

The drag for the landing gear was calculated in the same manner. The coefficient of drag for the landing gear was calculated as follows, neglecting pressure effects:

$$C_{D_{LG}} = C_{D_{oLG}} = C_{D_{FLG}}$$

$$C_{D_{FLG}} = C_{F_{LG}} \frac{S_{WET}}{S_{REF}}$$

where S_{WET} is the surface area of one landing gear, S_{REF} is the reference area (planform area) of one landing gear, and C_F is calculated the same way as for the endplate and the duct.

The total drag is calculated by adding up all of the drag from all of the components:

$$Drag_{tot} = 2 * Drag_W + 2 * Drag_E + Drag_D + 3 * Drag_{LG}$$

W - wing; E - endplate; D - duct; LG - landing gear

3.5 Lift Calculations

3.5.1 Introduction

The lift for *the Banshee '94* was an important consideration. Using an estimated weight of 13 pounds, it was necessary for the cruise conditions to generate 13 pounds of lift to overcome the weight.

3.5.2 Calculations

The following section describes the calculations used to calculate the lift at different cruise velocities. The only constants used in these calculations are the density of the air, the different coefficients of lift obtained from published experimental data, and the different reference areas for the sections of the wings. Since it was assumed that the cruise altitude would not be significant enough to warrant a change in the density, a standard sea level density was used; 0.076474 lbm/in³. The coefficients of lift and the reference areas can be found in the spreadsheet in Appendix A2.

Each wing was divided into three sections to represent the three different airfoils for which coefficient of lift data was available. An average chord length was used for each section to determine the planform area needed for the calculations.

The lift for each section was calculated using the following equation:

$$Lift = C_L \frac{1}{2} \rho V^2 S$$

Each lift was calculated and then summed to provide the total lift exerted on *the Banshee '94* by the wing. The lift calculations were iterated over a velocity interval to determine the necessary speed to keep *the Banshee '94* airborne.

3.6 Lift Versus Drag Calculations

3.6.1 Introduction

One of the major factors in considering an aircraft's performance and efficiency is the lift to drag ratio. The advantage of a flying wing in this area manifests itself in the high lift to drag ratio. This phenomenon is due simply to the high planform area of the lifting surfaces versus total planform area of the aircraft. For a flying wing, the ratio of lifting surface area to total area is nearly one. Below is a summary of the calculations for the lift to drag ratio.

3.6.2 Calculations

The lift and drag were determined from empirical methods which were explained in sections 3.3 and 3.4 of this report. The lift to drag ratio was calculated using the results of these sections.

3.7 Results and Conclusions

Below, in Figure 3.7, is a graph of the calculated lift in pounds versus velocity in miles per hour. It can be clearly seen from the graph the approximate cruise velocity necessary to

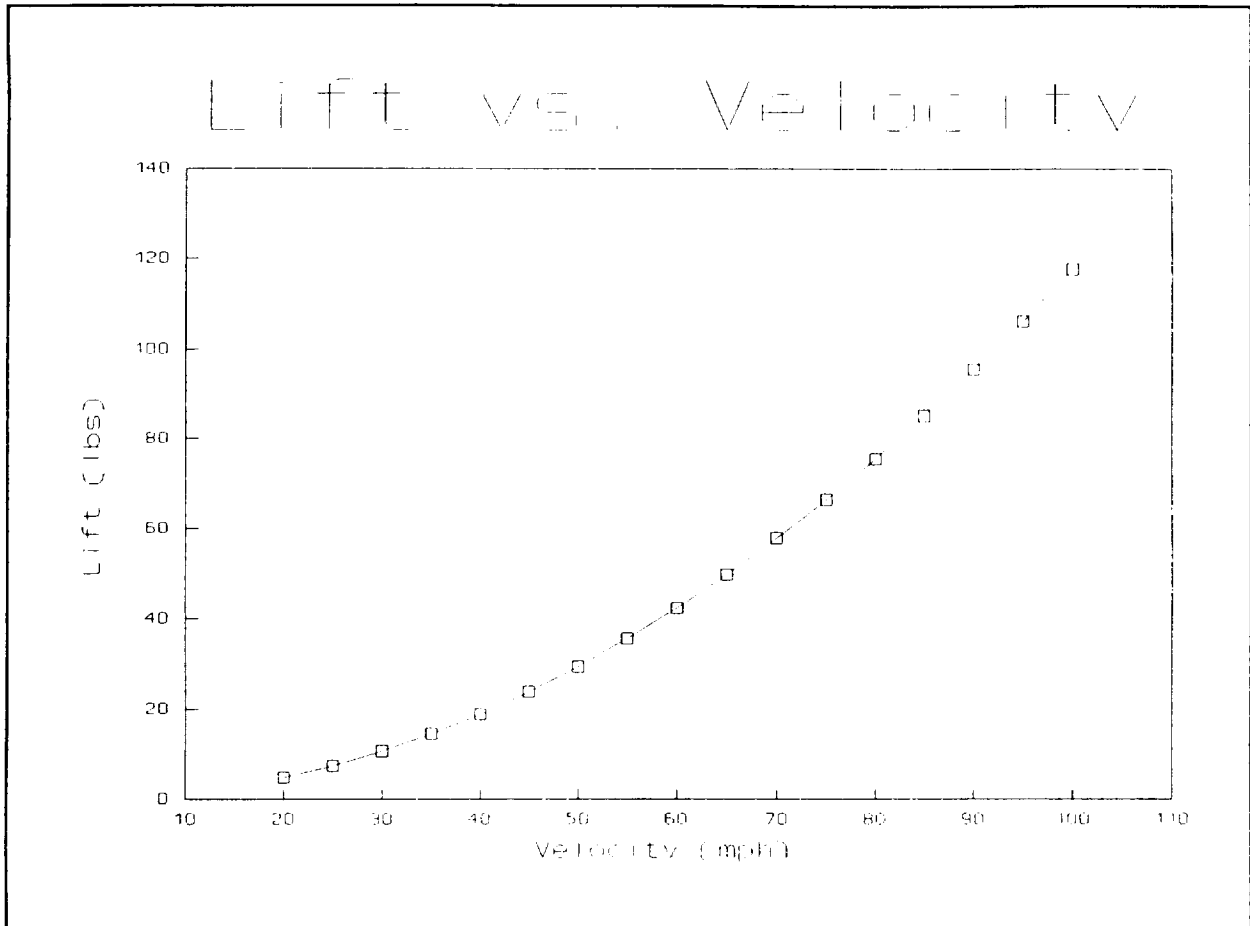


Figure 3.7 Lift vs. Velocity

maintain a steady altitude is thirty-three miles per hour. This velocity is reasonable for an aircraft of this size. *The Elang* had a cruise velocity of thirty-four miles per hour.

The spreadsheet that was used for the calculations can be found in Appendix A2. Using cruise condition of angle of attack of 4° and thirty-three miles per hour, the total drag exerted on *the Banshee '94* is calculated to be 0.617 pounds-force. This value is reasonable for an aircraft of this size and shape. The propulsion system being used should provide sufficient thrust to achieve cruise conditions. Figure 3.8 is a graph of the total drag force exerted on *the Banshee '94* in pounds versus the cruise velocity in miles per hour.

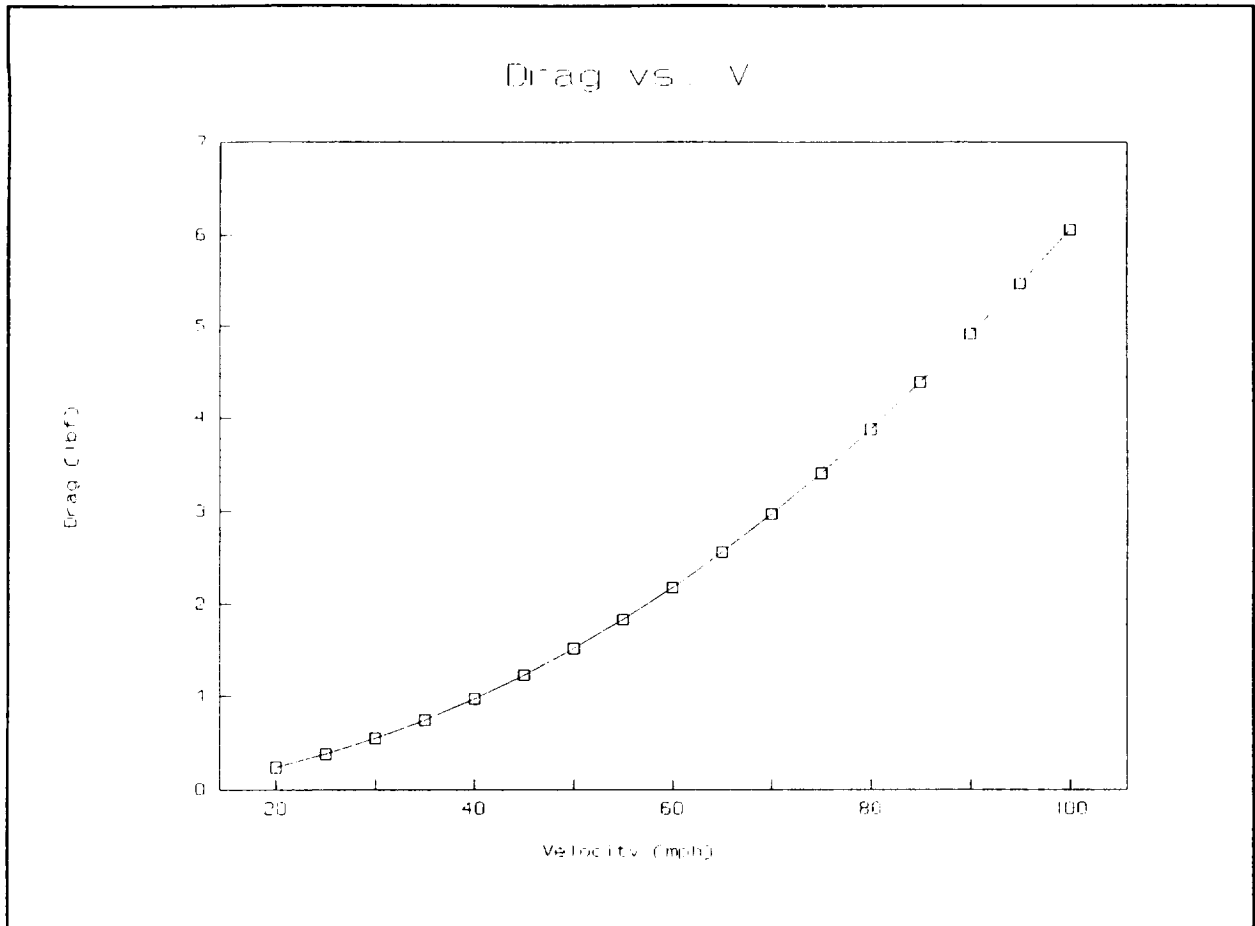


Figure 3.8 Drag vs. Velocity

From these results, the lift to drag ratio for *the Banshee '94* was calculated to be 19.44. This value is greater than that of a typical aircraft, as would be expected. However, this value is close to those found for other such flying wing aircraft such as *the Elang*. Below is a table of aircraft and their subsequent lift to drag ratios:

<u>Aircraft</u>	<u>L/D</u>
<i>Banshee '94</i>	19.44
<i>Elang</i>	19.69
<i>Surya NASA Advanced Aero MQP 91-92</i>	19.55

Concord (Trans-Atlantic)	7.5
XB-35 Flying Wing	20
Oblique Wing Aircraft	9.8
B-47	17.2
AVRO Vulcan	17.0

Figure 3.9 shows the thrust and drag versus velocity curve at different throttle settings. The thrust data is detailed in Chapter Five. The figure shows that at twenty-five percent power, the thrust equals the drag at the predicted cruise velocity of thirty-three miles per hour.

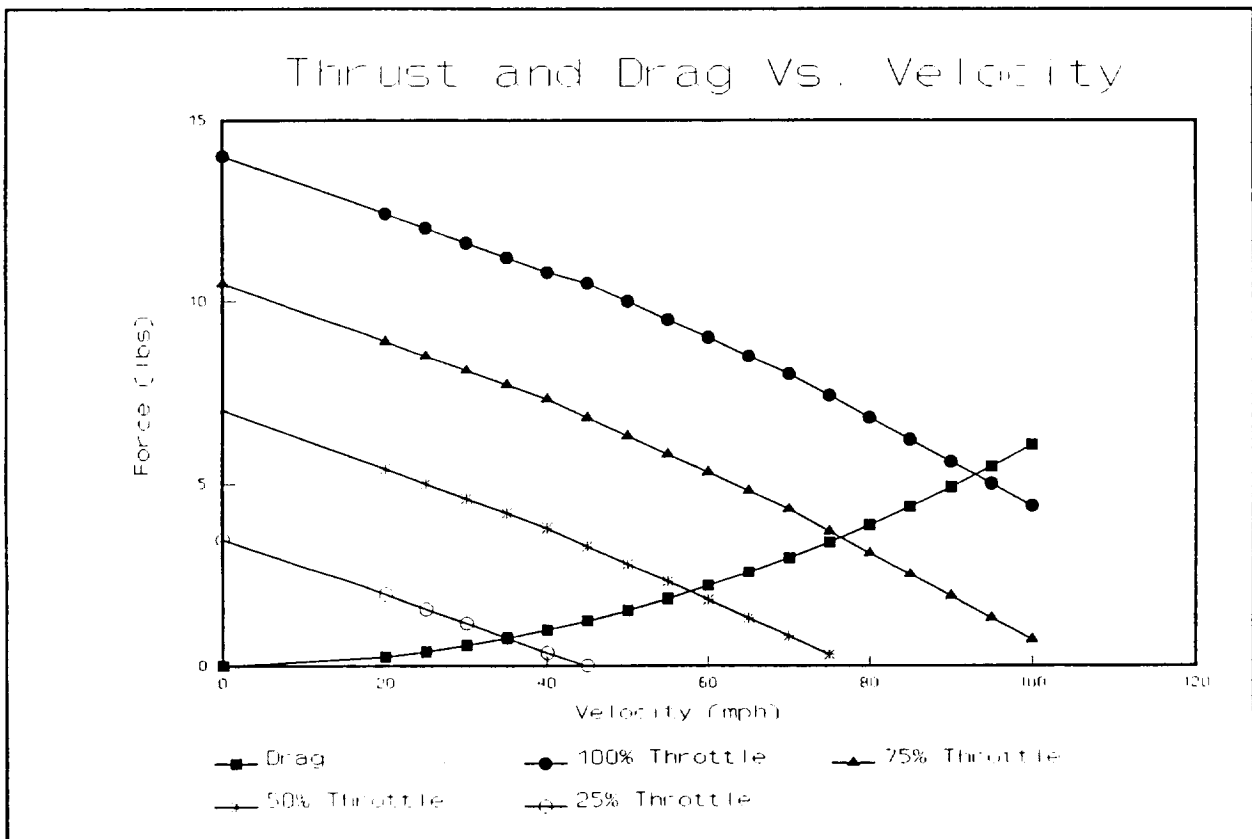


Figure 3.9 Thrust and Drag vs. Velocity

4. Stability and Controls

4.1 Introduction

The primary responsibilities of the stability/controls group was to determine the important flight parameters to ensure stable flight. The information provided by controls/stability is particularly important because of the intrinsic instability of the flying wing. The most important parameters such as the center of gravity, the flight condition angle of attack, and the static margin, are all crucial to the success of the flying wing.

Stability refers to the ability of a vehicle to return to its original equilibrium position, without pilot assistance, after a disturbance has pitched, yawed, or rolled it to a different angle or has caused a speed change.¹⁵ Static stability is present if the forces created by the disturbed condition displace it in the correct direction to return the aircraft to its original position, while dynamic stability pertains to the dynamic behavior of the motion of the aircraft before and after a disturbance. Dynamic stability is present if the dynamic motions of the aircraft will eventually return it to its initial state.

The rigid body motions of aircraft may be conveniently divided into two classifications, longitudinal and lateral motions. Longitudinal motions occur in the plane of symmetry, which remain in its original position. Lateral motions, such as rolling, yawing and sideslipping, displace the plane of symmetry.¹³ The technical significance of this distinction is that for normal symmetrical aircraft with small displacements these two types of motion are independent of each other.

In performing the stability analysis for *Banshee '94*, we considered the three primary axes of rotation: pitch, roll, and yaw, however our major concern was stability along the pitch axis. In conventional aircraft, a horizontal tail is placed so that it may offset the moments originated by the wing and fuselage. Consequently, a flying wing without a horizontal tail demands that a supplementary method for stabilization be used.

4.2 Static Stability

The goals of the static stability analysis were to find: 1) A workable cruise condition angle of attack for *Banshee '94*; and 2) A center of gravity for the wing which ensured static stability. Our primary objective was to focus on the stability of the aircraft in the pitch axis, which is anticipated to be more problematic than the other two axes. Stability in the yaw and roll axes is expected to be acceptable because of the symmetry of the wing in these axes.

The first objective was to derive the classic static stability curve: $C_{m_{cg}}$ vs α . The starting point was the lift, drag, and moment coefficients as determined by the aerodynamics group. (Table 4.1)

The moment coefficient about the center of gravity is arrived at through the equation:

$$C_{m_{cg}} = C_{m_{ac}} - C_l \frac{x}{c} - C_d \frac{x}{c}$$

Next, the lift and drag moment arms, which vary with changes in α , the angle of attack had to be considered. (Figure 4.1)

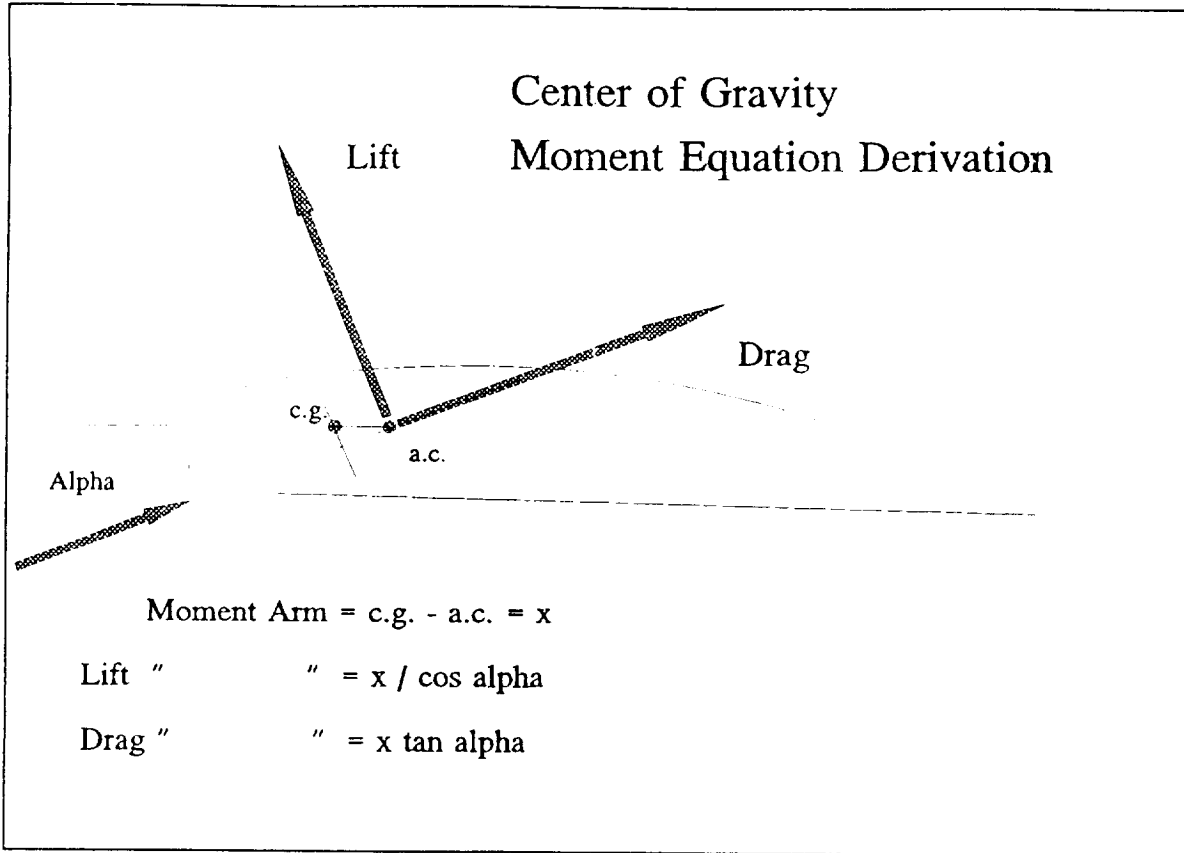


Figure 4.1 Moment Arm Analysis

Table 4.1, Experimental Airfoil Data⁵

α	E329			E327			E325		
	C_l	C_d	C_{mac}	C_l	C_d	C_{mac}	C_l	C_d	C_{mac}
2	0.53	0.0086	-0.05	0.35	0.008	0.0	0.15	0.0077	0.05
3	0.65	0.0091	-0.51	0.48	0.0085	-0.0024	0.27	0.0079	0.048
4	0.73	0.0094	-0.52	0.56	0.0087	-0.0048	0.38	0.0081	0.046
5	0.86	0.0102	-0.53	0.65	0.0094	-0.0072	0.45	0.0085	0.044
6	0.95	0.0108	-0.54	0.76	0.01	-0.0096	0.59	0.0094	0.042
7	1.03	0.0115	-0.55	0.87	0.0107	-0.012	0.69	0.0101	0.04

The final equation used is as follows:

$$C_{mcg} = C_{mac,329} \frac{S_{329}}{S_{tot}} + C_{mac,327} \frac{S_{327}}{S_{tot}} + C_{mac,325} \frac{S_{325}}{S_{tot}}$$

$$- \frac{1}{\cos \alpha} \left(C_{l,329} \frac{x_{329}}{c_{329}} \frac{S_{329}}{S_{tot}} + C_{l,327} \frac{x_{327}}{c_{327}} \frac{S_{327}}{S_{tot}} + C_{l,325} \frac{x_{325}}{c_{325}} \frac{S_{325}}{S_{tot}} \right)$$

$$- \tan \alpha \left(C_{d,329} \frac{x_{329}}{c_{329}} \frac{S_{329}}{S_{tot}} + C_{d,327} \frac{x_{327}}{c_{327}} \frac{S_{327}}{S_{tot}} + C_{d,325} \frac{x_{325}}{c_{325}} \frac{S_{325}}{S_{tot}} \right)$$

The derivation of this equation had to account for three different airfoils of the wing due to the fact that each airfoil had a different aerodynamic center (because of sweep-back) as well as a different planform area. Here, x is the center of gravity minus the aerodynamic center, which was assumed to be the quarter chord, and c & S respectively are the mean chord length and planform area of that particular airfoil.

An iterative process was employed through the use of a spreadsheet in order to determine a center of gravity of 7.43 inches behind the front of the duct and an angle of attack of four degrees for cruise conditions. The C_{mcg} vs α curve for this center of gravity was derived (Figure 4.2).

Static stability is ensured due to the negative slope of the plot. If the airplane is momentarily pitched to a higher angle, the pitching moment change will tend to restore the plane to its original attitude. If the airplane is pitched nose-down, the resulting moment change will tend to raise the nose.¹⁵

This spreadsheet was also used to determine the neutral point and the corresponding

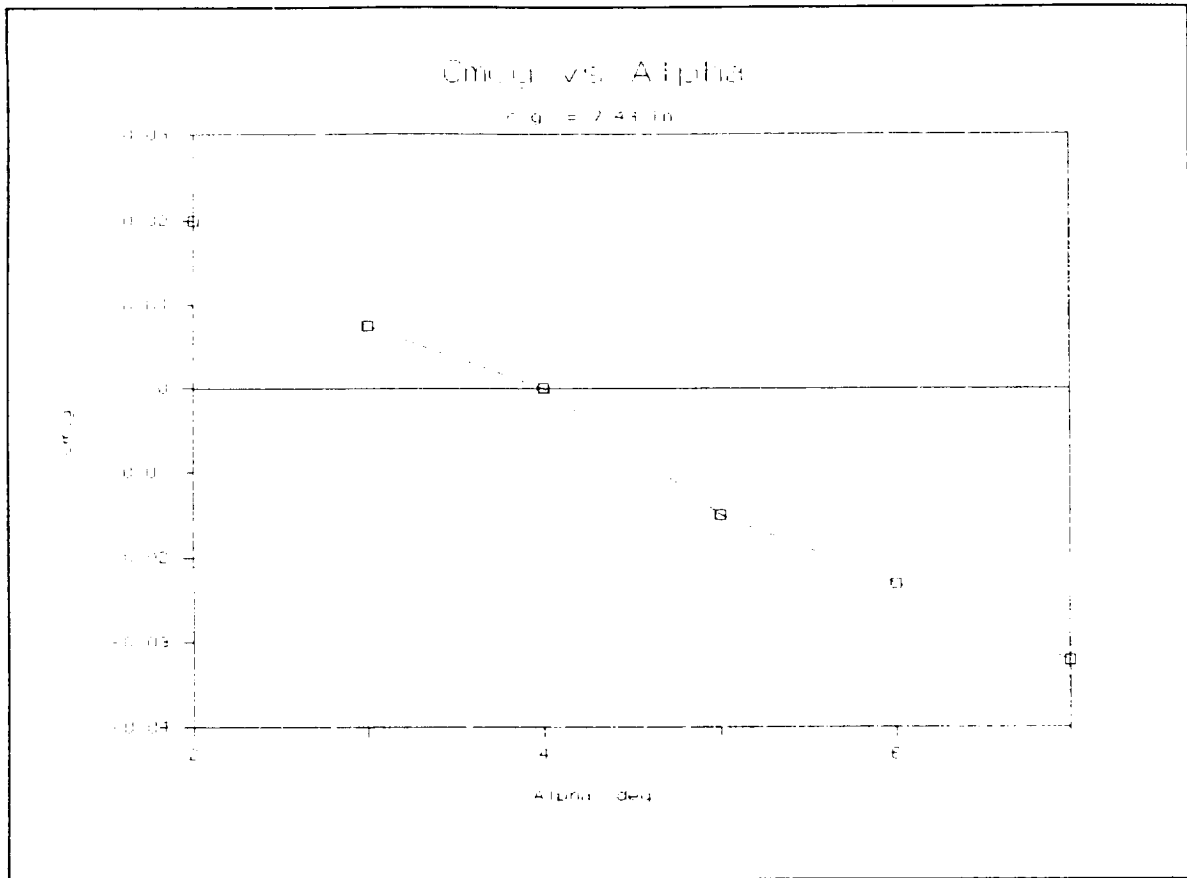


Figure 4.2 Static Stability Curve

static margin of the wing. To arrive at this, $C_{m_{cg}}$ was plotted against $C_{l_{ave}}$, the average lift of the three airfoils. When the slope of this curve is equal to zero, this is the point on the plane which has been labeled the neutral point. The neutral point of *Banshee '94* was found to be at 8.7252 inches behind the front of the duct or 1.2952 inches behind the center of gravity. The graph can be seen in Figure 4.3:

Note that while the slope of this curve doesn't appear to be zero, the average slope of this curve *is* zero. By placing the neutral point farther towards the front of the wing, the C_m vs C_l curve slopes upwards while placing the neutral point farther back causes the plot to slope downwards.

The static margin is defined as:

$$\text{Static Margin} = \frac{X_n - X_{cg}}{C}$$

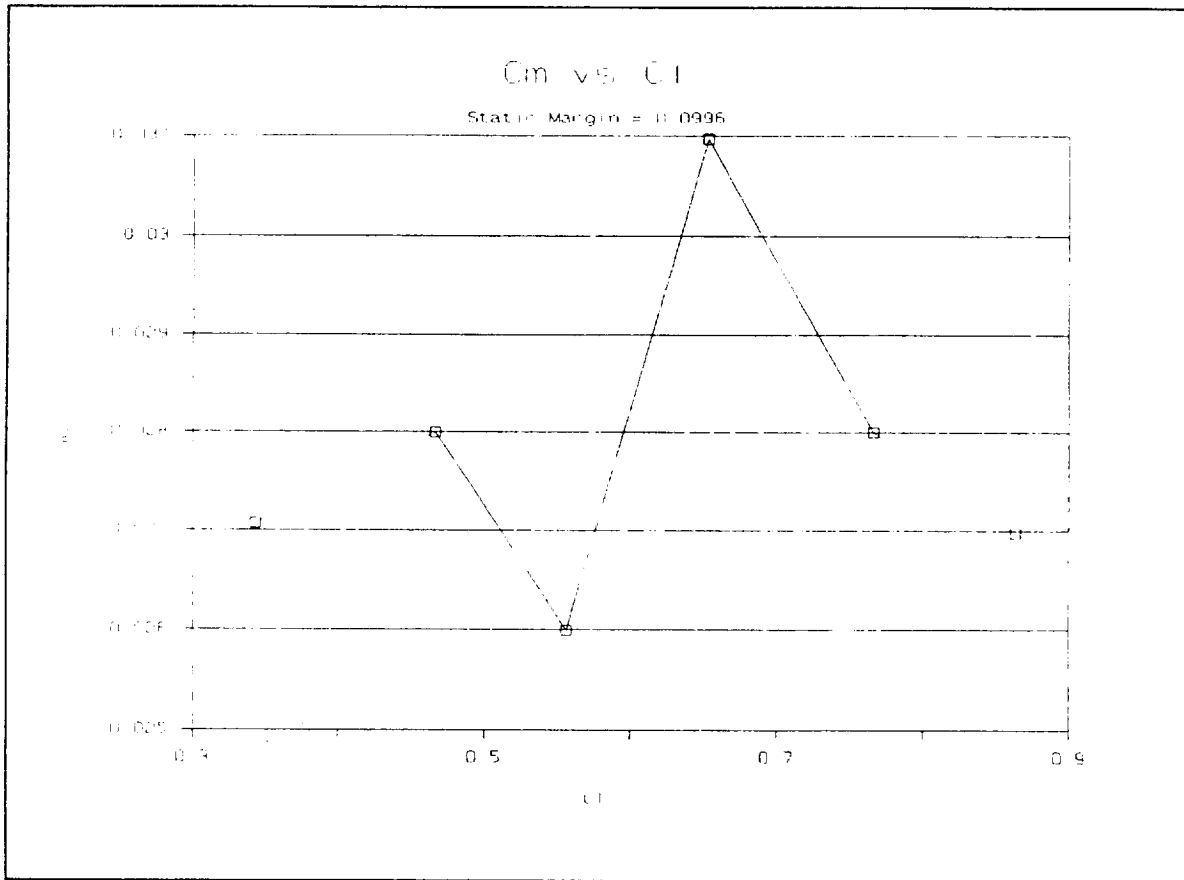


Figure 4.3 C_m vs C_l

Where X_n is the neutral point and C is the mean chord length. The static margin for *Banshee '94* was found to be 0.0996 or 9.96 percent, an acceptable number for conventional aircraft.

4.3 Dynamic Stability

The dynamic stability analysis entailed analyzing the wings reactions to sudden disturbances placed upon the wing during flight conditions, particularly along the pitch axis. A major concern with *Banshee '94* is a low moment of inertia about the pitch axis due to the absence of a horizontal tail. A horizontal tail would be used to provide damping effects so that the wing could retain an acceptable amount of controllability.

The governing equations of this analysis are:

$$M_{cs} = f(\delta)$$

Where M_{cs} is the moment caused by the deflected control surface, found through the use of the inviscid vortex panel code, and δ is the angle of deflection of the control surface. Also used is the equation:

$$\beta = \frac{M_{tot}}{I}$$

Where M_{tot} is the sum of the moments about the center of gravity derived from the wing, duct, etc., as well as the moment derived from the deflected control surface. I is the moment of inertia about a particular axis, found through a solid modeling program, ARIES, and β is the angular acceleration of the wing along that axis. Extremely high or low values for β denote poor controllability. By observing the angular accelerations, dynamic stability could be determined. Plots of β vs δ were arrived at for the pitch, roll, and yaw axes. (Figures 4.4, 4.5, 4.6)

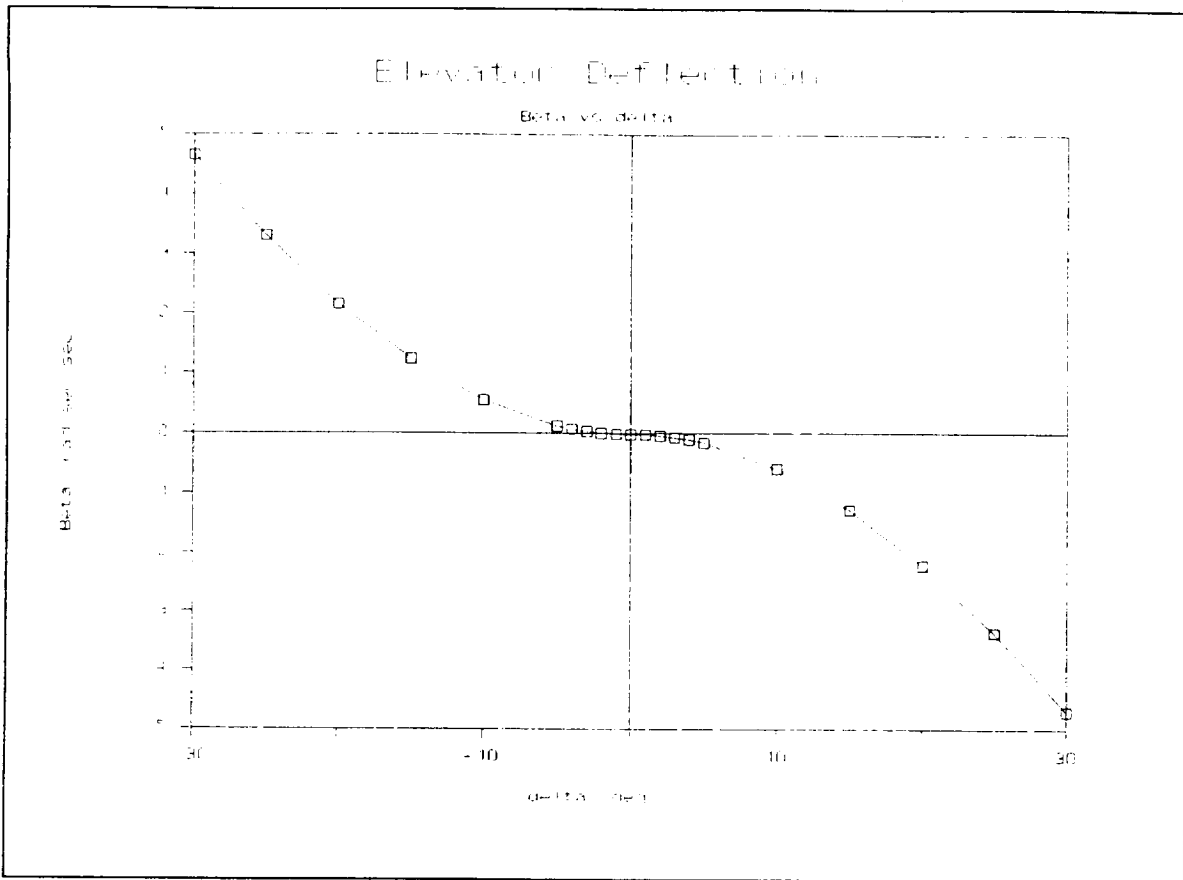


Figure 4.4 Angular Acceleration, Pitch Axis

4.3.1 Results

δ_{\max} in the roll axis was found to be around 70 rad/sec², indicating an acceptable amount of control. It can be seen in the plots for the elevators & rudders that the angular accelerations in the pitch and yaw axes are small, denoting low controllability. This isn't a foreseeable problem because of the symmetry in the yaw axis, however the absence of a tail in the pitch axis demands that further measures be taken. To conclude, it was determined that the wing has poor dynamic stability along the pitch axis.

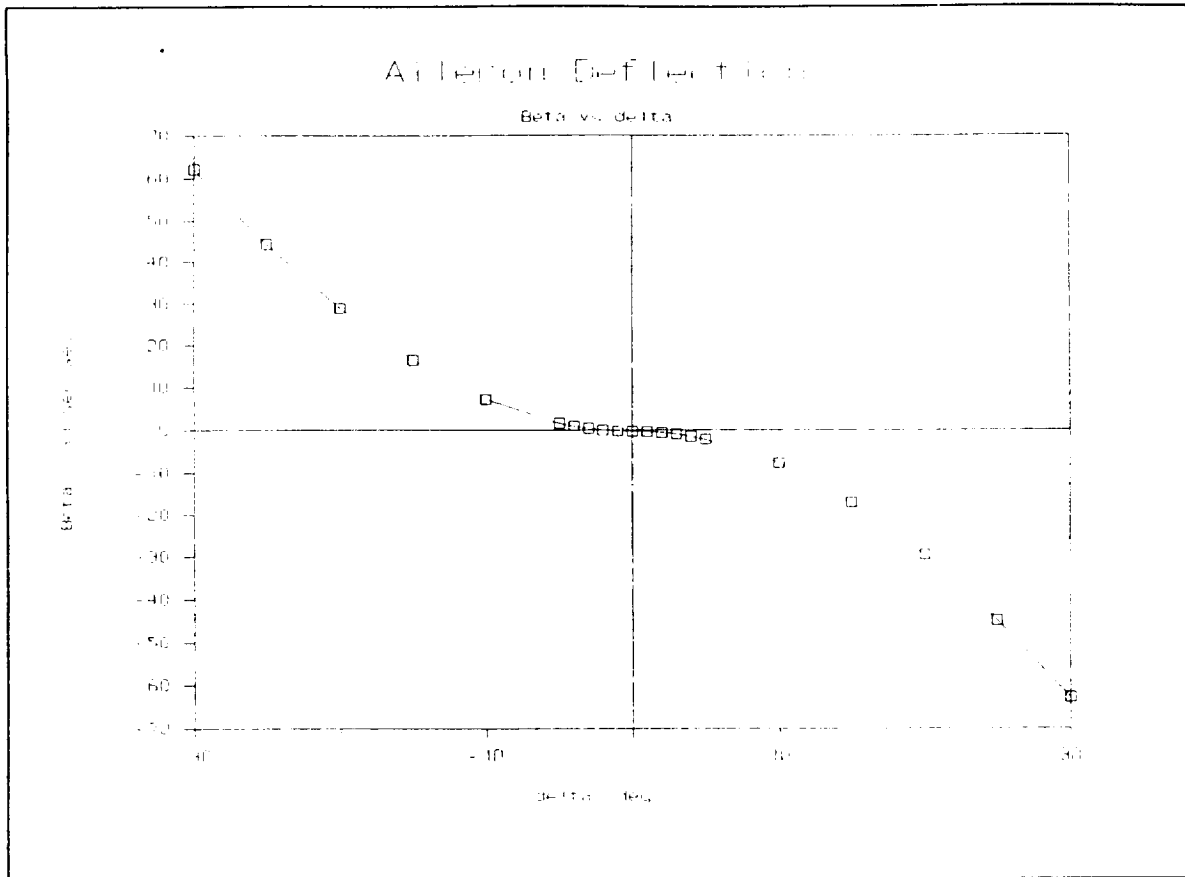


Figure 4.5 Angular Acceleration, Roll Axis

This analysis helped us to calculate the sizes for the control surfaces. Although our control surface size estimation was based on Elang's values, we decided to slightly oversize the elevators, ailerons and rudders to ensure better control. The final sizes appear in Table 4.2:

The dynamic stability analysis ascertained that several alternative design methods would have to be employed so that the wing would be stable during flight. Some of these design implementations are: 1) Sweeping the wings back for improved stability in all three axes; and 2) The use of an automatic electrostatic stability system.

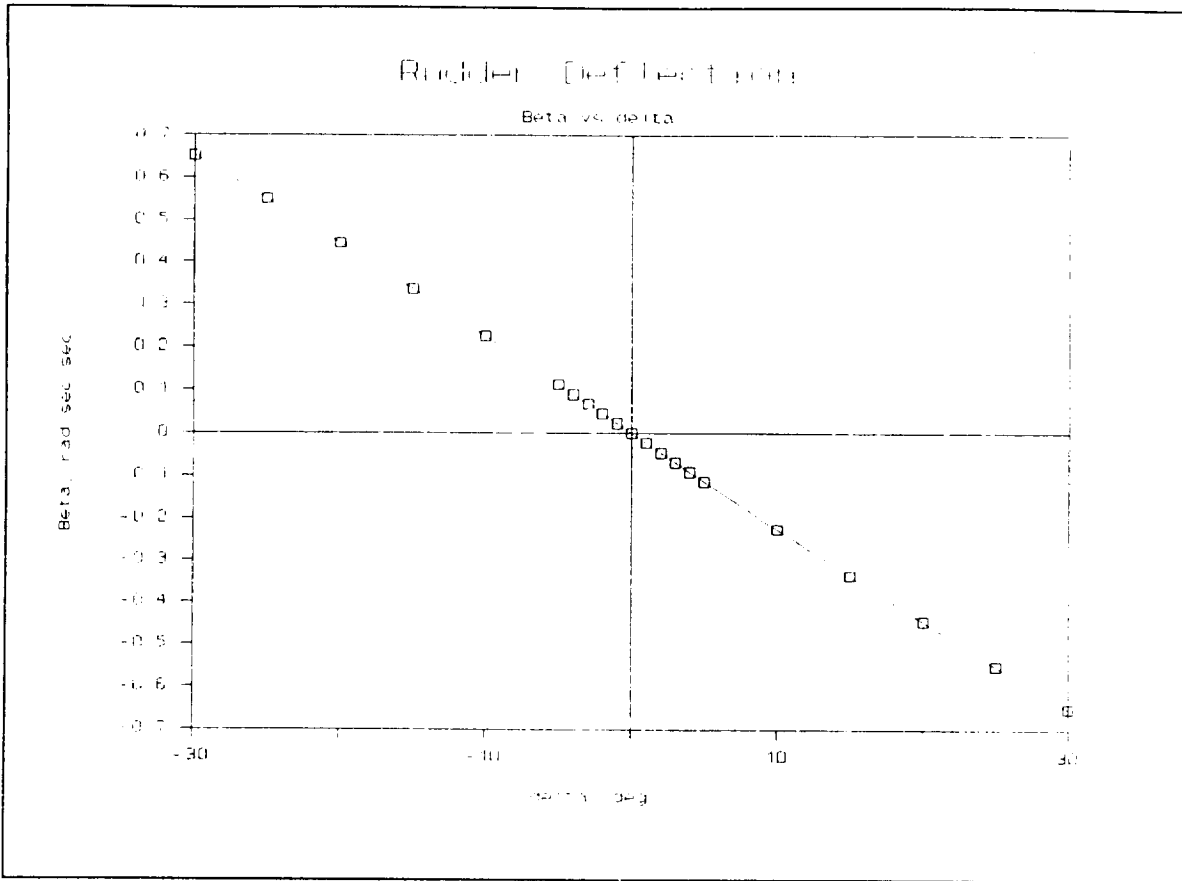


Figure 4.6 Angular Acceleration, Yaw Axis

Table 4.2, Control Surface Sizes:

Control Surface	Percent of Chord Length	Percent of Planform Area
Elevator	18.0	13.0
Aileron	18.0	2.9
Vertical Stabilizer	N/A	12.0
Rudder	N/A	31.7 percent of endplate planform

4.4 Sweep-back

One feature we decided to implement for the aircraft was to sweep-back the wings. From a stability point of view, sweep-back is important for three reasons:

1) Swept-back wings have large dihedral stability even when they have no dihedral angle. This arises because the effect of the angle of yaw is to increase the sweep-back angle of one wing panel and decrease it for the other side of the airplane. The change in sweep alters the effective dynamic pressure, increasing the lift on one side, lowering it on the other, and producing a restoring rolling moment.¹³

2) Sweep-back increases the moment of inertia along the pitch axis, helping to decrease the angular acceleration created by moments along this axis.

3) Sweep-back likewise aids in yaw stability. Figure 4.7 shows that a yawing moment produced by the differences in drag tends to restore the airplane to a straighter flight path.

Even with sweep-back, a flying wing is inherently unstable along the pitch axis. Normally, the horizontal tail would offset the moments generated by the fuselage and the wing. Because *Banshee '94* lacks a tail, it was decided that another method for stability would have to be utilized.

4.5 Electrostatic Stability System

The electrostatic stability system, (ESS) was invented by Maynard L. Hill of the John Hopkins Applied Physics Labs. It is a device that operates by measuring the earth's magnetic

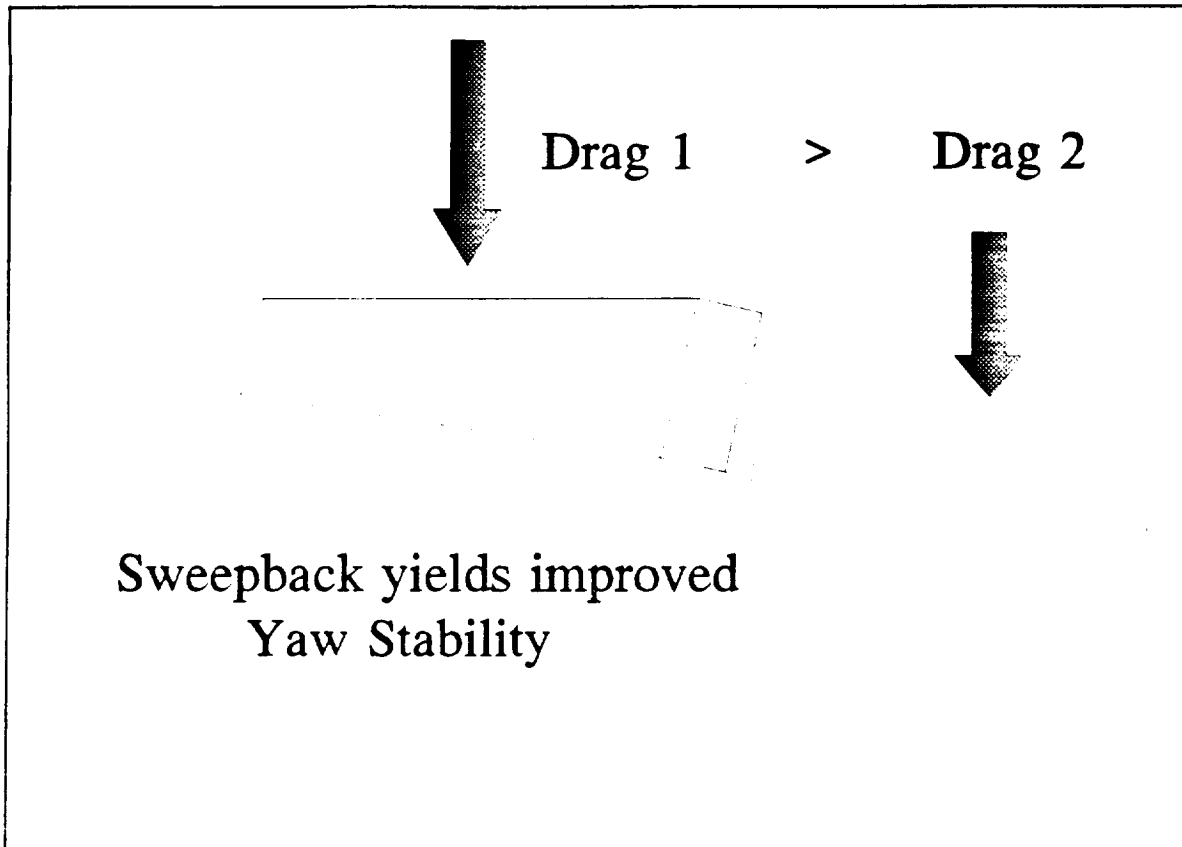


Figure 4.7 Effect of Sweep-back

field as a vertical reference, since the earth's electromagnetic field gradient is about 650 volts per foot.⁷ A complete two-axis system, functioning in the roll and pitch axes, weighs about one-tenth of a pound, uses 80 milliwatts of power and costs about \$130. Its principal component is the StaticMaster¹ a one inch square strip of radioactive polonium which measures static voltage. The alpha radiation that it emits is quite harmless and has a half-life of about six months. StaticMasters are also widely used in industrial and hobby applications for the elimination of electrostatic charges.

In a simplified sense, an electrostatic autopilot is a solid-state electronic unit that can be

¹ Supplied by NRD Corporation, 2937 Alt Blvd. Grand Island, NY.

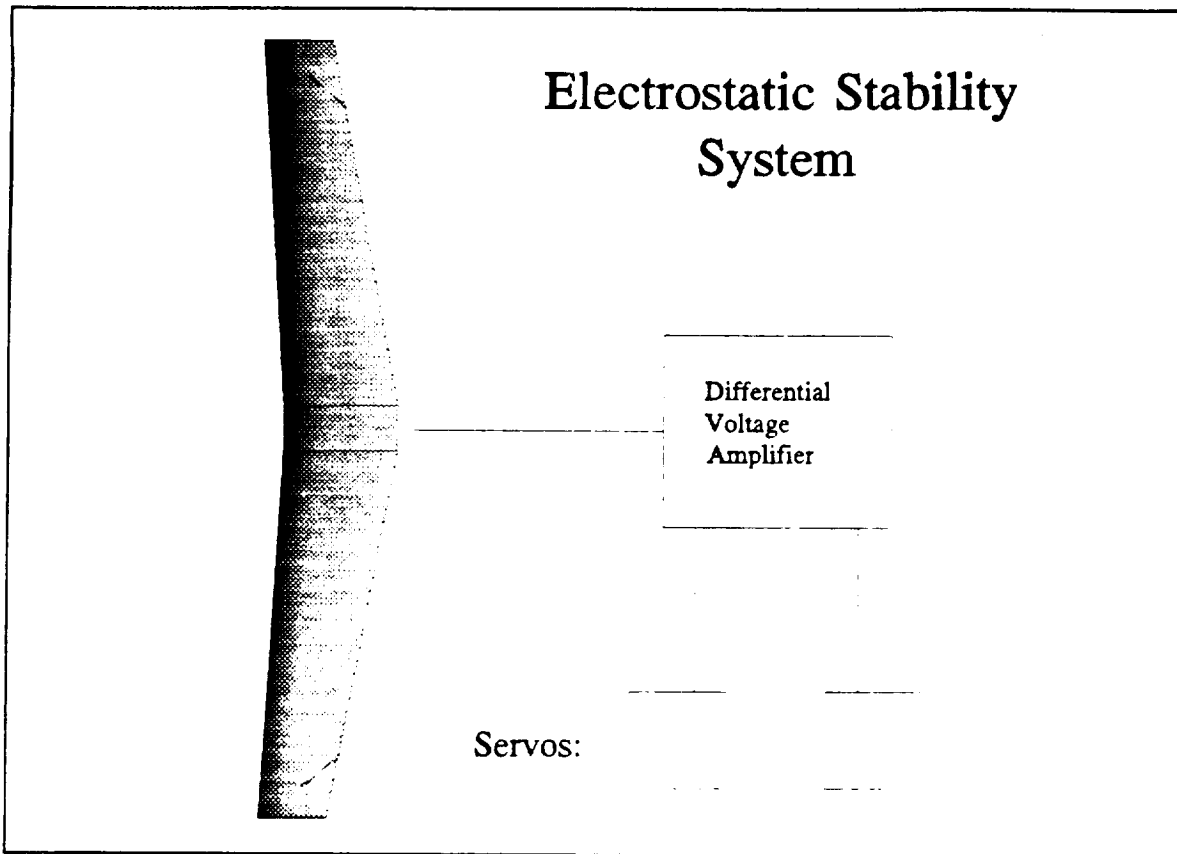


Figure 4.8 StaticMaster Placements for ESS

used in place of complex inertial gyroscopes whenever the electric field is vertical, a condition that on average exists about 90 percent of the time over 90 percent of the earth's surface.⁷ Electrical disturbances near thunderstorms cause malfunctions over distances that range out to about 10 kilometers from the edge of the storm. Also, the atmospheric electric field is sometimes useless over broader regions covered by frontal snow, rain, and sand storms. The method is not appropriate for use on manned aircraft where reliability is a prime requisite, and this is why the concept has not been seriously pursued for use on military weapons and aircraft.⁷

The StaticMaster displaces charged ions from the earth's magnetic field, and the signal from these ions are sent through a differential voltmeter (Figure 4.8). Next, the signal is sent

to mechanical servos which stabilize the aircraft accordingly. A more detailed view of the controls layout can be observed in Figure 4.9.

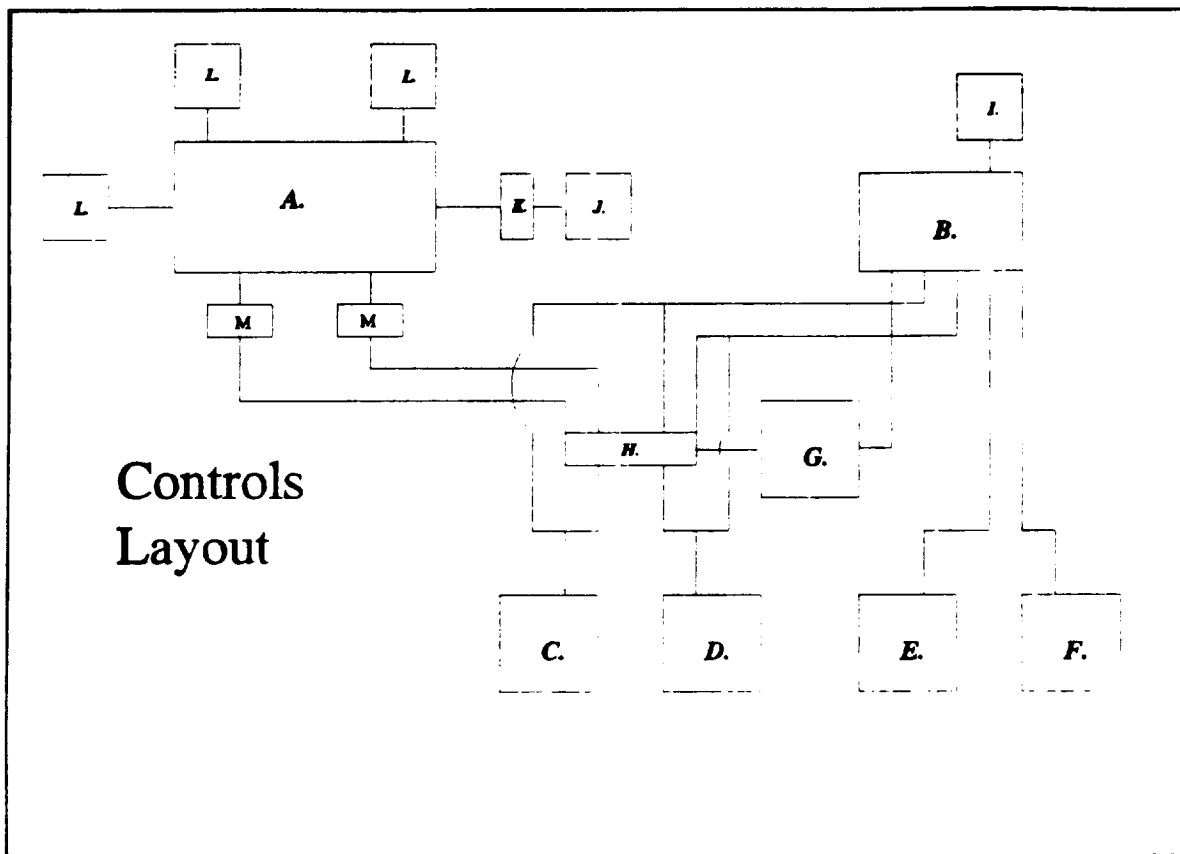
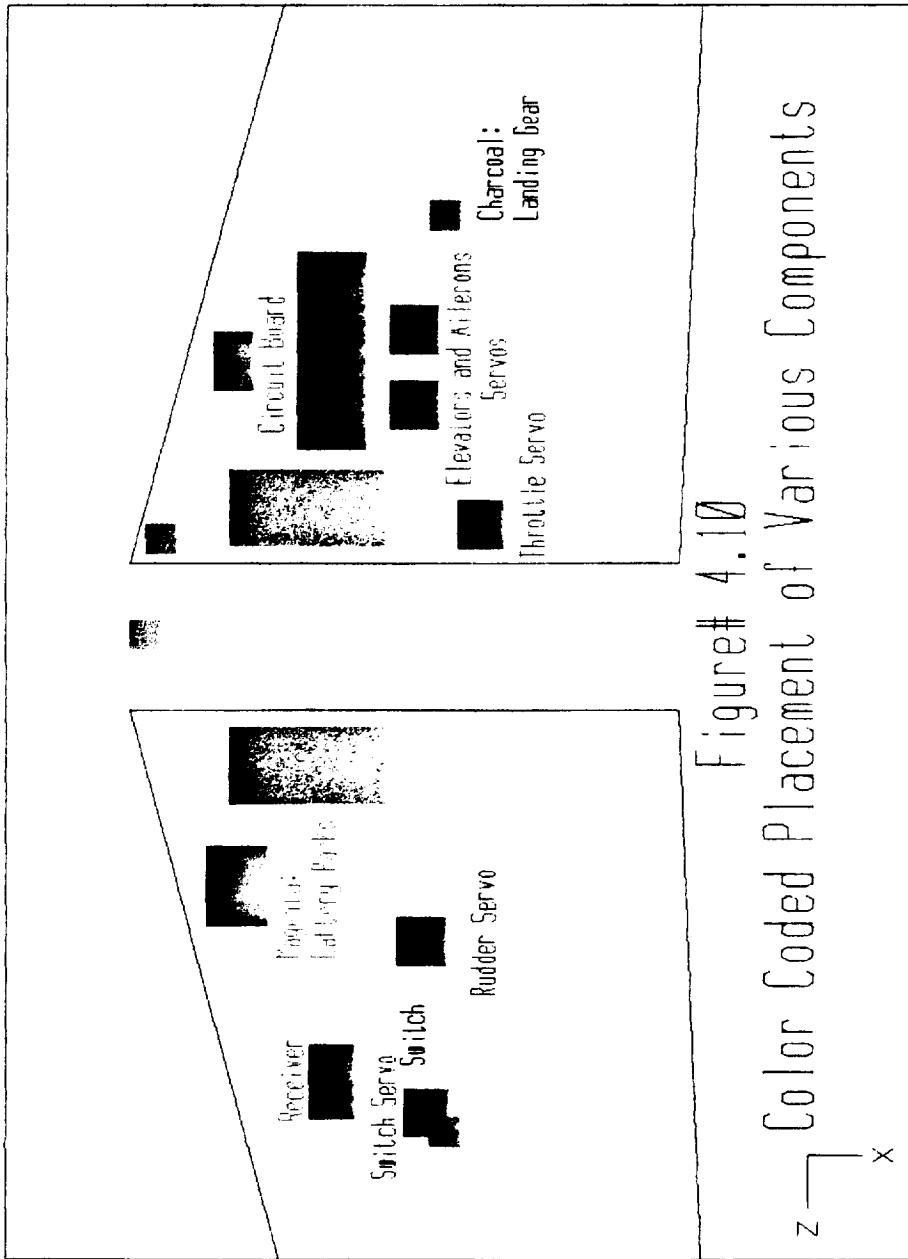


Figure 4.9 Electric Component Flowchart

- | | | |
|-----------------------------------|--------------------------|--------------------------|
| A. Differential Voltage Amplifier | E. Rudder Servo | J. ESS Battery Pack |
| B. Receiver | F. Throttle Servo | K. Op. Amp. (Gain = -1) |
| C. Elevator Servo | G. Switch Servo | L. StaticMaster |
| D. Aileron Servo | H. Switch | M. Servo Interface Board |
| | I. Receiver Battery Pack | |

This diagram represents the overall interaction between the servos, receiver, and the differential voltmeter, (DVA). A mechanical two channel switch, operated by a servo is employed here. When the switch is in its left position, the analog signal from the DVA travels first through a servo interface board, which converts the analog signal to a servo-compatible



Figure# 4.10

Color Coded Placement of Various Components

pulse-width signal. The signal then moves the control surfaces through the servos, automatically stabilizing the aircraft. When the switch is in its right position, a direct link exists between the servos and the receiver, so that the control surfaces can be displaced manually.

4.6 Component Placement - Planform

Two factors were kept in mind while the planform analysis was executed, center of gravity position and ease of wiring. The components and their appropriate weights can be seen in Table 4.3.

Table 4.3, Component Weights and Sizes

Component	Mass, lbm	Volume, in ³	Density, lbm/in ³
ESS Battery Pack	0.1647	2.4079	0.0684
Receiver Battery Pack	0.2093	3.0596	0.0684
Servos (A) ²	0.0664	1.1989	0.0554
Servos (B) ³	0.1106	1.9968	0.0554
Fuel Tank (Full)	0.6644	23.5590	0.0282
Receiver	0.0808	3.5459	0.0228
StaticMaster	0.0083	0.1709	0.0486
Switch	0.0245	0.8107	0.0302
Circuitboard	0.1909	10.9688	0.0174

ARIES was used to ensure that the center of gravity was 7.43 inches behind the front of the duct. Figure 4.10 displays the final overall planform of *Banshee '94*.

² Futaba Model FPS148

³ Futaba Model FPS3001

4.6 Conclusions

From the outset, the stability analysis was performed under the shadow of intrinsic instability. The static stability analysis proved that with the center of gravity placed at 7.43 inches behind the front of the duct, *Banshee '94* would be statically stable due to the $C_{m\alpha}$ vs α slope being negative. The dynamic stability analysis, as expected, showed that the deficiency of a horizontal tail would present a major design problem.

This plight was rectified through two pathways. First, sweeping back the wings was a simple measure which provided immediate stability in all three axes. Finally, placing an electrostatic stability system provided a more advanced system in which *Banshee '94* could be stabilized in both the roll and pitch axes.

As anticipated, our calculations showed that the wing would be inherently unstable along the pitch axis. sweep-back included. The electrostatic stability system has proven to be a working device and we fully expect it to be operational. Sweep-back along with the ESS will be welcome additions to our aircraft that will empower us with better control.

5. Propulsion System

5.1 Objective

In the process of designing *Banshee 94'* it was imperative to select a propulsion system which is suitable for the unique characteristics of a flying wing. As in all aircraft, there must be a light weight engine that will produce enough thrust suitable for runway take-offs and stable horizontal flight. In our circumstances the propulsion system should also conform to the shape of the wing to reduce drag and give the appearance of a flying wing (eliminate a fuselage). One of our desired factors was the ability to have excess power to recover from any flight difficulties.

5.2.1 Engine Selection

The engine selected for our task proved to meet the requirements expected for level flight and maneuverability. The engine selected was a single OS Max 91 VR-DF

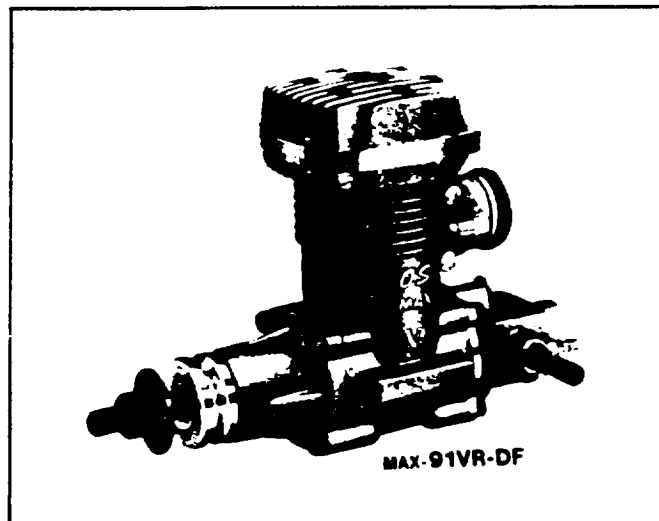


Figure 5.1 OS Max 91 VR-DF Engine

gas engine (figure 5.1), used in many high performance remote controlled aircraft.

Along with the OS Max 91, we selected a ducted fan instead of a propeller. The reason for this decision was to eliminate propeller wash and to best conform to the wings shape. The engine is positioned 4.5 inches from the center of gravity along the centerline of the aircraft.

5.2.2 Manufacture's Data

The OS Max 91 VR-DF Ducted Fan Gas Engine is a relatively new engine on the market. It is used in many remote controlled aircraft, such as F-16 and Sabers, to simulate jet engines. It is used for this task because it can be placed within the body of the aircraft and also because of the high exhaust velocities achieved by this engine.

The OS Max 91 engine is a two stroke gas engine made especially for ducted fan use. A ducted fan engine is designed differently from conventional propeller engines. Ducted fan engines perform at speeds of 22,000 RPM,¹² causing the engine to over heat during shorter periods of time than conventional engines. Because of this problem ducted fan engines are designed with large heat sinks to cool the engine at high RPM's. The OS Max 91 engine weights 25.77 ounces ¹² without the fan attached, and approximately 3.0 pounds with the entire assembly. The engine runs on a standard fuel for two stroke engines with 20% nitromethane and 20% lubricant. The high percentage of nitromethane enables the engine to run at high RPM's and enhances high performance abilities. This enhancement of performance gives the engine a total power output of 4.6 BHP and a static thrust of 14.0 lbs.¹² This engine surpasses the net power of the previous system and insures that there will be sufficient power to maneuver the aircraft.

5.3 Methods of Propulsion

Two main methods of propulsion were considered for the aircraft, propellers and ducted fans. Both methods are currently in use for remotely piloted aircraft, but propellers are extensively used while the ducted fans are just beginning to become accepted.

5.3.1 Propellers

Free propeller driven aircraft are the most widely used propulsion systems in the remotely piloted aircraft industry. Propeller engines are very reliable and take very little maintenance. The propeller can be easily mounted on to the driving shaft of the engine with a nose cone. The simplicity of the engine makes it useable for many aircraft.

There is one major disadvantage to the use of propellers on some aircraft. On all propeller engines there is a turbulent flow of air which is produced by the high speed rotation of the propeller, called propeller wash. Propeller wash originates from the engine and travels over the airfoil and past the control surfaces, mainly the elevators. The turbulent air over the elevators and ailerons makes the control of the aircraft difficult in many situations. Making the controls delayed or ineffective for a period of time. This lack of control is undesirable for a flying wing. Since a flying wing is an inherently unstable configuration, the lack of control would make the aircraft even more unstable. This undesired effect could possibly create an error in the performance of the elevators or ailerons, resulting in catastrophic consequences.

5.3.2 Ducted Fan

Ducted fan engines have only recently been accepted as a form of propulsion for remotely piloted aircraft. Ducted fan engines are primarily used in scaled jet aircraft with internal engines. The reason for their application in these aircraft is because of their ability to be mounted inside the frame of the aircraft.

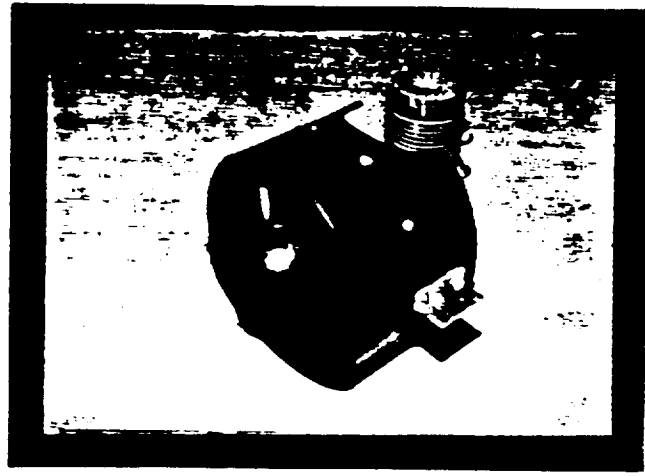


Figure 5.2 Ramtech Ducted fan Assembly

Ducted fan engines are high performance engines which run at high speeds and high temperatures. The high performance of the ducted fans makes them have a greater output than other two stroke propeller driven engine in its scale. One drawback is the fact that ducted fan engines are very sensitive due to their high performance, and have been known to overheat when not operated with the proper equipment.

Besides the possibility of overheating, the advantages over propeller driven engines pointed our team to work with a ducted fan. The Ducted Fan assembly being used with the OS Max 91 engine is made specifically for the OS Max 91. The fan unit is 5.25 inches in diameter with nine blades which substitute for a propeller. The nine fan blades rotate counter-clockwise and drive the flow of air into ten stator blades which directs the air to flow

parallel to the duct. The fan unit is mounted at the neck of the engine to the stator blades, and integrates itself to the engine to make an aerodynamic shape for parallel flow over the engines heat sinks. The assembly is mounted to the front of a 20 inch duct which passes through the center line of the aircraft. The entire assembly has a total weight of approximately 3.0 pounds and produces about 14 pounds of thrust. Giving more than adequate thrust for the purposes of our aircraft.

5.4 Single Engine

Last years flying wing design, The Elang, used two ducted fan engines. The engines used last year were the OS 25 Ducted Fan Gas Engines. These engines were placed 22 inches from the center line of the aircraft and 11 inches from the quarter chord. Each engine was predicted to produce 15.6 N (3.5 lbs) of thrust at static conditions. With the ducted fan attached, each engine assembly weighed approximately one pound and operated at a maximum speed of 22,000 RPM. Both engines received fuel from a central fuel tank located near the center of gravity of the aircraft. The central fuel tank was a 12 oz fuel tank, giving the approximate flight time of 10 minutes. The twin engine system was difficult to operate. In many cases, it was very difficult to run the engines at equal thrust levels. These conditions resulted in yaw and control problems.

As a result the current propulsion team decided to utilize a higher horsepower single engine. A single engine will eliminate the possibility of these problems reoccurring. It will also be simpler to adjust to the engine during preparations and flight tests. The possibility of unequal thrust will be eliminated with only one power source. The fuel mixture can be easily

adjusted by the needle valve to regulate the maximum power and fuel consumption.

5.5 Location

One of the major factors in the design is the location of the propulsion assembly. The engine is the heaviest object on the aircraft, and has the largest effect on the center of gravity of the aircraft. After determining the correct location of the center of gravity, the internal control components and fuel tanks can be placed accordingly. Then the engine can be placed to counteract the moments of the internal components. After placement of the internal components the engine assembly was placed 4.5 inches away from the center of gravity. This location is only several inches in front of the leading edge of the airfoil, and makes the duct of the airplane 20 inches in length.

5.6 Fuel System

The fuel system is composed of two 12 ounce tanks located on both sides of the duct. Twelve ounces of fuel will give the *Banshee 94'* an estimated engine running time of 20 minutes. This will give the aircraft adequate time to start the engine, taxi, and fly, without concerning about the amount of fuel remaining. The fuel tanks were placed on opposite sides of the center of gravity of the airplane. The positioning of the tanks is critical because they are the second heaviest internal component, and because of their unstable center of gravity. If the fuel tanks are not positioned correctly there is the possibility of reducing the stability of the aircraft. The fuel tanks are connected to the engine by a series of tubing which passes through the duct and attaches to a Y-connection on the left side of the duct, and then proceeds

to the engine inlet. This configuration enables the engine to draw from both tanks simultaneously. Both tanks will not need to be pressurized from an exhaust tube because the engine already produces an appropriate vacuum to draw the fuel.

5.7 Engine Type

The current engine was selected after a series of experiments using similar engines of lower power outputs. The engines were tested in the WPI wind tunnel to determine the effects of varying wind velocities on engine output.

In order to record the data from the experiments, several input devices were utilized to determine the variables, thrust, wind velocity, torque, and RPM. The constants of the tests were temperature, pressure, and fuel mixture. The input devices consisted of a strain gages, the wind tunnel pressure gages, and photocell tachometer or a fiber optic sensor. The engines were mounted on an aluminum mount. The mount was made of an aluminum rod which was attached to the engine and secured by a stand. The rod was attached to a flexible bar containing two pairs of strain gages to measure the thrust and torque of the engine. Each pair of the strain gages were connected to voltage meters which amplified the signal in to useful data. The thrust gage was calibrated before the experiments. A linear relationship between voltage and thrust was determined. The wind tunnel pressure gage was used to determine the freestream velocity during the experiment. The photocell tachometer and fiber optic sensor were used to measure engine RPM's during engine testing to determine when the engine is running at maximum power.

The tests were conducted on two engines available to the propulsion team. The

engines were, the OS 61 propeller engine and the OS 25 ducted fan. Each engine, running at max power, was tested at wind tunnel speeds from 0 to 100 mph. A resulting Thrust vs. Freestream Velocity plot was determined for each engine. The OS 61 engine had a maximum thrust of 5.5 lbs, which is slightly lower than the manufactures data of 6.0 lbs. The OS 25 ducted fan engine test resulted in 2.0 lbs of thrust, which was lower than the manufactures data of 3.5 lbs. The resulting curves of each engine proved to be very similar in shape. The experimental results were then scaled up to the current engines performance level using a maximum thrust of 14 lbs given by the manufactures data for the OS Max 91 VR-DF ducted fan engine.

In many cases the manufactures data is greater than the actual output of the engine. The output of the engine can fluxuate due to an improper mixture of air to fuel ratio or improper fuel choice. In the case of a improper air to fuel ratio, it takes practice to realize when the engine is working at its maximum RPM. Even though these mistakes may be corrected, the manufactures data may still not be accurate. For this reason the propulsion team calculated the thrust output of the engine at several engine speeds, 100% (22,000 RPM), 75% (16,500 RPM), 50% (11,000 RPM), and 25% (5500 RPM). The major assumption made for these calculations is that the engines have similar properties and react similarly to the change in velocity.

The first calculation was taken at one quarter (5,500 RPM) the power output of the engine. The purpose for this calculation is to verify the cruise velocity of the flying wing. During flight the engine will not be running a full throttle, but at about 25% to 30% its maximum output. This will ensure a reasonable cruise velocity which corresponds to the

figures calculated by the aerodynamics team.

The second series of experiments determined the thrust at half throttle (11,000 RPM). The main purpose of this calculation was to see the engine output at normal flying conditions, because a large percentage of the flight time will be within these limits.

The third experiment was taken at 75% output (16,500 RPM). This was to see the engines abilities during climbs and aerial maneuvers. The fourth calculation was taken at full throttle. These experiments to made to see the performance of the engine at the manufactures maximum thrust data.

Plans for tests on the current engine are now in progress. These tests were delayed because the current stand was not sufficient to handle the OS Max 91 engine's increased weight and power. The experiment will be run in a similar manner as the smaller engine tests were conducted. The proposed tests will coincide with the calculations previously taken, by performing the tests at 100%, 75%, 50% and 25% power.

The results from the engine testing and calculations can be seen in the Thrust - Drag vs. Velocity plot in figure 5.3.

At the intersection of the drag curve and the 25% thrust curve is the cruise velocity of the aircraft. The cruise velocity of the *Banshee 94'*, through the engine testing, has been estimated at 35 mph. The maximum velocity, assuming the manufactures data is accurate, is estimated at 93 mph. The maximum velocity at 75% power during horizontal flight is estimated at 76 mph.

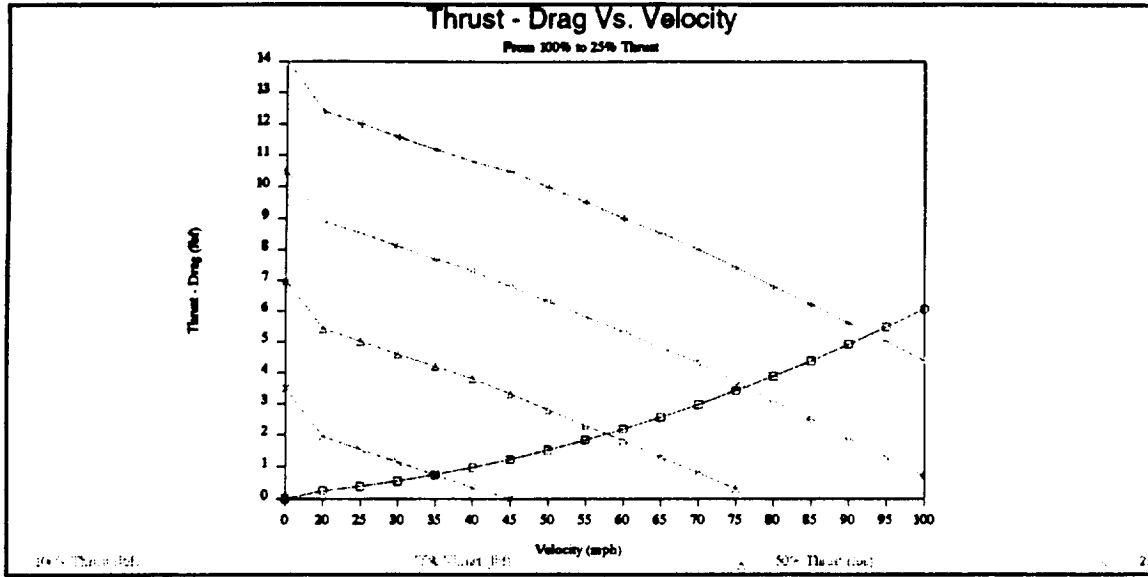


Figure 5.3 Thrust - Drag vs. Velocity

5.8 Excess Power

After reviewing the results of the current engines predicted performance, it is easy to notice the excess power delivered by the engine. One of the factors considered when choosing the OS Max 91 ducted fan engine was the ability to use extra thrust when needed. The extra thrust could be used for a variety of reasons.

When taking off from a static position, it is necessary to have a greater velocity than required for cruise conditions. Therefore cruise conditions can not be the maximum thrust of the engine, but only a small percentage of the available power. Take-off velocities are not significantly larger than cruise velocities, but the excess power is required in several other areas.

An additional need for power is required in the rate of climb of the aircraft. If a engine is selected to perform at only cruise velocity, the aircraft will not be able to climb. The greater the engines power the faster and higher an aircraft can climb. When selecting an

engine for the *Banshee 94'*, a main concern was the flight performance. We wished to give the pilot less limitations on the planes capabilities, and more room for error. This was another reason for extra power. If the pilot was to make an error in judgement, he would have greater chance to compensate for his mistake if there is more power available. The additional power would also allow the pilot to perform a larger array of aerial maneuvers.

Excess power was not only considered for flight conditions, but to compensate for errors in calculations. To compensate for the possibility of errors the designer must use a material or power source which is greater than the calculations limitations. Some of the possible errors in the *Banshee 94'* may have occurred in the assumptions made for the drag of the flying wing. There is also a large possibility of an error in the manufactures data on the maximum power output of the OS Max 91 engine. The engine must also compensate for unpredicted weight not estimated in the original design.

One additional factor not noticed in the early stages of design were the carbon fiber rod, used to connect the wings and as spars, and the control rods passing through the duct. These objects pass through the duct and partially block the air flow produced by the fan unit. This problem is solved by creating a symmetric airfoil shell which will contain the control rods and carbon fiber rods. The shell will be placed in the duct over the areas of interest to reduce the blockage and to make an easy transition for the airflow.

5.9 Rate of climb

As discussed previously, the rate of climb of the aircraft was one of the major reasons for utilizing an engine with excess power. From the test data the propulsion

group was able to make calculations on the rate of climb at various power outputs and velocities. These equation used to predict the rate of climb of the aircraft was

$$RC = \text{Climb rate} \quad T = \text{Thrust} \quad V = \text{Velocity} \quad W = \text{Weight} \quad D = \text{Drag}$$

$$RC = 60 * \frac{(TV-DV)}{W}$$

The results formed a plot of climb rate vs. velocity for power outputs of 75% and 50%, as shown in figure 5.4.

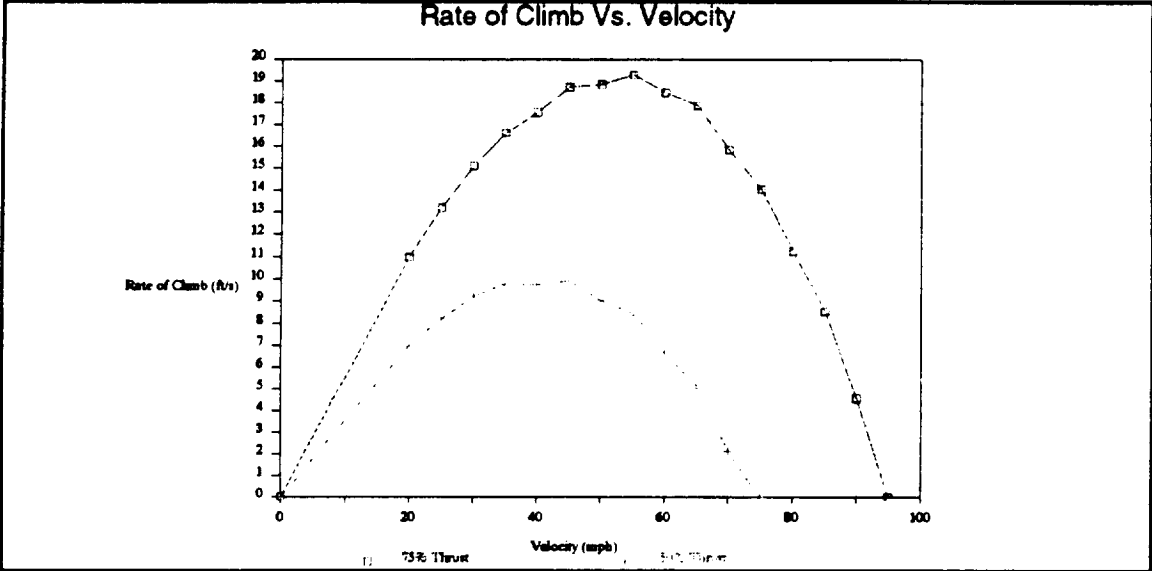


Figure 5.4 Climb Rate vs. Velocity

The maximum rate of climb with 75% thrust is 19 ft/s at 55 mph.

5.10 Equations

Other calculations which resulted from the Thrust - Drag vs. Velocity plot were, lift-

off velocity, lift-off distance, and landing distance. The lift-off velocity estimates the speed at which the aircraft is able to take off with a 4 degree angle of attack and without using the elevator control surfaces.

$$p = \text{density} \quad W = \text{Weight} \quad C_l = \text{Coefficient of lift}$$

$$S = \text{Surface Area} \quad V_s = \text{stall speed}$$

Lift-off Velocity

$$V_{lo} = 1.2 V_s = 1.2 * \sqrt{\frac{2W}{\rho S C_l}}$$

$$V_{lo} = 56.2 \text{ ft/s} = 38.81 \text{ mph}$$

As discussed before the lift-off velocity is slightly greater than the cruise velocity of 33 mph.

The lift-off distance was also determined using the same assumptions of a 4 degree angle of attack and without the use of elevator surfaces.

$$T = \text{Thrust} \quad D = \text{Drag} \quad g = \text{gravity}$$

Lift-off Distance

$$D_{lo} = 1.44 \frac{2W}{\rho S C_l \frac{2(T-D)}{Wg}}$$

Thrust at 75%

$$D_{lo} = 64.59 \text{ ft}$$

The estimated landing distance is predicted using a velocity at fifty feet of 40 mph and a landing velocity of 35 mph.

$$V_{50}^2 = \text{Velocity at 50 ft} \quad V_L = \text{Landing Velocity} \quad a = \text{acceleration}$$

$$D_{decel} = \frac{V_{50}^2}{2a} - \frac{V_L^2}{2a}$$

$$D_{decel} = 59.83 \text{ ft}$$

5.11 Conclusion

After considering the needs of the *Banshee 94'*, a light weight, high power, single engine with a adequate rate of climb, stable flight, and reasonable running time. The propulsion team decided upon the OS Max 91 DF-VR Ducted Fan Engine. The OS Max 91 engine satisfies the needs of the *Banshee 94'*, and leaves room flight or design changes. The OS Max 91 engine was also purchased to provide for next years Advanced Aerodynamics Design project, expecting that they will not increase the design parameters significantly. The engine meets the expectations of the current Advanced Aerodynamics Design group and will hopefully continue to meet the expectations of future design groups.

6. Structures

6.1. Introduction:

The structures group, working with the Aerodynamic group, the Control group and the Propulsion group surmounts the problems of maintaining the structural integrity of Banshee '94. The structures group is responsible for the structural integrity of the aircraft. The structural integrity has to be accomplished with the lightest possible weight since any excess weight has a detrimental effect upon the aircraft performance. Another responsibility of the group is to determine the geometric shape of the structures, the mechanical loads, the deformations acting through the structural boundary, and the material make-up of the structure. The deformations have also to be determined to assure that there is no excessive displacement existing in the structure, since a large deflection may make the plane stall and become unstable. The structures group analyses on stress not only to determine the kind of material to use, the appropriate thickness, the size and the cross sectional shape of the plane, but also to assist in designing of connections for all parts of the aircraft. Ultimately, the group is to determine the best structural arrangement for items such as power plants, built in fuel tanks, and landing gear, and to respond to the important requirement of the structural design safety with light weight.

In order to accomplish these tasks, as well as to obtain a detailed analysis for a given aircraft structure, the structures group uses two different Finite Element packages I-Deas and MSC/Nastran. The structures group used simple analytical methods for confirming the results from the Nastran Program; especially with regard to the displacement (or deformation) of the wing. In addition, the structures group conducted experimental tests on test beam section made of PVC foam covered on both top and bottom with Kevlar. This section was tested to failure; the data obtained was compared against the values given by the FEM codes.

6.2. Material selection:

For construction materials, there are two basic categories; conventional construction, and composite construction. Conventional construction (balsa wood, aluminum etc...) can lead to time consuming fabrication when applied to a complex wing shape. They are also brittle in nature, and damage easily if not handled with care. Composite construction, however, can afford great strength, and needs little attention for proper maintenance. Comparing these two factors, we decided that a composite structure of a face sheet, or "skin", laminated to a foam "core" would provide the best strength to weight ratio as well as the desired durability for the aircraft.

In the early 1960's, the emergence of boron filaments started a new generation of composites. Composites with modulus continuous filaments like boron and graphite are referred to as advanced composites. This remarkable class of material has had a profound impact on airframe design technology. An advanced composite material is defined as a material consisting of small-diameter, high strength, high modulus (or stiffness) fibers, which is embedded in an essentially homogeneous matrix. This makes the material anisotropic, since such materials have mechanical and physical properties that vary with direction. In addition to advanced composite materials such as Kevlar, and new matrix materials including polyimide, thermoplastics, and even metals such as aluminum, titanium, and nickel are also used. Using the properties of composite materials, the weight is reduced by 30%. Even though the resulting structures are more expensive than their metal counterparts, the composite materials are still ideal for the structural applications because of their important properties; high strength-to-weight and stiffness-to-weight ratios. Among the new materials, Kevlar has been chosen for the "Banshee 94".

6.2.1. Kevlar:

Kevlar Aramid is an aromatic organic compound of carbon, hydrogen, oxygen, and nitrogen, and is produced by spinning long-chained polyamide polymers. With its material properties of low density, and high tensile strength, and low-cost, Kevlar produces tough and impact-resistant structure; however, the compressive properties of Kevlar laminates are low, due to poor coupling of resin matrices to the aramid fibers. If compared to other organic fibers, the aromatic polyamide fibers of Kevlar, are characterized by their high tensile strength and high modulus.

There are two different types of Kevlar-- Kevlar 29 and Kevlar 49. Out of the myriad of numbers of fiber materials that exist today, we chose a Kevlar type 49 weave for the majority of the wing construction primarily for its high strength and low weight. It was also chosen for its failure quality. Kevlar does not bond directly to the resin matrix. This allows for the fiber to deform, yet still hold and maintain some structural integrity, in the case of an isolated impact. Other fibers will bond directly to the resin, causing the overall material to be brittle. In the same scenario these materials, if they fail, would fail catastrophically and shatter, leaving the aircraft structurally compromised. Moreover, Kevlar 49 aramid fiber is preferred for the Banshee '94 structural design because it is characterized by low density, high tensile strength and modulus. It is used in high-performance composite applications where light weight, high strength and stiffness, vibration damping, and resistance to damage, fatigue, and stress rupture are the main properties. If Kevlar 49 is applied for reinforcement, the reinforced composites can save up to 40% of the weight of glass fiber composites at the same stiffness.

The stress-strain behavior of Kevlar 49 is linear to ultimate failure in tension at 340 kips/in² and 1.8% elongation. Usable strength of Kevlar 49 reinforced epoxy is about 4 times of 7075-T6 aluminum at less than half the density. In addition, Kevlar 49

on a pound-for-pound basis is five times as strong as steel. The Figures 6.1a & 6.1b illustrates tensile stress/strain curves for tensile loading.¹¹

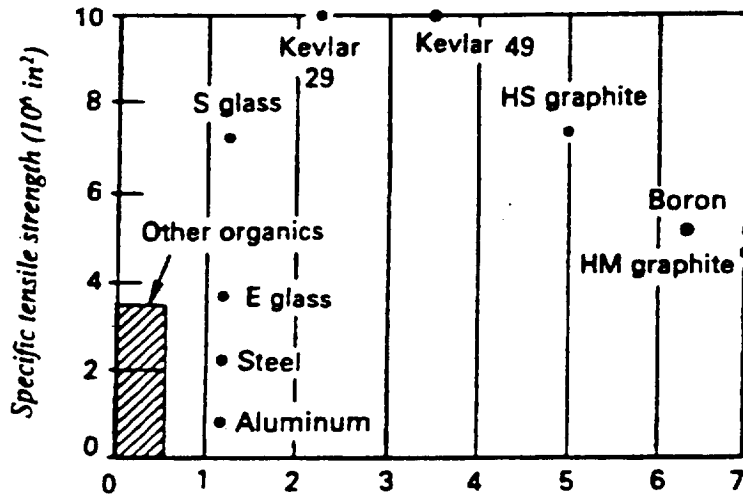


Figure 6.1a Specific tensile modulus. 10^6 in^2

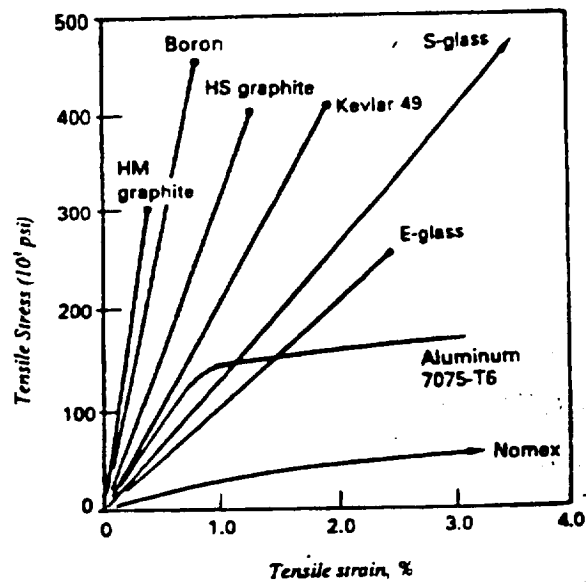


Figure 6.1b Stress and strain curves of various fibers/epoxy.

(Reproduced from Airframe Structural Analysis, by Michael C. Y. Niu)

Kevlar 49 is nonconductive and exhibits no galvanic reaction in contact with metal. In addition it can be combined with glass or graphite in hybrid composites to take advantage of the unique properties of each fiber.

Epoxy resins are used to reinforce Kevlar. Their high adhesion makes them useful in many high-performance applications in aircraft industry. Epoxy resins have also excellent water resistance and low shrinkage during cure or vacuum bagging (about 3%). Their conductive properties offer good fiber-matrix adhesion.

However, Kevlar does not cut well after it has been treated with a resin matrix. When cut, it has a tendency to fray, and the edge will look somewhat like a shag carpet. This would make it hard to cut the trailing edges of the control surfaces, which is done once the surface have been completed. For these reasons, we have also decided to use carbon fiber in designated areas of the craft

6.2.2. Carbon Fiber:

The carbon fiber was also applied to areas where high strength was needed. Since the area around the components in the upper surface have holes in them for access, it was decided that a layer of carbon fiber would be used around the holes to regain some of the strength lost. The duct was also made of carbon since it would have no foam for support and rigidity.

To further the strength in the duct, joint, and component areas, two carbon fiber spars were inserted through these areas. These extend to both rear landing gear placements to add support for their mountings.

6.2.3. PVC Foam Core:

The composite skin was built on a foam core. The purpose of this core is to act as a cushioning medium, to withstand the majority of the shear forces, and add to the rigidity of the wing.

There are two types of foam commonly used in composite structures: Polystyrene foams and polyvinyl chloride (PVC) foams. For the "Banshee 94", we opted to use the PVC foams for many reasons. First, PVC is much stronger than polystyrene. The foam has excellent tension, compression, and shear strengths that vary with the chosen density of foam. This reduces the load that the skin is required to support, and allows for fewer skin layers increasing strength. Another reason is its compatibility with composite skins. It has better adhesion qualities with resins for a superior bond and stress communication. PVC foams do not melt with resins, thus allowing good control of the wing shape. Due to the PVCs' closed cell construction, the resin cannot permeate the foam, causing undesired weight, and thus maintaining a uniform density. Lastly, PVC is easy to work with. It can be hot wired and sanded to shape without crumbling. For the Banshee '94, we chose the Klegecell, type 45, 3 lb. PVC. We felt that this foam would be the lightest while maintaining the wings strength and rigidity with only one skin layer.

6.3 Methods of analysis:

Today, there are many finite element methods which permit the efficient application of stress analysis :

- a) Abaqus and Ansys are used for non-linear dynamics. While good for anisotropic materials, but they are poor for composites
- b) Argus is an excellent method for analyzing composites, non-linear post buckling and vax.

- c) I-Deas is a graphical method of analysis.
- d) Nisa is good for doing an analysis on composite and vax.
- e) Msc/Natran is excellent for structural analysis, but poor for some non-linear structures¹.

The structure groups chose the graphical method I-DEAS and the structural method of analysis, Msc/Nastran.

6.3.1. I-DEAS CODE:

I-Deas is a finite element modeling code produced by Structural Dynamics Research Corporation. To run the program, one needs a CAD drawing of the object to be analyzed. After this the object has to be broken down to the desired number of nodes, or elements. The properties of the materials to be analyzed are then entered the code in the form of elastic, and shear modulus. The third step is to enter the forces and restraints to be applied to the model. The results are displayed graphically with different colors representing different stress, strain, or deflection ranges.

For our wing, we decided to break the wing into four elements in the chord-wise direction, and twenty three elements along the span. Since I-DEAS is not programmed to handle the complexities of composite structures, we were forced to make a number of assumptions. First, since I-DEAS models a shell with an arbitrary thickness, or as a solid, we chose the model our wing as a shell. The maximum thickness of the wing lies on the borderline between the definition of a solid and shell. Since our main structural component, the Kevlar skin, is a thin sheet on either side of the wing, we felt that the shell with arbitrary thickness would give the best results. This would also cause the program to over estimate the stress, allowing for a worst case scenario.

Since the model can be made of only one material for use of I-DEAS, our composite had to be converted to a single "material" to enter the material properties. Since the calculation for the ratio for Young's Modulus of the foam and Kevlas proved to be small, it was felt that the elastic modulus of the PVC could be neglected. However, for the shear modulus, the values for the PVC were entered since it was believed that it would be supporting the majority of these stresses.

Finally, the forces for level flight cruise conditions were applied to the model. The vertical loading was the resultant forces from the elliptical lift distribution, component weight, the weight of the wing, and the winglet at the tip combined. A graph of this load is shown in Figure 6.2. The drag loading was given by the Aerodynamic group, and is shown in Figure 6.3. The moment of 10 ft-lbs., applied at the quarter chord, was given by the Control group. Finally, the wing root was restrained in all three axis and restrained from rotation. A diagram of all forces applied to the wing can be seen in Figure 6.4.

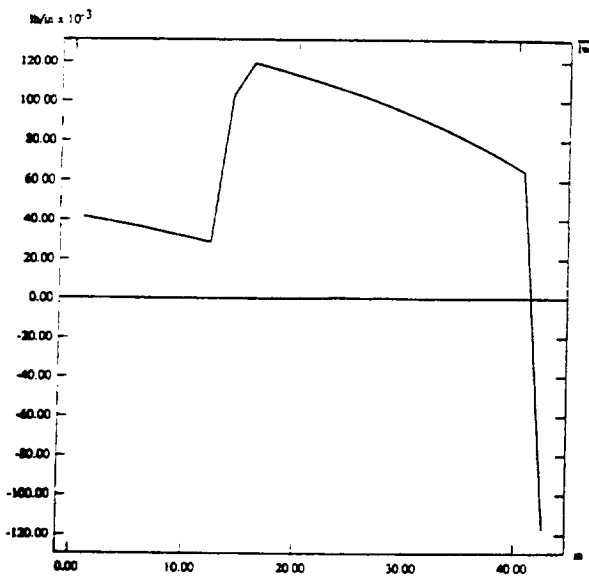


Figure 6.2: Lift-Weight Loading

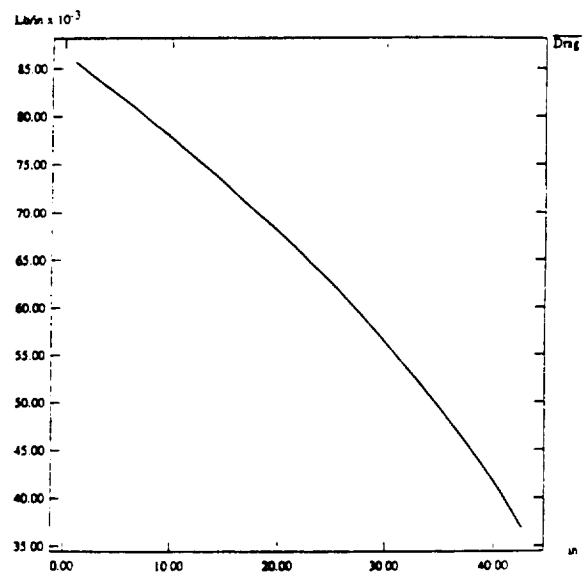


Figure 6.3: Drag Loading

After running the program, the results were printed. The readings for XY plane, Von Mises, and maximum principal stresses can be seen in Figures 6.5 and 6.6. The maximum stress occurs in the Von Mises diagram which, in short, is the total of all stresses occurring at a given point. This maximum value of 1.195 KSI falls well within the 238 KSI of the Kevlar skin. The diagram of the deflection, exaggerated in Figure 6.7, shows a maximum deflection as being almost two thousandths of an inch. We felt that these values are acceptable for confirming the soundness of the structure.

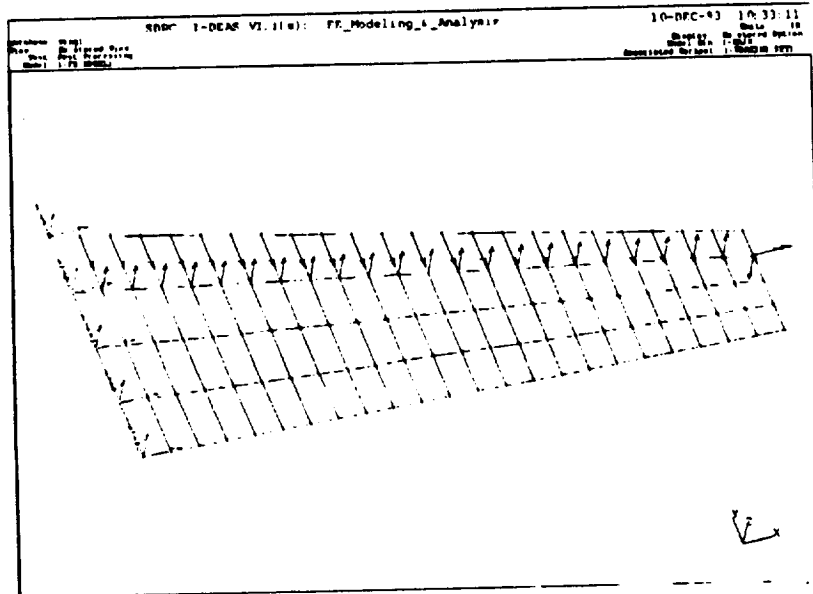


Figure 6.4: Load Forces Applied to Wing in I-Deas

Incabase: wing1
 View: No stored View
 Task: Post Processing
 Model: 1-FE MODEL1

SDRC I-DEAS V6.i(s): FE_Modeling_6_Analysis

10-DEC-93 10:28:26
 Units: IN
 Display: No stored Option
 Model Bin: 1-MAIN
 Associated Workset: 1-WORKING.SET1

wing1

LOAD SET: 8 - COMBO
 FRAME OF REF: GLOBAL
 STRESS - XY MIN: 66.71 MAX: 113.62

SHELL SURFACE: TOP

113.62
87.86
62.10
36.33
10.57
-15.19
-40.95
66.71

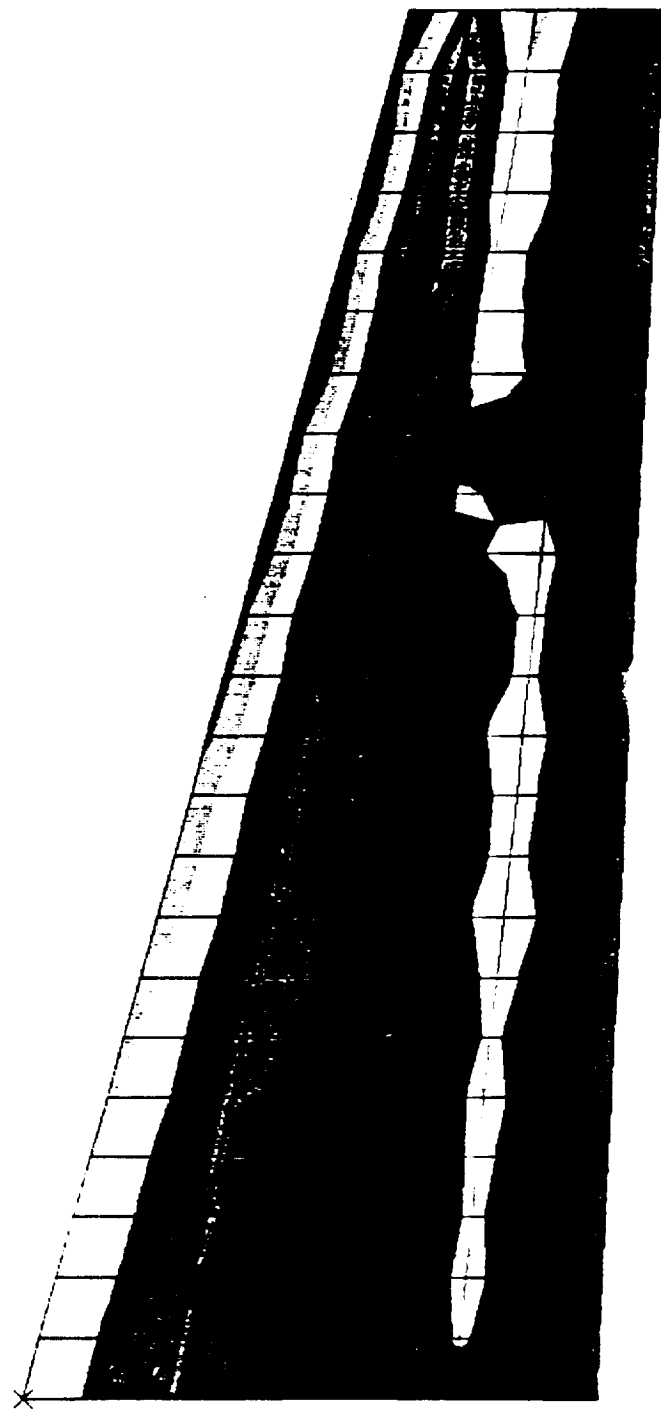
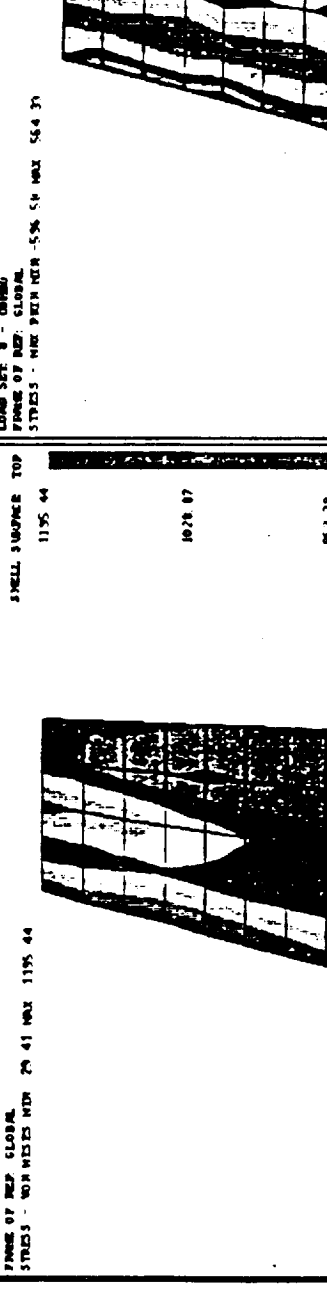


Figure 6.5: Stresses in the X-Y Plane

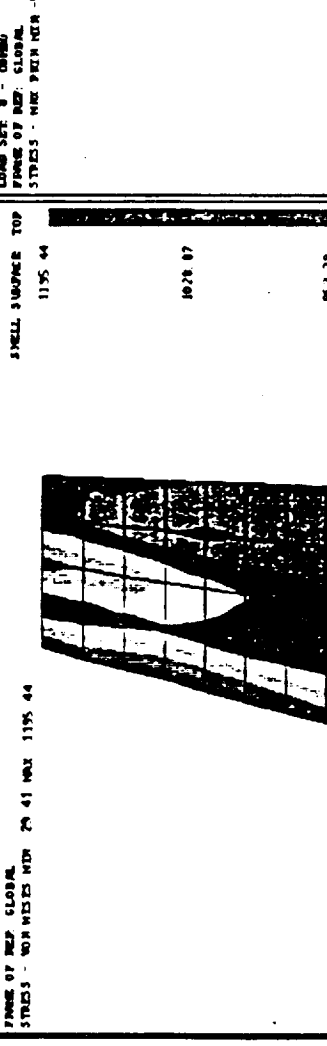
SDRC I-DEAS VI.i(s): FE_Modeling_&_Analysis
 10-DEC-93 10:31:27
 Unit: mm, mm
 Model Bin: I-MAILM
 Display: none, none
 Associated Worksheet: I-WORKING SET1

Unitbase: wing1
 View: none, none
 Task: Post Processing
 Model: I-FE MODEL1

LOAD SET: 8 - OTHER
 FRAME OF REF: GLOBAL
 STRESS: Von Mises MID: 29.41 MAX: 1135.44



LOAD SET: 8 - OTHER
 FRAME OF REF: GLOBAL
 STRESS: Max PRIN FOR: 55% 54 MAX: 564.37



Von-Mises Stresses

Maximum Principle stresses

Figure 6.6: Von-Mises and Maximum Principle Stresses

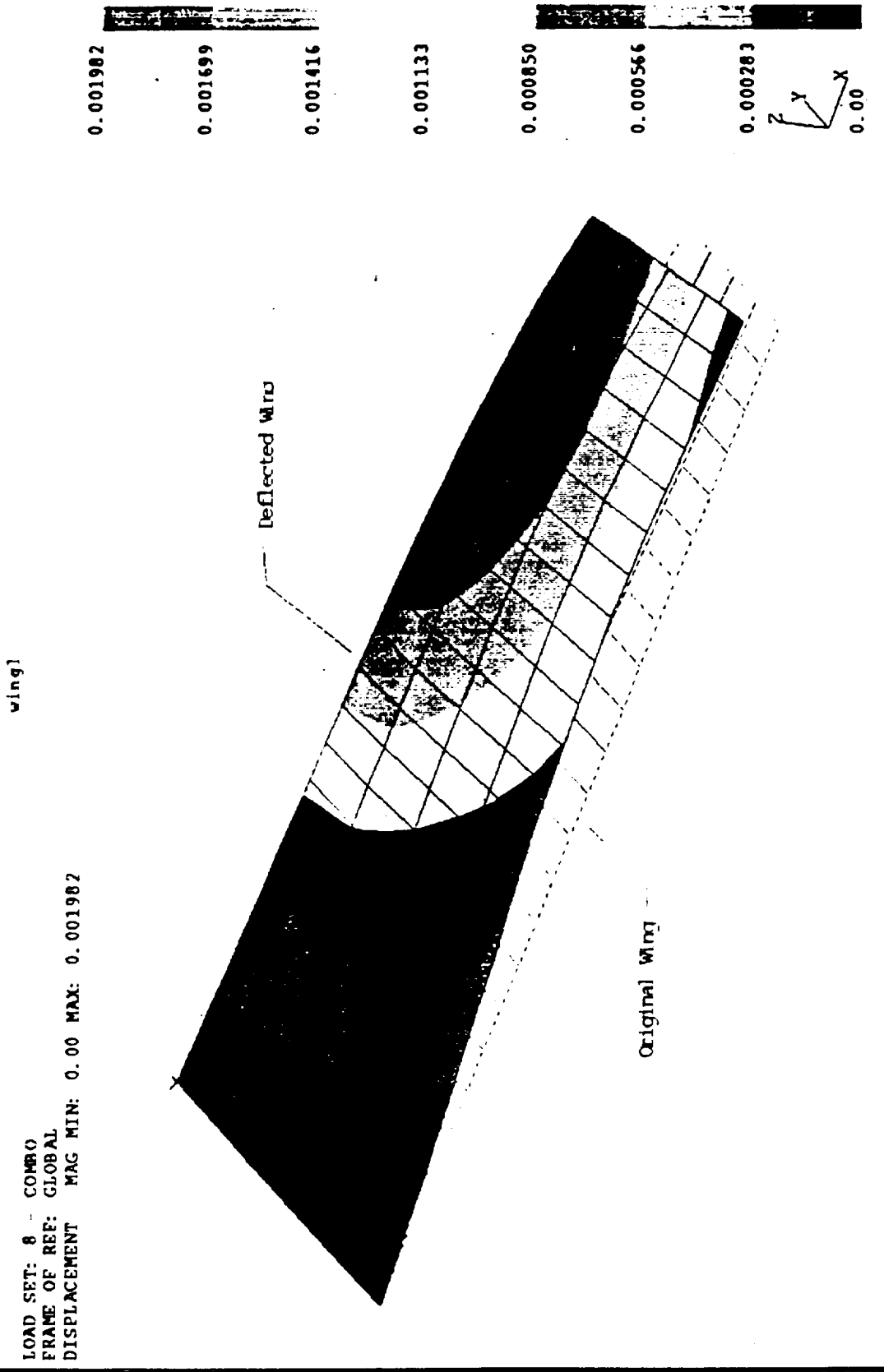


Figure 6.7: Wing Deflection

6.3.2 Msc/Nastran Code:

Msc/Nastran is a new analysis technique which generates a data file for one of the four types of problems³.

- a) Plane stress analysis (Using CQUAD4 OR CQUAD8 elements).
- b) Beam (Using bar elements).
- c) Plate (Using CQUAD4 elements).
- d) Solid (Using CHEXA elements).

Msc/Nastran uses a Finite Element Structural model, wherein the distributed physical properties of a structure are represented by a finite number of structure elements, which are interconnected at a finite number of grid points. Loads are applied to grid points and for which displacement are calculated. With the specific assumptions, the procedures for defining and loading a structural model for "Banshee'94", are generated through eight steps. (see Appendix D1.)

1. Executive control deck- problem identification
2. Case control deck - title (Winfem Nastran Output, page1)
3. Grid point definition - Grid point identifications and coordinates (pages 3 to 6)
4. Grid point constraints - Grid point identifications and constraint codes (p.3 to 6)
5. Elements - Elements identifications, property identifications ,and grid point connectives (pages 3 to 6)
6. Properties - Material identifications and thickness (or section properties , if required) (pages 3 to 6)
7. Material - Young Modulus, Poison ratio (pages 3 to 6)

8. Load grid point identifications and Cartesian components of forces (p. 3to 6)

In comparing the results from Msc/Nastran to those from the I-Deas code, we find that the differences are great. The Maximum Principal Stress for Msc/Nastran and I-Deas respectively, at the point of maximum value for I-Deas, is 3.983 lb/in² and 564.33 lb/in². For the shear in the X-Y they are 0.0436 lb/in² and 113.62 lb/in². Finally, for the Von-Mises Stresses, we have 2.766 lb/in² and 1195 lb/in². The large differences in these values suggest that the different assumptions have a great impact on the results of these codes. From these numbers we can also find that the I-Deas values may be higher than they should be. To further investigate this, we performed an experimental test with a beam section.

6.3.3 Experimental Analysis:

To check whether the assumptions used for the FEM codes were correct, it was decided to compare the strains and deflection of a composite test specimen with the data obtained of a computer simulation of the same specimen. The specimen was cantilever beam 20 inches long, 2 inches thick, and 1 inch wide. It was made of foam core with a layer of Kevlar laminated to the top and bottom surfaces. At the fixed end of this beam where the maximum strain would occur, a strain gauge was affixed. Weight between zero to fifteen pounds were then hung from the free end, and the strain was measured with 15% experimental error (Fig 6.8). The deflection was also measured, and found to be near zero until the specimen failed. The test beam withstood approximately 13.5 lbs before failing. Upon failure, the lower surface Kevlar buckled, and the beam suffered massive deformation. The beam was then simulated with the FEM codes and assumptions used for

the wing. All forces were applied, including the distributed weight of the beam itself. The results are shown in Figure 6.9. From this, we can conclude that the I-Deas codes are a worst case scenario.

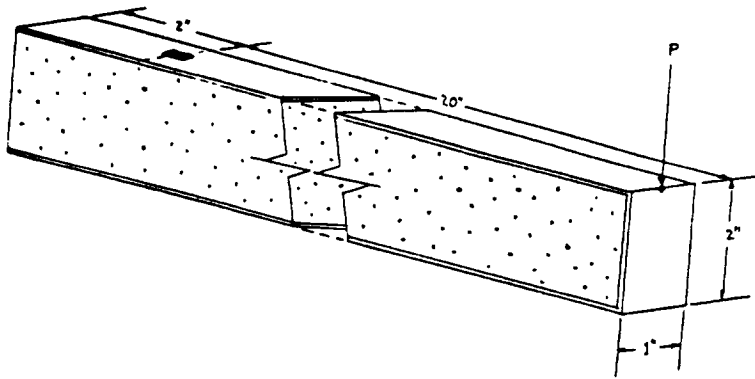


Figure 6.8: Test Beam Dimensions

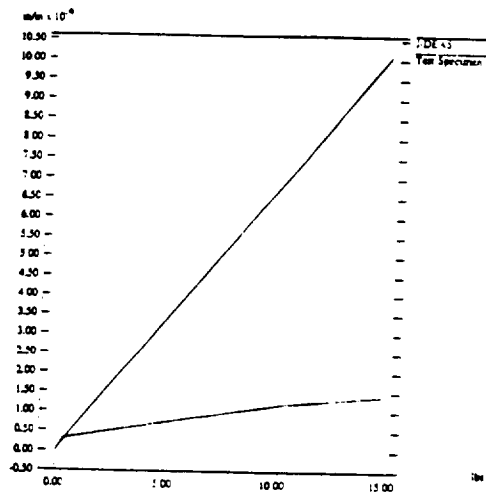


Figure 6.9: Comparison of Test and I-Deas Data

6.3.4 Comparison of analytical methods with Msc/Nastran

6.3.4.1. Weight/Strength

Minimizing the weight of the aircraft has been a major consideration in the present design. This led to the use of composite materials such as PVC, Kevlar, and Graphite, as well as new types of structures such as a geometrical block wing containing all loads.

From the design point of view, with a given loading systems and the limitations on the outside dimensions (geometry) of the structure (if such limitations exist), a designer can figure out the optimum configuration of the internal structure. The loading system may include all the requirements as to breaking strength, deflection, fatigue etc....

In determining the optimum design, the most important loading criterion is the ultimate strength. Stiffness may also be required to modify the optimum structure and in some cases, may be very important as to outweigh strength completely. Because of the importance of providing adequate strength at minimum weight, it has become customary to evaluate materials and structures via their strength/weight ratios.

A strength/weight factor can be obtained by dividing the ultimate tensile strength of material by its density ²:

$$\text{Strength/Weight} = \sigma_u \div \rho = (\sigma \times F.S) \div \rho \quad (\text{equation 6.1 a})$$

$$\text{Strength/Weight} = (p \times F.S) \div (A \times \rho) \quad (\text{equation 6.1 b})$$

where

σ_u : Ultimate tensile strength

ρ : Density

F.S : Factor of Safety

p : Normal Force

A : Area

Such a factor has the dimension of length. It represents the length of vertical member, of a uniform section, at which the material fail in tension under its own weights. Moreover, the factor is considered as the limit of maximum displacement at which the materials can withstand (Appendix D2)

$$\text{Factor (Strength/Weight) PVC} = 1.52 \text{ inches}$$

$$\text{Factor (Strength/Weight) PVC+Kevlar} = 1.60 \text{ inches}$$

6.3.4.2. Check Shear Stress and Bending Moments

An additional method for checking shear stress and bending moments along the spanwise and the chordwise is based on the total area of the given geometrical tapered wing. The total area of the whole wing (565.57 in^2) is considered as a total load, which is assumed acting on the half wing in the Z direction and through the aerodynamic center of the airfoil section, and which is distributed along spanwise (see Appendix D3).

6.3.4.3. Section Properties of the Composite Materials

PVC foam "Q45" is considered as a homogeneous material with its Young Modulus (E), being a constant value. However, the flexural rigidity which is defined as a product of a Young Modulus and the Moment of Inertia of each section (EI), varies along the beam of varying its thickness. In the case the wing is treated as a beam, the product EI takes an important role in analysis of deflection due to bending and torsion, therefore, the flexural rigidity must be calculated and their results are

1 For PVC foam only:

$$EI_{(E329)} = 922480 \text{ lbin}^2 \quad EI_{(E327)} = 330174 \text{ lbin}^2$$

$$EI_{(E328)} = 512193 \text{ lbin}^2 \quad EI_{(E326)} = 150195 \text{ lbin}^2$$

$$EI_{(E325)} = 42279 \text{ lbin}^2$$

The procedure of flexural rigidity calculation is described and shown in the Appendix D4.

2 For the composites of PVC foam and Kevlar:

$$EI_{(E329)} = 4460000 \text{ lbin}^2 \quad EI_{(E327)} = 2050000 \text{ lbin}^2$$

$$EI_{(E328)} = 3240000 \text{ lbin}^2 \quad EI_{(E326)} = 1180000 \text{ lbin}^2$$

$$EI_{(E325)} = 360000 \text{ lbin}^2$$

The procedure to calculate sections properties of the composites is described in (Appendix D4).

With respect to aeroelastic effects, a tapered swept wing of a control surface is specifically important. In the case, the deflection is due to bending, and torsion contributes considerably to the twist angle of the wing section. The deflection at the tip on the elastic curve of the wing, treated as a beam, from a tangent to the elastic curve at the root is defined as the moment of the area under the M/EI diagram between points taken about the tip³.

$$\delta_{RT} = \int_R^T (M\bar{y} / EI) dy \text{ (equation 6.2)}$$

where

δ_{RT} : the spanwise deflection

\bar{y} : the distance between centroid of elastic load (M/EI) and the tip

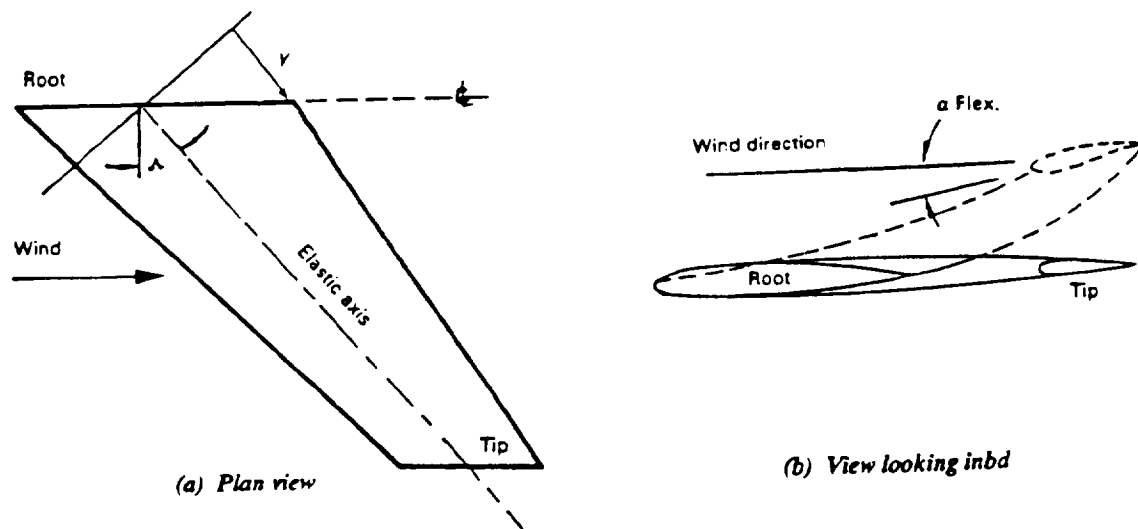


Figure 6.10 Wing twist angle caused by swept.

(Reproduced from Airframe Structural Analysis, by Michael N. Y. Niu)

The result for the deflection due the bending moment of the PVC foam is 1.14 inches; whereas, the deflection due to the bending moment of the composites of PVC and Kevlar decreases to the value of 0.0249 inches. As its results is compared to the deflection of the composites obtained from the Nastran program (0.0284 inches), the value from hand-calculation is short off about 0.0035 inches. This means that, as the commercial program is run, it produces the total deflection, being defines as:

$$\delta_{(total)} = \delta_{bM} + \delta_{(shearforce)} \quad (\text{equation 6.3})$$

However, for the engineering calculation, the deflection due to the shear force is considered so small that its value can be neglected. This is the reason why the value from the hand calculating is smaller than that obtained from Nastran program (see Appendix D5).

Taking into account the limit of the factor of Strength/Weight of the materials for the composites (1.60 inches), as well as comparing the results obtained from the Nastran program (maximum displacement = 0.0284 inches, including PVC foam and Kevlar) and from hand-calculating(maximum displacement = 0.0249 inches), the structures group can conclude that the wing in the static case can withstand under its basic loads

The concept of structural elastic axis is also applied for Torsion (or chordwise deflection) The angular deflection due to torsion about the elastic axis between point A and B is given by the equation¹¹:

$$\theta_A - \theta_B = \int_B^A (T / GJ) dy \quad (\text{equation 6.4})$$

Where: GJ is known as the torsional stiffness

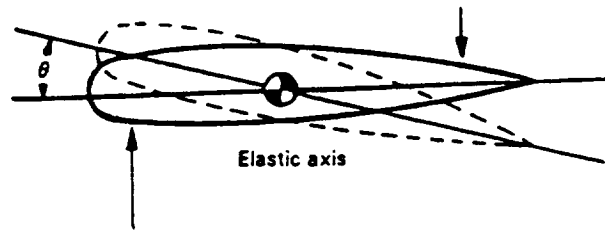


Figure 6.11 Wing chordwise deflection.

(Reproduced from Airframe Structural Analysis, by Michael N. Y. Niu)

The values of torsional stiffness are obtained for each section as:

$$\begin{aligned}
 JG_{(E329)} &= 637200 \text{ lbin}^2 & JG_{(E327)} &= 227610 \text{ lbin}^2 \\
 JG_{(E328)} &= 334800 \text{ lbin}^2 & JG_{(E326)} &= 101520 \text{ lbin}^2 \\
 JG_{(E325)} &= 26783 \text{ lbin}^2
 \end{aligned}$$

The above equations show that changes in airload due to structural deflection are due to torsional loads and that bending loads contribute more and more as sweep increases

6.4. Construction Methods:

Construction of the wing was begun by cutting the foam core. This was done by first cutting the block of foam to the shape of the wing planform. Obtaining the desired airfoil shape was made easy by designing the wing in such a way that the midspan airfoils were linear extrapolations of the root and tip foils. This meant that by making templates for the root and tip airfoils, affixing them to their respective ends of the foam block, and dragging the hot wire to coincide at specific chordlengths at each template, the midspan airfoils were automatically produced.

When the core had been cut, the control surfaces were cut out. Since the components were to build into the wings, small cavities were hollowed out for them as well as the channels for the controls rods and electrical wiring. On the bottom of the wing cavities were hollowed out for the landing gear fixtures. Into these were fitted blocks made of alternating layers of 1/32 inch plywood and 1/4 inch balsa. The effect of these blocks are to dampen the shock of landing from the landing gear.

After fitting the control rods and electrical wiring, the foam received a thin layer of micro balloons on the surfaces that would be covered by the skin layer. Micro-balloons are small, hollow spheres made of glass or phenolic resin that is mixed with the resin to reduce its weight while maintaining its strength. The effect of this layer was to reduce weight of the aircraft by filling the small nooks on the surface of the foam with something that is lighter than untreated resin.

On top of this the Kevlar skin was added in a wet lay-up, and then vacuum-bagged. Vacuum-bagging is the process in which the component is placed between layers of absorbent material and then in an air tight bag. Then a pressure of 25 inches Hg is applied to the component. This process eliminates air bubbles in the resin that could cause stress build up in the skin as well as removing excess resin. The duct was produced by molding layers of carbon fibers on a polystyrene form, and then melting out the polystyrene.

The wing were then connected to the duct by means of two carbon fiber rods that passed through the duct. At the joints, we also applied gussets of Kevlar, 2 to 3 inches wide, for reinforcement. We, then, applied another layer of micro-balloonmixture to fill the small "dimplies" that are caused by the weave in the skin. After this was completed, the components were mounted on balsa blocks in their respective compartments.

Lastly, we mounted the engine and fan unit. This was done by simply connecting the fan unit directly to the duct with eight screws, and rubber washers to dampen vibration.

Reference List

1. Anderson, William J.; *MSC/Nastran Interactive Training Program*
2. Beer, Ferdinand P. & Johnston, E. Russel, Jr.; *Mechanics of Materials*
3. Bruhn, E. F.; *Analysis and Design of Flight Vehicle Structure* Section A5.11
4. Constance, Joseph; "The All-Composite Aircraft" *Machine Design* Jan 1992
5. Eppler, Richard; *Airfoil Design and Data*
6. Hill, Maynard L.; *Electro-static Autopilots*
7. Hollman, Martin; *Aircraft Design, Practical Aircraft Design Utilizing Composite Materials*
8. Jones, R. T.; "The Supersonic Flying Wing" *Aerospace America* Oct 1987
9. Kuethy, Arnold M. & Chow, Chuen-Yen; *Foundations of Aerodynamics: Bases of Aerodynamic Design*
10. Meppenheimer, T. A.; "The Dream of the Flying Wing" *Invention and Technology* Winter 1994
11. Niu, Michael Chun Yung; *Airframe Structural Design*
12. O.S. Engines Mfg. Co. Ltd.; *O.S. Engines Catalog*
13. Raymer, Daniel P.; *Aircraft Design: A Conceptual Approach*
14. Shanley, F. R.; *Weight-Strength Analysis of Aircraft Structures*
15. Shevell, Richard S.; *Fundamentals of Flight*
16. Taylor, Michael J. H.; *Jet Warplanes: The 21st Century*
17. Van der Velden, Alexander J. M.; "The Conceptual Design of a Mach 2.0 Oblique Flying Wing Supersonic Transport" *NASA CR177529* May 1989

7. Conclusions and Recommendations

Many difficulties were encountered during the design and construction of *the Banshee '94*. In retrospect, many of these difficulties could have been either avoided or lessened, however these revelations were not obvious to the project team.

As was expected, the series of calculations for the aerodynamic analysis of *the Banshee '94* proved to be tedious and time-consuming. The use of a previously published vortex panel computer code proved to be more of a hindrance than a help due to debugging and difficulties in deciphering the output. If such a code is to be used in the future, it would be best to know exactly how the code works and have a better than working knowledge of the language in which it is written. Another problem experienced by the Aerodynamics group is the wind tunnel testing apparatus. WPI does not have a working force-balance capable of measuring lift, drag, and moments on an airfoil simultaneously. An apparatus does exist, but it is not in working order. If the desire for such an apparatus is apparent, it is advised that work begin on making this apparatus operational early on in the project's development. The Aerodynamics team concluded that *the Banshee '94* will fly at a cruise condition of angle of attack of 4 degrees and a cruise velocity of 33 miles per hour.

Stability was one of the primary problems addressed in the design of *the Banshee '94*. The group decided that the best way to handle the stability problems inherent to a flying wing was to oversize the control surfaces. In conjunction with the Aerodynamics group, a series of airfoils were selected which had a positive moment coefficient. This is essential in counteracting the instability of the flying wing. As experienced by the Aerodynamics group, computer codes proved to be a hindrance due to their difficulty in interpretation. Another problem addressed

by the Stability/Controls group was the implementation of the Electro-static Stability System. The existing literature available on the electrostatic stability system was rather minimal to the extent that several ambitious design implementations had to be undertaken. It is recommended that before an undertaking such as this, a better than working knowledge of electronics is acquired. From the analysis performed, *the Banshee '94* will maintain stable flight and will be able to maneuver without any major difficulty.

The propulsion system that was used in *the Banshee '94* proved to have sufficient power. This helped insuring that enough power was available for take-off and maneuvering. It is recommended that future projects use the ducted fan engine assembly as their primary propulsion system. Testing of the engine proved to be a major problem due to an inappropriate force balance. Future projects should restrain the thrust gage in the wind tunnel before engaging the test, in order to ensure that no injuries or damages to the apparatus occur.

The Structures group used two different finite element analysis codes to estimate the shear forces and displacements of the wing. Such codes are not entirely accurate due to the anisotropic nature of composites. The assumptions that had to be made when entering the data into the code proved to be difficult. The materials should prove to be more than adequate in handling the aerodynamic forces as well as the shocks from landing.

The project team was very satisfied with the outcome of this project. The group found that the areas mentioned above were difficulties that could have been avoided had the team had the foresight to compensate for them. It is the view of this team that these areas be addressed early when tackling such a project. Further research and development may have provided a better design. More experimental data would have proven useful in determining some of the necessary values needed for calculations.

APPENDIX A

AERODYNAMICS

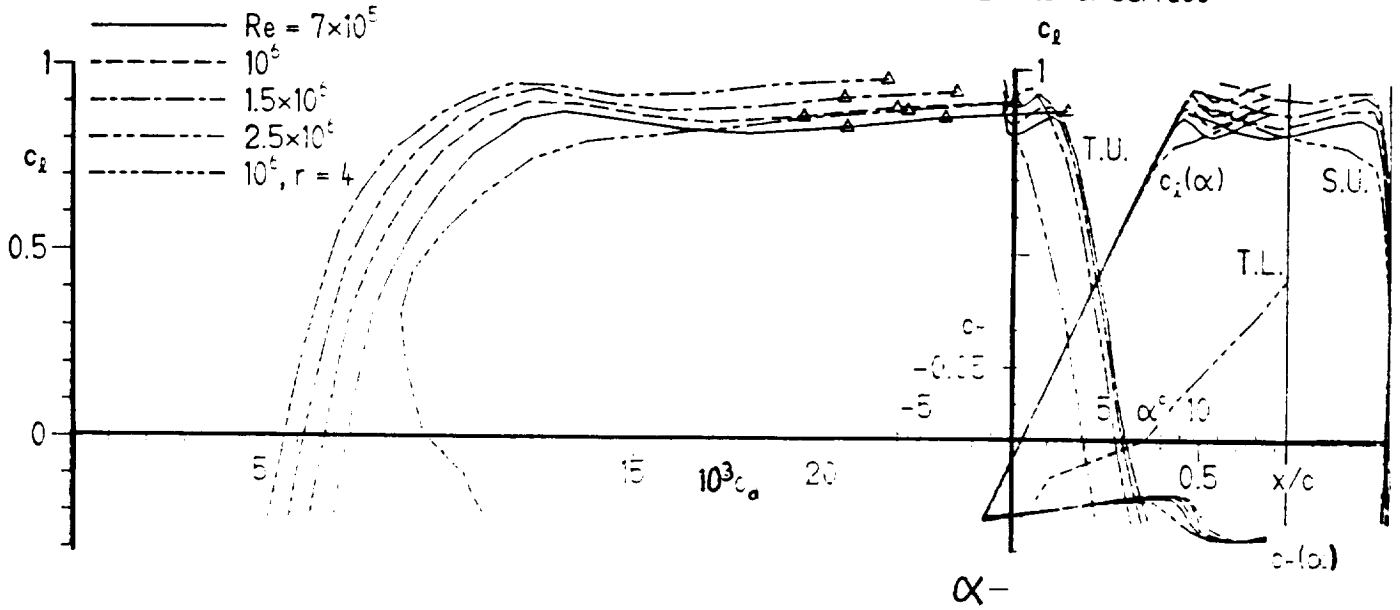
APPENDIX A1

The Eppler E325 Series Aerodynamic Data⁵

E 325 12.63% c_2 mod.

Separation bubble warning
 Δ upper surface
 ∇ lower surface

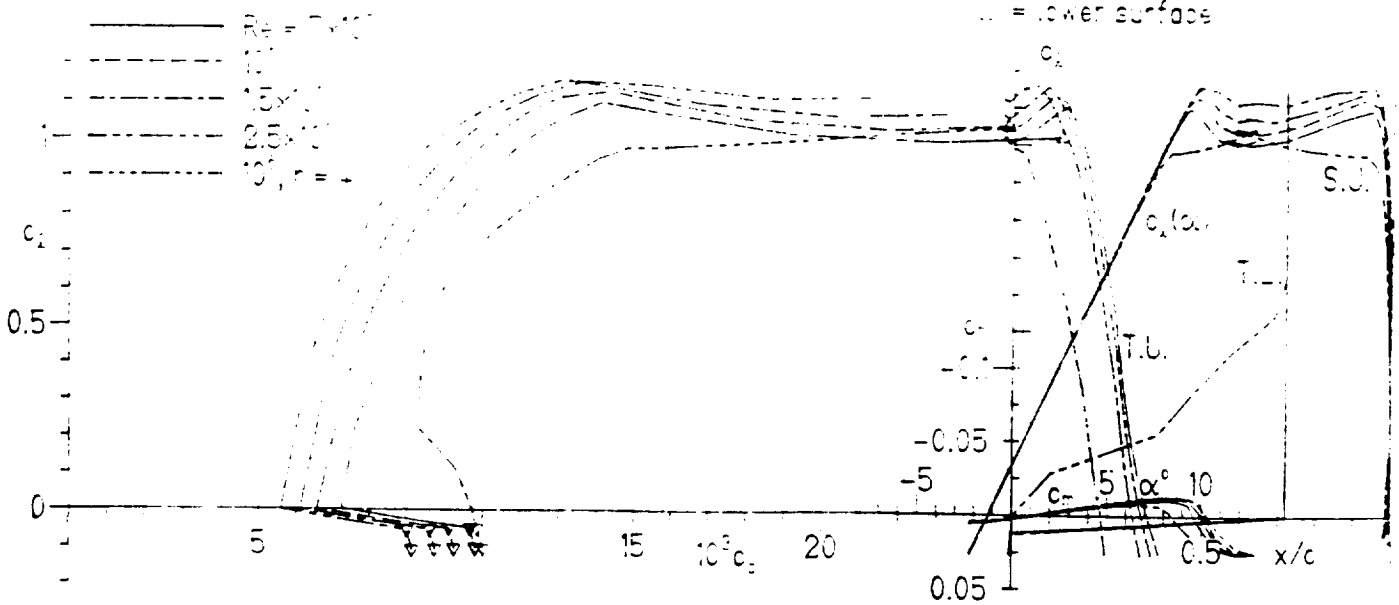
T. = boundary layer transition
 S. = boundary layer separation
 U. = upper surface
 L. = lower surface



E 327 13.1% c_2 mod.

Separation bubble warning
 Δ upper surface
 ∇ lower surface

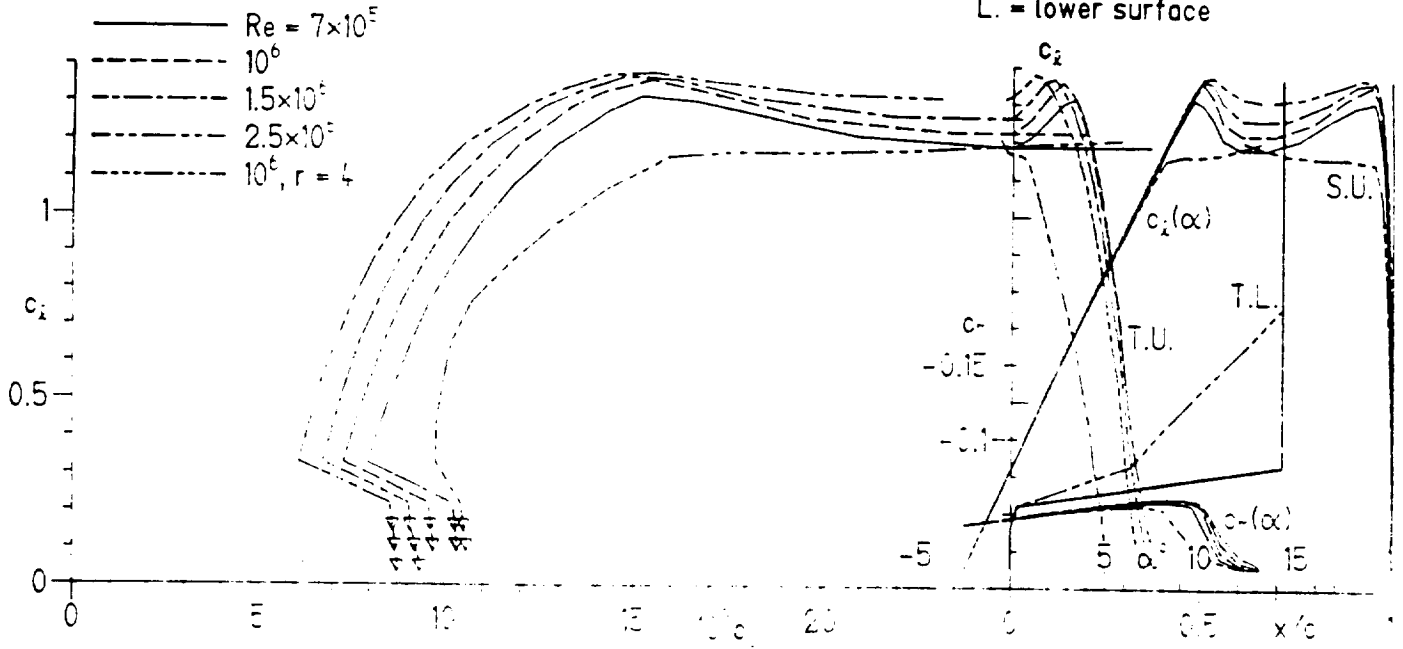
T. = boundary layer transition
 S. = boundary layer separation
 U. = upper surface
 L. = lower surface



E 329 13.5% c_p mod.

Separation bubble warning
 Δ upper surface
 ∇ lower surface

T. = boundary layer transition
 S. = boundary layer separation
 U. = upper surface
 L. = lower surface



ORIGINAL PAGE IS
 OF POOR QUALITY

APPENDIX A2

Lotus Spreadsheet for Drag and Lift Calculations

c329=	c327=	c325=	cg=	Stot4wng	b	AR
0.4148	0.3302	0.2455	13.6925	0.73	2.2098	6.689337
Stot=	q=	b=	Cmac:			Cm _{cg}
0.3648	48.95320	0.3683	329	327	325	
a.c.			-0.05	0	0.05	0.550416
329	327	325	-0.051	-0.0024	0.048	0.290020
16.33333	13	9.666666	-0.052	-0.0048	0.046	-0.00192
x/c:			-0.053	-0.0072	0.044	-0.00457
329	327	325	-0.054	-0.0096	0.042	-0.41482
-6.36652	2.097213	16.39850	-0.055	-0.012	0.04	-0.68975
S ratio:			K			
329	327	325	0.048555			
0.418859	0.333333	0.247807				
alpha	Cl:			Cd:		
2	0.53	0.35	0.15	0.0086	0.008	0.0077
3	0.65	0.48	0.27	0.0091	0.0085	0.0079
4	0.73	0.56	0.38	0.0094	0.0087	0.0081
5	0.86	0.65	0.45	0.0102	0.0094	0.0085
6	0.95	0.76	0.59	0.0108	0.01	0.0094
7	1.03	0.87	0.69	0.0115	0.0107	0.0101
L(lbf)	L(N)	D (wing)	D(e-plat)	D(L-gear)	D tot (N)	D (lbf)
3.017521	13.42254	0.146024	0.036206	0.003362	0.423644	0.095239
4.007816	17.82757	0.153626			0.438847	0.098657
4.709871	20.95045	0.157945	D (duct)		0.447486	0.100599
5.527216	24.58616	0.169866	0.049093		0.471327	0.105959
6.402903	28.48139	0.181909			0.495413	0.111373
7.165359	31.87295	0.194409			0.520414	0.116994
v (m/s)=	v (m/h)=	q	D (wing)	D(e-plat)	D (duct)	D(L-gear)
8.94	20	48.95320	0.157945	0.036206	0.049093	0.003362
11.175	25	76.48938	0.246789	0.056572	0.076708	0.005254
13.41	30	110.1447	0.355377	0.081464	0.110460	0.007566
15.645	35	149.9191	0.483708	0.110882	0.150348	0.010298
17.88	40	195.8128	0.631782	0.144825	0.196374	0.013451
20.115	45	247.8256	0.799599	0.183295	0.248535	0.017024
22.35	50	305.9575	0.987159	0.226290	0.306834	0.021018
24.585	55	370.2086	1.194462	0.273811	0.371269	0.025431
26.82	60	440.5788	1.421509	0.325858	0.441841	0.030266
29.055	65	517.0682	1.668299	0.382430	0.518550	0.035520
31.29	70	599.6767	1.934832	0.443529	0.601395	0.041195
33.525	75	688.4044	2.221108	0.509153	0.690377	0.047290
35.76	80	783.2512	2.527128	0.579303	0.785496	0.053806
37.995	85	884.2172	2.852890	0.653979	0.886751	0.060742
40.23	90	991.3024	3.198396	0.733181	0.994143	0.068098
42.465	95	1104.506	3.563645	0.816908	1.107672	0.075875
44.7	100	1223.830	3.948637	0.905161	1.227337	0.084072
D(induc)	D tot (N)	D (lbf)	L tot (N)	L (lbf)	L/D	
0.315198	1.077883	0.242319	20.95045	4.709871	19.43665	
0.492497	1.684193	0.378623	32.73508	7.359174		
0.709197	2.425238	0.545217	47.13852	10.59721	Cl	
0.965295	3.301018	0.742101	64.16076	14.42398	0.586258	
1.260794	4.311534	0.969276	83.80182	18.83948		
1.595693	5.456785	1.226739	106.0616	23.84372	Cd	
1.969991	6.736772	1.514493	130.9403	29.43669	0.030162	

2.383690 8.151494 1.832537 158.4378 35.61840

2.836788 9.700952 2.180871 188.5540 42.38884
3.329286 11.38514 2.559494 221.2891 49.74802
3.861183 13.20407 2.968407 256.6430 57.69592
4.432481 15.15773 3.407611 294.6157 66.23257
5.043178 17.24613 3.877104 335.2072 75.35794
5.693276 19.46927 4.376887 378.4175 85.07205
6.382773 21.82714 4.906959 424.2467 95.37490
7.111670 24.31974 5.467322 472.6946 106.2664
7.879967 26.94708 6.057975 523.7613 117.7467

APPENDIX B

STABILITY ANALYSIS

B.1 CONTROLS/STABILITY SPREADSHEET

	Cl:			Cd:		
alpha	329	327	325	329	327	325
2	0.53	0.35	0.15	0.0086	0.008	0.0077
3	0.65	0.48	0.27	0.0091	0.0085	0.0079
4	0.73	0.56	0.38	0.0094	0.0087	0.0081
5	0.86	0.65	0.45	0.0102	0.0094	0.0085
6	0.95	0.76	0.59	0.0108	0.01	0.0094
7	1.03	0.87	0.69	0.0115	0.0107	0.0101
	Cmac:			Cdi:		
alpha	329	327	325	329	327	325
2	-0.05	0	0.05	0.015309	0.006676	0.001226
3	-0.051	-0.0024	0.048	0.023026	0.012557	0.003973
4	-0.052	-0.0048	0.046	0.029043	0.017091	0.00787
5	-0.053	-0.0072	0.044	0.040308	0.023026	0.011036
6	-0.054	-0.0096	0.042	0.049186	0.031479	0.018971
7	-0.055	-0.012	0.04	0.057819	0.041251	0.025947
alpha	Cmac1	Ci1	Cd1	Cmcg		
2	-0.00855	0.035529	0.002128	0.027073		
3	-0.01027	0.038073	0.002644	0.027997		
4	-0.01198	0.037683	0.002914	0.025998		
5	-0.0137	0.044169	0.003703	0.030965		
6	-0.01541	0.042763	0.00394	0.028002		
7	-0.01713	0.04326	0.004253	0.026982		
	Clave	slope:	aveslp:	Cdave	Cl/Cd	
	0.343333	0.007495	-6.1e-06	0.015837	21.67894	
	0.466667	-0.02222		0.021685	21.51989	

	Cl:			Cd:		
	0.556667	0.05139		0.026735	20.82189	
	0.653333	-0.02615		0.034157	19.12742	
	0.766667	-0.01055		0.043279	17.71453	
	0.863333			0.052439	16.46352	
Chord, m:						
c329=	c327=	c325=	cg (m)=	SM:	Cd(eplt)	Cd(edl)
0.4148	0.3302	0.2455	0.232334	0.132077	0.00647	0.032978
a.c.			cg (in)=	rho	Cd(duct)	
329	327	325	9.147	0.000043	0.004996	
0.1514	0.2255	0.2997	Stot=	V, in/s	Cd(lgr)	
x/c:			0.3648	616	0.005014	
329	327	325	b/3, m.	Ar, in2		
0.195115	0.020696	-0.2744	0.3683	25.34		
S ratio:			Ix	Iy	Iz	
329	327	325	270	3390.69	3610.24	
0.41886	0.333333	0.247807				

B.2 INVISCID VORTEX PANEL CODE

PROGRAM VORCODE

INTEGER Z,ZZ

PARAMETER (Z=36)

PARAMETER (ZZ=37)

DIMENSION XB(ZZ),YB(ZZ),X(Z),Y(Z),S(Z),SINE(Z),COSINE(Z)
 DIMENSION V(Z),CP(Z),GAMA(Z),RHS(Z),CN1(Z,Z),CN2(Z,Z)
 DIMENSION CT2(Z,Z),AN(ZZ,ZZ),AT(Z,ZZ),THETA(Z),CT1(Z,Z)

OPEN (UNIT=11, FILE='juju', STATUS='NEW')

OPEN (UNIT=12, FILE='e327', STATUS='OLD')

M = 36

MP1 = M+1

DO 13 I=1,MP1

-13 READ (12,*) XB(I),YB(I)

PI = 4.0 * ATAN(1.0)

ALPHA = (4.) * PI/180

DO 1 I=1,M

IP1= I+1

X(I)=0.5*(XB(I)+XB(IP1))

Y(I)=0.5 * (YB(I) + YB(IP1))

S(I)=SQRT((XB(IP1)-XB(I))**2+(YB(IP1)-YB(I))**2)

THETA(I)=ATAN2((YB(IP1)-YB(I)), (XB(IP1)-XB(I)))

SINE(I)=SIN(THETA(I))

COSINE(I)=COS(THETA(I))

1 RHS(I)=SIN(THETA(I)-ALPHA)

DO 3 I= 1,M

DO 3 J= 1,M

IF (I.EQ.J) GO TO 2

A=-(X(I)-XB(J))*COSINE(J) - (Y(I)-YB(J))*SINE(J)

B=(X(I)-XB(J))**2+(Y(I)-YB(J))**2

C=SIN(THETA(I)-THETA(J))

D=COS(THETA(I)-THETA(J))

E=(X(I)-XB(J))*SINE(J)-(Y(I)-YB(J))*COSINE(J)

F=ALOG(1.0+S(J)*(S(J)+2.*A)/B)

G=ATAN2(E*S(J),B+A*S(J))

P=(X(I)-XB(J))*SIN(THETA(I)-2.*THETA(J))

+ (Y(I)-YB(J))*COS(THETA(I)-2.*THETA(J))

Q=(X(I)-XB(J))*COS(THETA(I)-2.*THETA(J))

+ -(Y(I)-YB(J))*SIN(THETA(I)-2.*THETA(J))

CN2(I,J)=D+.5*Q*F/S(J)-(A*C+D*E)*G/S(J)

CN1(I,J)=.5*D*F+C*G-CN2(I,J)

CT2(I,J)=C+.5*P*F/S(J)+(A*D-C*E)*G/S(J)

CT1(I,J)=.5*C*F-D*G-CT2(I,J)

GO TO 3

2 CN1(I,J)=-1.0

```
CN2(I,J)=1.0
CT1(I,J)=0.5*PI
CT2(I,J)=0.5*PI
```

```
3 CONTINUE
```

```
DO 4 I=1,M
```

```
AN(I,1)=CN1(I,1)
AN(I,MP1)=CN2(I,M)
AT(I,1)=CT1(I,1)
AT(I,MP1)=CT2(I,M)
DO 4 J=2,M
```

```
AN(I,J)=CN1(I,J)+CN2(I,J-1)
```

```
4 AT(I,J)=CT1(I,J)+CT2(I,J-1)
```

```
AN(MP1,1)=1.0
AN(MP1,MP1)=1.0
```

```
DO 5 J=2,M
```

```
5 AN(MP1,J)=0.0
RHS(MP1)=0.0
```

```
CALL CRAMER(AN,RHS,GAMA,MP1)
```

```
DO 8 I=1,M
```

```
V(I)=COS(THETA(I)-ALPHA)
```

```
DO 7 J=1,MP1
```

```
V(I)=V(I)+AT(I,J)*GAMA(J)
```

```
7 CP(I)=1.0-V(I)**2
```

```
8 WRITE (11,9) I,X(I),Y(I),THETA(I),S(I),GAMA(I),V(I),CP(I)
```

```
9 FORMAT(10X,I2,F8.4,F9.4,F10.4,F8.4,2F9.4,F10.4)
```

```
WRITE (11,10) MP1,GAMA(MP1)
```

```
10 FORMAT (10X,I2,35X,F9.4)
```

```
END FILE (UNIT=11)
```

```
END FILE (UNIT=12)
```

```
CLOSE (UNIT=11)
```

```
CLOSE (UNIT=12)
```

```
STOP
```

```
END
```

```
SUBROUTINE CRAMER(C,A,X,N)
```

```
INTEGER ZZ
```

```
PARAMETER (ZZ=37)
```

```
DIMENSION C(ZZ,ZZ),CC(ZZ,ZZ),A(ZZ),X(ZZ)
```

```
DENOM=DETERM(C,N)
```

```
DO 3 K=1,N
```

```
DO 1 I=1,N
```

```
DO 1 J=1,N
```

```
1 CC(I,J)=C(I,J)
```

```
DO 2 I=1,N
```

```
CC(I,K)=A(I)
```

```
3 X(K)=DETERM(CC,N)/DENOM  
RETURN  
END
```

```
FUNCTION DETERM(ARRAY,N)
```

```
INTEGER ZZ  
PARAMETER(ZZ=37)  
DIMENSION ARRAY(ZZ,ZZ),A(ZZ,ZZ)  
DO 1 I=1,N  
DO 1 J=1,N
```

```
1 A(I,J)=ARRAY(I,J)
```

```
M=1  
2 K=M+1
```

```
DO 3 I=K,N
```

```
RATIO=A(I,M)/A(M,M)  
DO 3 J=K,N
```

```
3 A(I,J)=A(I,J)-A(M,J)*RATIO
```

```
IF (M.EQ.N-1) GO TO 4
```

```
M=M+1  
GO TO 2  
4 DETERM=1
```

```
DO 5 L=1,N
```

```
5 DETERM=DETERM*A(L,L)
```

```
RETURN  
END
```


Appendix C

Data from Trust - Drag vs. Velocity Plot

V (mph)	Drag (lbf)	Thrust (100%)	Thrust (75%)	Thrust (50%)	Thrust (25%)
0	0	14	10.5	7	3.5
20	0.2423	12.4	8.9	5.4	1.95
25	0.3786	12	8.5	5	1.55
30	0.5452	11.6	8.1	4.6	1.15
35	0.7421	11.2	7.7	4.2	0.75
40	0.9693	10.8	7.3	3.8	0.35
45	1.2267	10.5	6.8	3.3	0
50	1.5145	10	6.3	2.8	
55	1.8325	9.5	5.8	2.3	
60	2.1809	9	5.3	1.8	
65	2.5595	8.5	4.8	1.3	
70	2.9684	8	4.3	0.8	
75	3.4076	7.4	3.7	0.3	
80	3.8771	6.8	3.1		
85	4.3769	6.2	2.5		
90	4.9069	5.6	1.9		
95	5.4673	5	1.3		
100	6.0579	4.4	0.7		

Data from the Climb Rate vs. Velocity

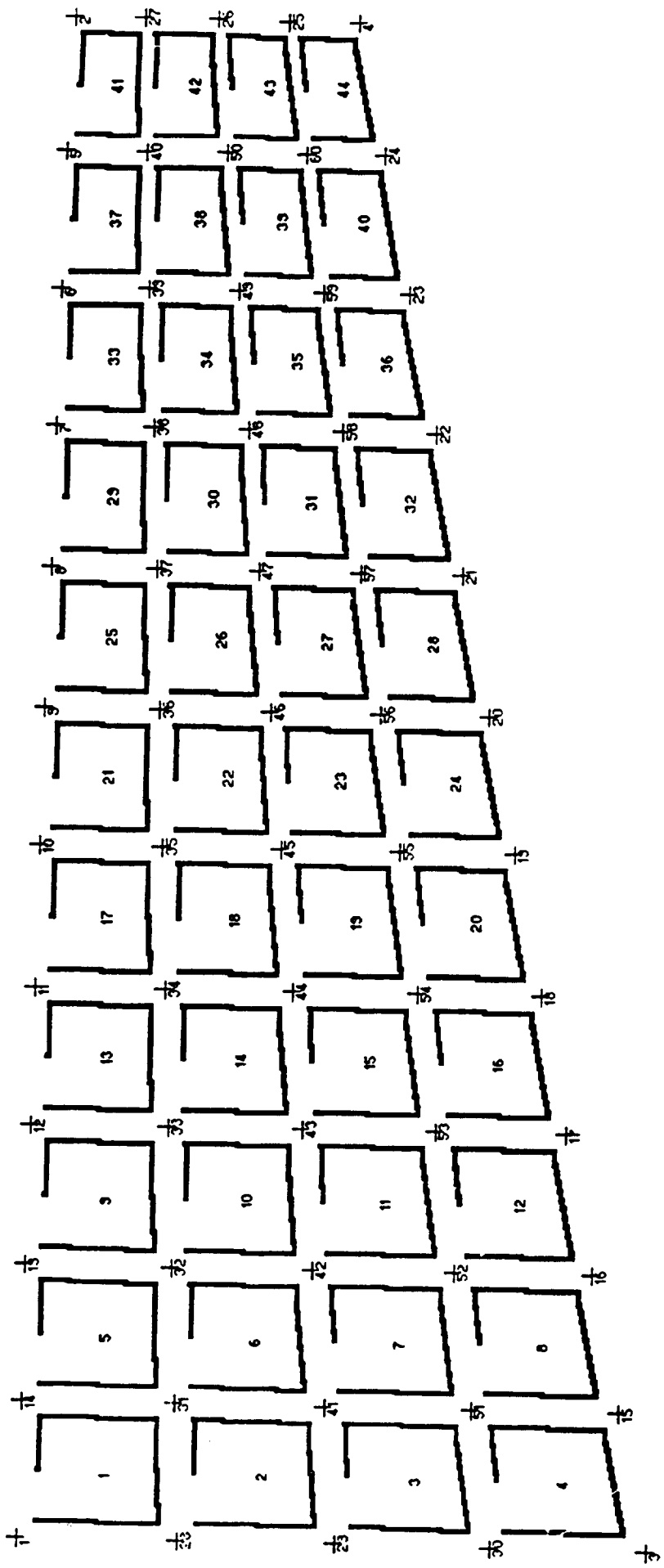
and calculations for Acceleration

Velocity (mph)	RC (ft/s)(100%)	RC (ft/s)(75%)	RC (ft/s)(50%)	Thrust (100%)	Thrust (75%)	Thrust (50%)
0	0	0	0	14	10.5	7
20	32.16	10.974366	6.9971998	13.4	9.9	6.4
25	39.02	13.169251	8.1977928	13.15	9.65	6.15
30	45.3	15.093007	9.2124816	12.9	9.4	5.95
35	51.15	16.620381	9.7597681	12.7	9.1	5.65
40	55.39	17.569304	9.7286042	12.3	8.7	5.25
45	60.08	18.723847	9.9030598	12.15	8.55	5.1
50	62.55	18.85035	9.0494746	11.75	8.15	4.7
55	65.67	19.272924	8.491961	11.6	8	4.55
60	66.14	18.473712	6.7126619	11.2	7.6	4.15
65	67.06	17.87637	5.1352324	11	7.4	3.95
70	64.87	15.835487	2.1142618	10.55	6.95	3.5
75	63.18	14.02974	0	10.3	6.7	3.25
80	59.38	11.240155		9.95	6.35	2.9
85	55.82	8.5630387		9.75	6.15	2.7
90	49.43	4.5668669		9.4	5.8	2.35
95	41.02	0		9	5.1	1.95
100	27.41			8.3	4.4	1.25
Drag (lbs)	Accel (100%)	Accel (75%)	Accel (50%)	Accel (25%)		Velocity (mph)
0	37.56675	28.17506	18.78337	9.33917		0
0.2423	35.30657	25.91488	16.5232	7.1315		20
0.3786	34.27	24.87831	15.48662	6.0949		25
0.5452	33.15212	23.76043	14.50291	4.977		30
0.7421	32.0871	22.42708	13.16956	3.6437		35
0.9693	30.40411	20.74409	11.48657	1.9607		40

1.2267	29.31092	19.6509	10.39338	0.8675		45
1.5145	27.46532	17.8053	8.547777	0		50
1.8325	26.2013	16.54946	7.291974			55
2.1809	24.2013	14.54128	5.283763			60
2.5595	22.64872	12.9887	3.731183			65
2.9684	20.344	10.68398	1.426463			70
3.4076	18.49465	8.834626	0			75
3.8771	16.29565	6.635629				80
4.3769	14.41785	4.757829				85
4.9069	12.05651	2.39649				90
5.4673	9.479432	0				95
6.0579	6.016315					100

APPENDICES D

APPENDIX D1 :
MSC/NASTRAN RESULTS



M S C / N A S T R A N

VERSION - 67

JAN 30, 1992

IBM 370/390 SERIES

MODEL 9021 SCALAR

MVS/XA NCPU= 6

CARD COUNT	1	2	3	4	5	6	7	8	9	10	ECHO
1-	1	1	1	1	1	1	1	1	1	1	1
2-	1	1	1	1	1	1	1	1	1	1	1
3-	1	1	1	1	1	1	1	1	1	1	1
4-	1	1	1	1	1	1	1	1	1	1	1
5-	1	1	1	1	1	1	1	1	1	1	1
6-	1	1	1	1	1	1	1	1	1	1	1
7-	1	1	1	1	1	1	1	1	1	1	1
8-	1	1	1	1	1	1	1	1	1	1	1
9-	1	1	1	1	1	1	1	1	1	1	1
10-	1	1	1	1	1	1	1	1	1	1	1
11-	1	1	1	1	1	1	1	1	1	1	1
12-	1	1	1	1	1	1	1	1	1	1	1
13-	1	1	1	1	1	1	1	1	1	1	1
14-	1	1	1	1	1	1	1	1	1	1	1
15-	1	1	1	1	1	1	1	1	1	1	1
16-	1	1	1	1	1	1	1	1	1	1	1
17-	1	1	1	1	1	1	1	1	1	1	1
18-	1	1	1	1	1	1	1	1	1	1	1
19-	1	1	1	1	1	1	1	1	1	1	1
20-	1	1	1	1	1	1	1	1	1	1	1
21-	1	1	1	1	1	1	1	1	1	1	1
22-	1	1	1	1	1	1	1	1	1	1	1
23-	1	1	1	1	1	1	1	1	1	1	1
24-	1	1	1	1	1	1	1	1	1	1	1
25-	1	1	1	1	1	1	1	1	1	1	1
26-	1	1	1	1	1	1	1	1	1	1	1
27-	1	1	1	1	1	1	1	1	1	1	1
28-	1	1	1	1	1	1	1	1	1	1	1
29-	1	1	1	1	1	1	1	1	1	1	1
30-	1	1	1	1	1	1	1	1	1	1	1
31-	1	1	1	1	1	1	1	1	1	1	1
32-	1	1	1	1	1	1	1	1	1	1	1
33-	1	1	1	1	1	1	1	1	1	1	1
34-	1	1	1	1	1	1	1	1	1	1	1
35-	1	1	1	1	1	1	1	1	1	1	1
36-	1	1	1	1	1	1	1	1	1	1	1
37-	1	1	1	1	1	1	1	1	1	1	1
38-	1	1	1	1	1	1	1	1	1	1	1
39-	1	1	1	1	1	1	1	1	1	1	1
40-	1	1	1	1	1	1	1	1	1	1	1
41-	1	1	1	1	1	1	1	1	1	1	1
42-	1	1	1	1	1	1	1	1	1	1	1
43-	1	1	1	1	1	1	1	1	1	1	1
44-	1	1	1	1	1	1	1	1	1	1	1
45-	1	1	1	1	1	1	1	1	1	1	1
46-	1	1	1	1	1	1	1	1	1	1	1
47-	1	1	1	1	1	1	1	1	1	1	1
48-	1	1	1	1	1	1	1	1	1	1	1
49-	1	1	1	1	1	1	1	1	1	1	1
50-	1	1	1	1	1	1	1	1	1	1	1

5

CARD COUNT	1	2	3	4	5	6	7	8	9	10
101-	GRID	0.000	0.000	43.500	0.000	0.000				
102-	GRID	18.000	0.000	0.000	0.000	0.000				
103-	GRID	8.000	43.500	0.000	0.000	0.000		123456		
104-	GRID	0.000	0.000	39.545	0.000	0.000				
105-	GRID	0.000	0.000	35.591	0.000	0.000				
106-	GRID	0.000	0.000	31.636	0.000	0.000				
107-	GRID	0.000	0.000	27.682	0.000	0.000				
108-	GRID	0.000	0.000	23.727	0.000	0.000				
109-	GRID	0.000	0.000	19.773	0.000	0.000				
110-	GRID	0.000	0.000	15.818	0.000	0.000				
111-	GRID	0.000	0.000	11.864	0.000	0.000				
112-	GRID	0.000	0.000	7.909	0.000	0.000				
113-	GRID	0.000	0.000	3.955	0.000	0.000				
114-	GRID	17.091	3.955	0.000	0.000	0.000				
115-	GRID	16.182	7.909	0.000	0.000	0.000				
116-	GRID	15.273	11.864	0.000	0.000	0.000				
117-	GRID	14.364	15.818	0.000	0.000	0.000				
118-	GRID	13.455	19.773	0.000	0.000	0.000				
119-	GRID	12.545	23.727	0.000	0.000	0.000				
120-	GRID	11.636	27.682	0.000	0.000	0.000				
121-	GRID	10.727	31.636	0.000	0.000	0.000				
122-	GRID	9.818	35.591	0.000	0.000	0.000				
123-	GRID	8.909	39.545	0.000	0.000	0.000				
124-	GRID	8.000	43.500	0.000	0.000	0.000				
125-	GRID	4.000	43.500	0.000	0.000	0.000				
126-	GRID	2.000	43.500	0.000	0.000	0.000				
127-	GRID	4.500	0.000	0.000	0.000	0.000				
128-	GRID	9.000	0.000	0.000	0.000	0.000				
129-	GRID	13.500	0.000	0.000	0.000	0.000				
130-	GRID	4.273	3.955	0.000	0.000	0.000				123456
131-	GRID	4.045	7.909	0.000	0.000	0.000				123456
132-	GRID	3.818	11.864	0.000	0.000	0.000				123456
133-	GRID	3.591	15.818	0.000	0.000	0.000				
134-	GRID	3.364	19.773	0.000	0.000	0.000				
135-	GRID	3.136	23.727	0.000	0.000	0.000				
136-	GRID	2.909	27.682	0.000	0.000	0.000				
137-	GRID	2.682	31.636	0.000	0.000	0.000				
138-	GRID	2.455	35.591	0.000	0.000	0.000				
139-	GRID	2.227	39.545	0.000	0.000	0.000				
140-	GRID	8.545	3.955	0.000	0.000	0.000				
141-	GRID	8.091	7.909	0.000	0.000	0.000				
142-	GRID	7.636	11.864	0.000	0.000	0.000				
143-	GRID	7.182	15.818	0.000	0.000	0.000				
144-	GRID	6.727	19.773	0.000	0.000	0.000				
145-	GRID	6.273	23.727	0.000	0.000	0.000				
146-	GRID	5.818	27.682	0.000	0.000	0.000				
147-	GRID	5.364	31.636	0.000	0.000	0.000				
148-	GRID	4.909	35.591	0.000	0.000	0.000				
149-	GRID	4.455	39.545	0.000	0.000	0.000				
150-	GRID	12.818	3.955	0.000	0.000	0.000				

CARD COUNT	1	2	3	4	5	6	7	8	9	10
151- GRID	52		12.136	7.909	0.000					
152- GRID	53		11.455	11.864	0.000					
153- GRID	54		10.773	15.818	0.000					
154- GRID	55		10.091	19.773	0.000					
155- GRID	56		9.409	23.727	0.000					
156- GRID	57		8.727	27.682	0.000					
157- GRID	58		8.045	31.636	0.000					
158- GRID	59		7.364	35.591	0.000					
159- GRID	60		6.682	39.545	0.000					
160- MAT1	1		4.4E+06	0.30	0.108					
161- PARAM	AUTOSPC	YES								
162- PARAM	BAILOUT	-1								
163- PARAM	DBC	124								
164- PARAM	EST	+1								
165- PARAM	GRDPNT	0								
166- PARAM	POST	0								
167- PARAM	WTMASS	.00259								
168- PSHELL	1	1	0.046	1	7611.0					
169- PSHELL	2	1	0.046	1	3571.0					
170- PSHELL	3	1	0.046	1	1041.0					
ENDDATA										

TOTAL COUNT= 171

SEQUENCE PROCESSOR OUTPUT

THERE ARE 60 POINTS DIVIDED INTO 1 GROUP(S).

CONNECTION DATA

ELEMENT TYPE NUMBER ASSEMBLY TIME(SEC)

QUAD4 44 0.28

TOTAL MATRIX ASSEMBLY TIME FOR 44 ELEMENTS IS 0.28 SECONDS.

ORIGINAL PERFORMANCE DATA

SUPER(GROUP) ID NO. GRIDS AV. CONNECTIVITY C-AVERAGE C-RMS C-MAXIMUM P-GROUPS P-AVERAGE DECOMP TIME(SECS)
 (6.0 DOF/GRID)

0 60 7.37 17.27 18.70 27 0 0.00 0.028

RESEQUENCED PERFORMANCE DATA

SUPER(GROUP) ID NO. GRIDS AV. CONNECTIVITY C-AVERAGE C-RMS C-MAXIMUM P-GROUPS P-AVERAGE DECOMP TIME(SECS)
 (6.0 DOF/GRID)

0 60 7.37 6.28 6.41 7 0 0.00 0.010 ACTIVE

AFB1511 VDIOS : 1800 RECORDS OF LENGTH 4096 FORMATTED ON FILE DBC.
 VDIOS : LAST EXECUTED FORTRAN STATEMENT IN PROGRAM OPNPFL AT ISN 606 (OFFSET 000062EC).

ELEMENT TYPE = QUAD4

ELEMENT ID	AREA	VOLUME	ELEMENT ID	AREA	VOLUME	ELEMENT ID	AREA	VOLUME	ELEMENT ID	AREA	VOLUME
1	17.3486	.798034	2	17.3486	-.797944	3	17.3486	.798034	4	17.3486	.798034
5	16.4447	.756454	6	16.4447	-.756454	7	16.4447	.756454	8	16.4466	.756544
9	15.5491	.715257	10	15.551	-.715348	11	15.551	.715348	12	15.551	.715347
13	14.6476	.673789	14	14.6476	-.673789	15	14.6496	.67388	16	14.6476	.673789
17	13.7535	.63266	18	13.7515	-.632569	19	13.7535	.63266	20	13.7535	.63266
21	12.8505	.591122	22	12.8505	-.591122	23	12.8505	.591122	24	12.8505	.591122
25	11.954	.549883	26	11.956	-.549974	27	11.954	.549883	28	11.954	.549883
29	11.0534	.508455	30	11.0534	-.508456	31	11.0514	.508364	32	11.0534	.508456
33	10.1584	.467287	34	10.1564	-.467196	35	10.1564	.467196	36	10.1584	.467196
37	9.25633	.425791	38	9.25633	-.425791	39	9.25633	.425791	40	9.25436	.4257
41	8.35886	.384507	42	8.36084	-.384598	43	8.35886	.384507	44	8.35886	.384507

OUTPUT FROM GRID POINT WEIGHT GENERATOR

REFERENCE POINT = 0

* 2.809401E+00 0.000000E+00 0.000000E+00 0.000000E+00 0.000000E+00 0.000000E+00 -5.327007E+01 *
 * 0.000000E+00 2.809401E+00 0.000000E+00 0.000000E+00 0.000000E+00 0.000000E+00 1.916167E+01 *
 * 0.000000E+00 0.000000E+00 2.809401E+00 5.327007E+01 -1.916167E+01 0.000000E+00 0.000000E+00 *
 * 0.000000E+00 0.000000E+00 5.327007E+01 1.438556E+03 -3.140774E+02 0.000000E+00 0.000000E+00 *
 * 0.000000E+00 0.000000E+00 -1.916167E+01 -3.140774E+02 1.874879E+02 0.000000E+00 0.000000E+00 *
 * -5.327007E+01 1.916167E+01 0.000000E+00 0.000000E+00 0.000000E+00 0.000000E+00 1.626044E+03 *

S

* 1.000000E+00 0.000000E+00 0.000000E+00 0.000000E+00 *
 * 0.000000E+00 1.000000E+00 0.000000E+00 0.000000E+00 *
 * 0.000000E+00 0.000000E+00 1.000000E+00 1.000000E+00 *

DIRECTION

MASS AXIS SYSTEM (S)

		MASS	X-C.G.	Y-C.G.	Z-C.G.
X	2.809401E+00	0.000000E+00	1.896135E+01	0.000000E+00	0.000000E+00
Y	2.809401E+00	6.820553E+00	0.000000E+00	0.000000E+00	0.000000E+00
Z	2.809401E+00	6.820553E+00	1.896135E+01	0.000000E+00	0.000000E+00

I(S)

* 4.284844E+02 -4.925317E+01 0.000000E+00 *
 * -4.925317E+01 5.679480E+01 0.000000E+00 *
 * 0.000000E+00 0.000000E+00 4.852793E+02 *

I(Q)

* 5.037889E+01 *
 * 4.348997E+02 *
 * 4.852793E+02 *

Q

* 1.291718E-01 9.916222E-01 0.000000E+00 *
 * -9.916222E-01 1.291718E-01 0.000000E+00 *
 * 0.000000E+00 0.000000E+00 1.000000E+00 *

WINFEM NASTRAN OUTPUT

	LOAD	RESULTANT				
	T1	T2	T3	R1	R2	R3
1	0.000000E+00	0.000000E+00	7.9749985E+00	1.8922488E+02	-5.0024963E+01	0.0000000E+00

GRID POINT SINGULARITY TABLE

POINT ID	TYPE	FAILED DIRECTION	STIFFNESS RATIO	OLD USET EXCLUSIVE UNION	NEW USET EXCLUSIVE UNION
2	G	6	0.00E+00	B	SB
4	G	6	0.00E+00	B	SB
5	G	6	0.00E+00	B	SB
6	G	6	0.00E+00	B	SB
7	G	6	0.00E+00	B	SB
8	G	6	0.00E+00	B	SB
9	G	6	0.00E+00	B	SB
10	G	6	0.00E+00	B	SB
11	G	6	0.00E+00	B	SB
12	G	6	0.00E+00	B	SB
13	G	6	0.00E+00	B	SB
14	G	6	0.00E+00	B	SB
15	G	6	0.00E+00	B	SB
16	G	6	0.00E+00	B	SB
17	G	6	0.00E+00	B	SB
18	G	6	0.00E+00	B	SB
19	G	6	0.00E+00	B	SB
20	G	6	0.00E+00	B	SB
21	G	6	0.00E+00	B	SB
22	G	6	0.00E+00	B	SB
23	G	6	0.00E+00	B	SB
24	G	6	0.00E+00	B	SB
25	G	6	0.00E+00	B	SB
26	G	6	0.00E+00	B	SB
27	G	6	0.00E+00	B	SB
31	G	6	0.00E+00	B	SB
32	G	6	0.00E+00	B	SB
33	G	6	0.00E+00	B	SB
34	G	6	0.00E+00	B	SB
35	G	6	0.00E+00	B	SB
36	G	6	0.00E+00	B	SB
37	G	6	0.00E+00	B	SB
38	G	6	0.00E+00	B	SB
39	G	6	0.00E+00	B	SB
40	G	6	0.00E+00	B	SB
41	G	6	0.00E+00	B	SB
42	G	6	0.00E+00	B	SB
43	G	6	0.00E+00	B	SB
44	G	6	0.00E+00	B	SB
45	G	6	0.00E+00	B	SB
46	G	6	0.00E+00	B	SB
47	G	6	0.00E+00	B	SB
48	G	6	0.00E+00	B	SB
49	G	6	0.00E+00	B	SB
50	G	6	0.00E+00	B	SB
51	G	6	0.00E+00	B	SB
52	G	6	0.00E+00	B	SB
53	G	6	0.00E+00	B	SB
54	G	6	0.00E+00	B	SB
55	G	6	0.00E+00	B	SB

MAXIMUM SPCFORCES

	T1	T2	T3	R1	R2	R3
1	0.0000000E+00	0.0000000E+00	3.3643913E+00	5.9949631E+01	1.1310131E+01	0.0000000E+00

WINFEM NASTRAN OUTPUT
 WINFEM NASTRAN OUTPUT

SUBCASE 1

D I S P L A C E M E N T V E C T O R

POINT ID.	TYPE	T1	T2	T3	R1	R2	R3
51	G	0.0	0.0	2.621617E-04	1.269192E-04	1.175654E-05	0.0
52	G	0.0	0.0	1.014851E-03	2.424571E-04	3.351587E-05	0.0
53	G	0.0	0.0	2.221921E-03	3.492981E-04	5.378420E-05	0.0
54	G	0.0	0.0	3.834229E-03	4.416518E-04	6.843377E-05	0.0
55	G	0.0	0.0	5.950335E-03	5.957312E-04	8.189050E-05	0.0
56	G	0.0	0.0	8.625716E-03	7.210914E-04	9.303399E-05	0.0
57	G	0.0	0.0	1.174846E-02	8.188677E-04	1.008929E-04	0.0
58	G	0.0	0.0	1.520486E-02	8.884768E-04	1.069754E-04	0.0
59	G	0.0	0.0	1.908078E-02	1.020119E-03	1.121666E-04	0.0
60	G	0.0	0.0	2.335005E-02	1.090081E-03	1.149607E-04	0.0

SUBCASE 1

LOAD VECTOR

POINT ID.	TYPE	T1	T2	T3	R1	R2	R3
2	G	0.0	0.0	1.450000E-01	0.0	0.0	0.0
4	G	0.0	0.0	1.450000E-01	0.0	0.0	0.0
5	G	0.0	0.0	1.450000E-01	0.0	0.0	0.0
6	G	0.0	0.0	1.450000E-01	0.0	0.0	0.0
7	G	0.0	0.0	1.450000E-01	0.0	0.0	0.0
8	G	0.0	0.0	1.450000E-01	0.0	0.0	0.0
9	G	0.0	0.0	1.450000E-01	0.0	0.0	0.0
10	G	0.0	0.0	1.450000E-01	0.0	0.0	0.0
11	G	0.0	0.0	1.450000E-01	0.0	0.0	0.0
12	G	0.0	0.0	1.450000E-01	0.0	0.0	0.0
13	G	0.0	0.0	1.450000E-01	0.0	0.0	0.0
14	G	0.0	0.0	1.450000E-01	0.0	0.0	0.0
15	G	0.0	0.0	1.450000E-01	0.0	0.0	0.0
16	G	0.0	0.0	1.450000E-01	0.0	0.0	0.0
17	G	0.0	0.0	1.450000E-01	0.0	0.0	0.0
18	G	0.0	0.0	1.450000E-01	0.0	0.0	0.0
19	G	0.0	0.0	1.450000E-01	0.0	0.0	0.0
20	G	0.0	0.0	1.450000E-01	0.0	0.0	0.0
21	G	0.0	0.0	1.450000E-01	0.0	0.0	0.0
22	G	0.0	0.0	1.450000E-01	0.0	0.0	0.0
23	G	0.0	0.0	1.450000E-01	0.0	0.0	0.0
24	G	0.0	0.0	1.450000E-01	0.0	0.0	0.0
25	G	0.0	0.0	1.450000E-01	0.0	0.0	0.0
26	G	0.0	0.0	1.450000E-01	0.0	0.0	0.0
27	G	0.0	0.0	1.450000E-01	0.0	0.0	0.0
31	G	0.0	0.0	1.450000E-01	0.0	0.0	0.0
32	G	0.0	0.0	1.450000E-01	0.0	0.0	0.0
33	G	0.0	0.0	1.450000E-01	0.0	0.0	0.0
34	G	0.0	0.0	1.450000E-01	0.0	0.0	0.0
35	G	0.0	0.0	1.450000E-01	0.0	0.0	0.0
36	G	0.0	0.0	1.450000E-01	0.0	0.0	0.0
37	G	0.0	0.0	1.450000E-01	0.0	0.0	0.0
38	G	0.0	0.0	1.450000E-01	0.0	0.0	0.0
39	G	0.0	0.0	1.450000E-01	0.0	0.0	0.0
40	G	0.0	0.0	1.450000E-01	0.0	0.0	0.0
41	G	0.0	0.0	1.450000E-01	0.0	0.0	0.0
42	G	0.0	0.0	1.450000E-01	0.0	0.0	0.0
43	G	0.0	0.0	1.450000E-01	0.0	0.0	0.0
44	G	0.0	0.0	1.450000E-01	0.0	0.0	0.0
45	G	0.0	0.0	1.450000E-01	0.0	0.0	0.0
46	G	0.0	0.0	1.450000E-01	0.0	0.0	0.0
47	G	0.0	0.0	1.450000E-01	0.0	0.0	0.0
48	G	0.0	0.0	1.450000E-01	0.0	0.0	0.0
49	G	0.0	0.0	1.450000E-01	0.0	0.0	0.0
50	G	0.0	0.0	1.450000E-01	0.0	0.0	0.0
51	G	0.0	0.0	1.450000E-01	0.0	0.0	0.0
52	G	0.0	0.0	1.450000E-01	0.0	0.0	0.0
53	G	0.0	0.0	1.450000E-01	0.0	0.0	0.0
54	G	0.0	0.0	1.450000E-01	0.0	0.0	0.0
55	G	0.0	0.0	1.450000E-01	0.0	0.0	0.0

SUBCASE 1

L O A D V E C T O R

POINT ID.	TYPE	T1	T2	T3	R1	R2	R3
56	G	0.0	0.0	1.450000E-01	0.0	0.0	0.0
57	G	0.0	0.0	1.450000E-01	0.0	0.0	0.0
58	G	0.0	0.0	1.450000E-01	0.0	0.0	0.0
59	G	0.0	0.0	1.450000E-01	0.0	0.0	0.0
60	G	0.0	0.0	1.450000E-01	0.0	0.0	0.0

SUBCASE 1

FORCES OF SINGLE-POINT CONSTRAINT

POINT ID.	TYPE	T1	T2	T3	R1	R2	R3
1	G	0.0	0.0	-3.547325E-01	-2.092920E+01	1.131013E+01	0.0
3	G	0.0	0.0	5.586644E-01	-9.528893E+00	-8.691465E+00	0.0
28	G	0.0	0.0	-3.364391E+00	-5.994963E+01	3.713194E+00	0.0
29	G	0.0	0.0	-2.649501E+00	-5.363058E+01	-4.649229E+00	0.0
30	G	0.0	0.0	-2.165038E+00	-4.518658E+01	-9.814965E+00	0.0

WINFEM NASTRAN OUTPUT

SUBCASE 1

FORCES IN QUADRILATERAL ELEMENTS (QUAD4)

ELEMENT ID	MEMBRANE FORCES -			BENDING MOMENTS -			TRANSVERSE SHEAR FORCES -		
	FX	FY	FXV	MX	MY	MXV	QX	QY	QZ
1	0.0	0.0	0.0	2.491438E+00	1.059808E+01	5.523085E-01	-1.523708E-03	4.817711E-01	
2	0.0	0.0	0.0	3.247677E+00	1.115523E+01	1.269674E-01	1.958368E-02	5.578814E-01	
3	0.0	0.0	0.0	2.793676E+00	1.012796E+01	2.641160E-02	2.690110E-02	4.687011E-01	
4	0.0	0.0	0.0	1.781461E+00	7.809033E+00	-4.440301E-01	2.582401E-02	2.981315E-01	
5	0.0	0.0	0.0	9.792652E-01	9.142017E+00	4.288534E-01	-1.110991E-01	4.504421E-01	
6	0.0	0.0	0.0	1.888896E+00	8.681191E+00	-5.774407E-02	3.304183E-02	4.569342E-01	
7	0.0	0.0	0.0	1.683712E+00	8.502654E+00	-5.289294E-01	7.084936E-02	4.330508E-01	
8	0.0	0.0	0.0	9.517034E-01	8.511098E+00	-9.975463E-01	1.199285E-01	3.895956E-01	
9	0.0	0.0	0.0	1.984234E-01	7.572354E+00	-2.134433E-01	-8.701903E-02	4.273285E-01	
10	0.0	0.0	0.0	6.532668E-01	7.396354E+00	-2.018381E-01	-2.133584E-03	4.110470E-01	
11	0.0	0.0	0.0	6.708822E-01	7.339574E+00	-5.200430E-01	7.232195E-02	4.062396E-01	
12	0.0	0.0	0.0	2.738851E-01	7.564283E+00	-5.829919E-01	8.853531E-02	4.088879E-01	
13	0.0	0.0	0.0	-2.799790E-01	6.356520E+00	-3.720208E-01	-7.390767E-02	3.914745E-01	
14	0.0	0.0	0.0	-1.766050E-01	6.280845E+00	-4.104772E-01	-1.257731E-02	3.861265E-01	
15	0.0	0.0	0.0	-1.601062E-01	6.241873E+00	-4.330670E-01	3.043471E-02	3.895513E-01	
16	0.0	0.0	0.0	-2.676837E-01	6.230234E+00	-4.741845E-01	4.551711E-02	4.014108E-01	
17	0.0	0.0	0.0	3.752341E-01	5.180422E+00	-2.619521E-01	-3.327882E-02	3.848199E-01	
18	0.0	0.0	0.0	4.626753E-01	5.086769E+00	-1.678323E-01	-6.458897E-02	3.664811E-01	
19	0.0	0.0	0.0	4.540854E-01	5.056809E+00	-6.709737E-02	1.609548E-02	3.559520E-01	
20	0.0	0.0	0.0	3.354231E-01	5.020164E+00	-2.454071E-02	-2.912935E-02	3.487672E-01	
21	0.0	0.0	0.0	1.871374E-02	3.923165E+00	-4.028698E-01	2.912935E-02	3.487672E-01	
22	0.0	0.0	0.0	9.317148E-02	3.948080E+00	-2.118065E-01	-2.457521E-03	3.305492E-01	
23	0.0	0.0	0.0	8.433080E-02	4.001216E+00	-8.081609E-02	6.330527E-03	3.261869E-01	
24	0.0	0.0	0.0	-2.258503E-03	4.139894E+00	6.771410E-02	2.039972E-02	3.376218E-01	
25	0.0	0.0	0.0	-9.356719E-02	2.865709E+00	-3.887329E-01	-1.071462E-02	3.111618E-01	
26	0.0	0.0	0.0	-1.791834E-01	2.955791E+00	-2.025229E-01	-7.761177E-03	2.958418E-01	
27	0.0	0.0	0.0	-1.854114E-01	3.026046E+00	-5.996224E-02	-5.974591E-03	2.949134E-01	
28	0.0	0.0	0.0	-1.251113E-01	3.106761E+00	1.512318E-01	-1.447678E-02	3.064834E-01	
29	0.0	0.0	0.0	-2.469372E-01	2.045205E+00	-2.863203E-01	-1.277473E-03	2.640591E-01	
30	0.0	0.0	0.0	-3.902671E-01	2.072139E+00	-1.957286E-01	-1.747753E-02	2.598812E-01	
31	0.0	0.0	0.0	-4.059278E-01	2.093821E+00	-6.598895E-02	-3.142205E-02	2.613999E-01	
32	0.0	0.0	0.0	-2.903033E-01	2.099220E+00	5.823481E-02	-5.403478E-02	2.668344E-01	
33	0.0	0.0	0.0	1.206159E-01	1.278478E+00	-8.780938E-02	-4.414350E-04	2.191309E-01	
34	0.0	0.0	0.0	1.141374E-01	1.255267E+00	-3.185914E-02	6.607637E-03	2.126546E-01	
35	0.0	0.0	0.0	1.100704E-01	1.253093E+00	3.384198E-02	1.323308E-02	2.087178E-01	
36	0.0	0.0	0.0	1.049548E-01	1.254295E+00	8.041638E-02	1.941824E-02	2.070866E-01	
37	0.0	0.0	0.0	-3.412861E-02	5.649182E-01	-1.140088E-01	-4.331484E-03	1.587872E-01	
38	0.0	0.0	0.0	-3.098023E-02	6.008345E-01	-4.473559E-02	4.104804E-03	1.545656E-01	
39	0.0	0.0	0.0	-3.306207E-02	6.285371E-01	9.112764E-03	3.083591E-03	1.531541E-01	
40	0.0	0.0	0.0	-3.396520E-02	6.677556E-01	7.526475E-02	1.015851E-02	1.557613E-01	
41	0.0	0.0	0.0	-5.340894E-02	1.464387E-01	-7.589912E-02	-1.788895E-03	8.816111E-02	
42	0.0	0.0	0.0	-9.612647E-02	1.653169E-01	-3.769567E-02	-9.041380E-03	8.687776E-02	
43	0.0	0.0	0.0	-1.023386E-01	1.800566E-01	2.890768E-03	-1.428624E-02	8.680427E-02	
44	0.0	0.0	0.0	-6.719130E-02	1.889840E-01	5.300003E-02	-2.417379E-02	8.680385E-02	

STRESSES AT GRID POINTS - - SURFACE 1

GRID ID	ELEMENT ID	FIBER	SURFACE X-AXIS X NORMAL(Z-AXIS) Z STRESSES IN ELEMENT SYSTEM			REFERENCE COORDINATE SYSTEM FOR SURFACE			MAX SHEAR	VON MISES	DEFINITION CID
			NORMAL-X	NORMAL-Y	SHEAR-XY	ANGLE	MAJOR	MINOR			
1	0	Z1	1.055E+00	4.211E+00	3.137E-01	84.3778	4.242E+00	1.024E+00	1.609E+00	3.834E+00	0
		Z2	-1.055E+00	-4.211E+00	-3.137E-01	-5.6222	-1.024E+00	-4.242E+00	1.609E+00	3.834E+00	
		MID	0.000E+00	0.000E+00	0.000E+00	0.0	0.000E+00	0.000E+00	0.000E+00	0.000E+00	
2	0	Z1	-1.434E-01	-2.083E-01	-2.280E-01	-40.9525	5.442E-02	-4.062E-01	2.303E-01	4.359E-01	0
		Z2	1.434E-01	2.083E-01	2.280E-01	49.0474	4.062E-01	-5.442E-02	2.303E-01	4.359E-01	
		MID	0.000E+00	0.000E+00	0.000E+00	0.0	0.000E+00	0.000E+00	0.000E+00	0.000E+00	
3	0	Z1	6.558E-01	2.563E+00	-1.498E-01	-85.5378	2.575E+00	6.441E-01	9.654E-01	2.321E+00	0
		Z2	-6.558E-01	-2.563E+00	1.498E-01	4.4621	-6.441E-01	-2.575E+00	9.654E-01	2.321E+00	
		MID	0.000E+00	0.000E+00	0.000E+00	0.0	0.000E+00	0.000E+00	0.000E+00	0.000E+00	
4	0	Z1	-2.050E-01	-1.046E-01	1.932E-01	52.2810	4.485E-02	-3.544E-01	1.996E-01	3.788E-01	0
		Z2	2.050E-01	1.046E-01	-1.932E-01	-37.7190	3.544E-01	-4.485E-02	1.996E-01	3.788E-01	
		MID	0.000E+00	0.000E+00	0.000E+00	0.0	0.000E+00	0.000E+00	0.000E+00	0.000E+00	
5	0	Z1	-9.091E-02	9.317E-01	-3.318E-01	-73.5085	1.030E+00	-1.892E-01	6.096E-01	1.136E+00	0
		Z2	9.091E-02	-9.317E-01	3.318E-01	16.4915	1.892E-01	-1.030E+00	6.096E-01	1.136E+00	
		MID	0.000E+00	0.000E+00	0.000E+00	0.0	0.000E+00	0.000E+00	0.000E+00	0.000E+00	
6	0	Z1	1.200E-01	2.502E+00	-3.601E-01	-81.5873	2.555E+00	6.677E-02	1.244E+00	2.522E+00	0
		Z2	-1.200E-01	-2.502E+00	3.601E-01	8.4127	-6.677E-02	-2.555E+00	1.244E+00	2.522E+00	
		MID	0.000E+00	0.000E+00	0.000E+00	0.0	0.000E+00	0.000E+00	0.000E+00	0.000E+00	
7	0	Z1	-9.907E-02	2.564E+00	-2.893E-01	-83.3927	2.597E+00	6.555E-02	1.266E+00	2.565E+00	0
		Z2	9.907E-02	-2.564E+00	2.893E-01	6.6073	-6.555E-02	-2.597E+00	1.266E+00	2.565E+00	
		MID	0.000E+00	0.000E+00	0.000E+00	0.0	0.000E+00	0.000E+00	0.000E+00	0.000E+00	
8	0	Z1	-8.975E-02	1.926E+00	-3.229E-01	-81.1185	1.977E+00	-1.402E-01	1.059E+00	2.051E+00	0
		Z2	8.975E-02	-1.926E+00	3.229E-01	8.8814	1.402E-01	-1.977E+00	1.059E+00	2.051E+00	
		MID	0.000E+00	0.000E+00	0.000E+00	0.0	0.000E+00	0.000E+00	0.000E+00	0.000E+00	
9	0	Z1	-2.750E-02	2.673E+00	-3.892E-01	-81.9596	2.728E+00	-8.248E-02	1.405E+00	2.770E+00	0
		Z2	2.750E-02	-2.673E+00	3.892E-01	8.0404	-8.248E-02	-2.728E+00	1.405E+00	2.770E+00	
		MID	0.000E+00	0.000E+00	0.000E+00	0.0	0.000E+00	0.000E+00	0.000E+00	0.000E+00	
10	0	Z1	1.242E-01	3.828E+00	-3.206E-01	-84.8150	3.657E+00	9.516E-02	1.781E+00	3.610E+00	0
		Z2	-1.242E-01	-3.828E+00	3.206E-01	5.1850	-9.516E-02	-3.657E+00	1.781E+00	3.610E+00	
		MID	0.000E+00	0.000E+00	0.000E+00	0.0	0.000E+00	0.000E+00	0.000E+00	0.000E+00	
11	0	Z1	6.981E-02	3.266E+00	-1.884E-01	-86.6386	3.277E+00	5.875E-02	1.609E+00	3.248E+00	0
		Z2	-6.981E-02	-3.266E+00	1.884E-01	3.3613	-5.875E-02	-3.277E+00	1.609E+00	3.248E+00	
		MID	0.000E+00	0.000E+00	0.000E+00	0.0	0.000E+00	0.000E+00	0.000E+00	0.000E+00	
12	0	Z1	-6.719E-02	2.618E+00	-1.066E-01	-87.7310	2.622E+00	-7.141E-02	1.347E+00	2.659E+00	0
		Z2	6.719E-02	-2.618E+00	1.066E-01	2.2690	7.141E-02	-2.622E+00	1.347E+00	2.659E+00	
		MID	0.000E+00	0.000E+00	0.000E+00	0.0	0.000E+00	0.000E+00	0.000E+00	0.000E+00	
13	0	Z1	9.231E-02	3.173E+00	8.439E-02	88.4321	3.175E+00	9.000E-02	1.543E+00	3.131E+00	0
		Z2	-9.231E-02	-3.173E+00	-8.439E-02	-88.4321	-3.175E+00	-9.000E-02	-1.543E+00	-3.131E+00	
		MID	0.000E+00	0.000E+00	0.000E+00	0.0	0.000E+00	0.000E+00	0.000E+00	0.000E+00	

PROCEEDING PAGE BLANK NOT FILMED

1 SUBCASE = 1

STRESSES AT GRID POINTS -- SURFACE 1

GRID ID ELEMENT ID SURFACE X-AXIS X STRESSES IN ELEMENT SYSTEM Z NORMAL(Y) SHEAR(XY) REFERENCE COORDINATE SYSTEM FOR SURFACE DEFINITION CID

GRID ID	ELEMENT ID	SURFACE	STRESSES IN ELEMENT SYSTEM Z			REFERENCE COORDINATE SYSTEM FOR SURFACE DEFINITION CID			MAX SHEAR	VON MISES
			NORMAL-X	NORMAL-Y	SHEAR-XY	ANGLE	MAJOR	MINOR		
14	0	Z1	4.913E-01	3.688E+00	2.677E-01	85.2167	3.691E+00	4.689E-01	1.611E+00	3.480E+00
		Z2	-4.913E-01	-3.668E+00	-2.677E-01	-4.7833	-4.689E-01	-3.691E+00	1.611E+00	3.480E+00
		MID	0.000E+00	0.000E+00	0.000E+00	0.0	0.000E+00	0.000E+00	0.000E+00	0.000E+00
15	0	Z1	3.466E-01	2.825E+00	-3.560E-01	-81.9851	2.875E+00	2.965E-01	1.289E+00	2.739E+00
		Z2	-3.466E-01	-2.825E+00	3.560E-01	8.0149	-2.965E-01	-2.875E+00	1.289E+00	2.739E+00
		MID	0.000E+00	0.000E+00	0.000E+00	0.0	0.000E+00	0.000E+00	0.000E+00	0.000E+00
16	0	Z1	1.232E-01	3.016E+00	-3.439E-01	-83.3125	3.057E+00	8.283E-02	1.487E+00	3.016E+00
		Z2	-1.232E-01	-3.016E+00	3.439E-01	6.6875	-8.283E-02	-3.057E+00	1.487E+00	3.016E+00
		MID	0.000E+00	0.000E+00	0.000E+00	0.0	0.000E+00	0.000E+00	0.000E+00	0.000E+00
17	0	Z1	-4.585E-02	2.589E+00	-2.066E-01	-85.5440	2.606E+00	-6.195E-02	1.334E+00	2.637E+00
		Z2	4.585E-02	-2.589E+00	2.066E-01	4.4560	6.195E-02	-2.606E+00	1.334E+00	2.637E+00
		MID	0.000E+00	0.000E+00	0.000E+00	0.0	0.000E+00	0.000E+00	0.000E+00	0.000E+00
18	0	Z1	4.971E-02	3.145E+00	-9.347E-02	-88.2720	3.148E+00	4.689E-02	1.551E+00	3.125E+00
		Z2	-4.971E-02	-3.145E+00	9.347E-02	1.7280	-4.689E-02	-3.148E+00	1.551E+00	3.125E+00
		MID	0.000E+00	0.000E+00	0.000E+00	0.0	0.000E+00	0.000E+00	0.000E+00	0.000E+00
19	0	Z1	9.420E-02	3.657E+00	5.509E-02	89.1143	3.658E+00	9.334E-02	1.782E+00	3.612E+00
		Z2	-9.420E-02	-3.657E+00	-5.509E-02	-0.8856	-9.334E-02	-3.658E+00	1.782E+00	3.612E+00
		MID	0.000E+00	0.000E+00	0.000E+00	0.0	0.000E+00	0.000E+00	0.000E+00	0.000E+00
20	0	Z1	-5.309E-02	2.921E+00	1.583E-01	86.9612	2.929E+00	-6.150E-02	1.495E+00	2.960E+00
		Z2	5.309E-02	-2.921E+00	-1.583E-01	-3.0388	6.150E-02	-2.929E+00	1.495E+00	2.960E+00
		MID	0.000E+00	0.000E+00	0.000E+00	0.0	0.000E+00	0.000E+00	0.000E+00	0.000E+00
21	0	Z1	-1.300E-01	2.084E+00	1.497E-01	86.1480	2.094E+00	-1.401E-01	1.117E+00	2.167E+00
		Z2	1.300E-01	-2.084E+00	-1.497E-01	-3.8520	1.401E-01	-2.094E+00	1.117E+00	2.167E+00
		MID	0.000E+00	0.000E+00	0.000E+00	0.0	0.000E+00	0.000E+00	0.000E+00	0.000E+00
22	0	Z1	4.713E-02	2.543E+00	1.890E-01	85.6947	2.558E+00	3.290E-02	1.262E+00	2.541E+00
		Z2	-4.713E-02	-2.543E+00	-1.890E-01	-4.3053	-3.290E-02	-2.558E+00	1.262E+00	2.541E+00
		MID	0.000E+00	0.000E+00	0.000E+00	0.0	0.000E+00	0.000E+00	0.000E+00	0.000E+00
23	0	Z1	9.256E-02	2.645E+00	2.888E-01	83.6251	2.677E+00	6.030E-02	1.309E+00	2.648E+00
		Z2	-9.256E-02	-2.645E+00	-2.888E-01	-6.3749	-6.030E-02	-2.677E+00	1.309E+00	2.648E+00
		MID	0.000E+00	0.000E+00	0.000E+00	0.0	0.000E+00	0.000E+00	0.000E+00	0.000E+00
24	0	Z1	-1.144E-01	1.200E+00	2.539E-01	79.4381	1.247E+00	-1.618E-01	7.044E-01	1.335E+00
		Z2	1.144E-01	-1.200E+00	-2.539E-01	-10.5619	1.618E-01	-1.247E+00	7.044E-01	1.335E+00
		MID	0.000E+00	0.000E+00	0.000E+00	0.0	0.000E+00	0.000E+00	0.000E+00	0.000E+00
25	0	Z1	-3.007E-01	1.289E-01	5.672E-02	73.2825	-1.119E-01	-3.177E-01	1.029E-01	2.792E-01
		Z2	3.007E-01	-1.289E-01	-5.672E-02	-16.7175	3.177E-01	1.119E-01	-1.029E-01	-2.792E-01
		MID	0.000E+00	0.000E+00	0.000E+00	0.0	0.000E+00	0.000E+00	0.000E+00	0.000E+00

SUBCASE 1

1 S T R E S S E S A T G R I D P O I N T S - - S U R F A C E 1

GRID ID	ELEMENT ID	FIBER	SURFACE X-AXIS X STRESSES IN ELEMENT SYSTEM			ANGLE	REFERENCE COORDINATE SYSTEM FOR SURFACE DEFINITION CID			VON MISES
			NORMAL-X	NORMAL-Y	SHEAR-XY		MAJOR	MINOR	MAX SHEAR	
26	0	Z1	-3.659E-01	-1.315E-01	-4.685E-02	-79.1057	-1.275E-01	-3.749E-01	1.262E-01	3.311E-01
		Z2	3.659E-01	1.315E-01	4.685E-02	10.8943	3.749E-01	1.225E-01	1.262E-01	3.311E-01
		MID	0.000E+00	0.000E+00	0.000E+00	0.0	0.000E+00	0.000E+00	0.000E+00	0.000E+00
27	0	Z1	-2.652E-01	-1.569E-01	-1.239E-01	-56.8047	-7.579E-02	-3.463E-01	1.353E-01	3.153E-01
		Z2	2.652E-01	1.569E-01	1.239E-01	33.1953	3.463E-01	7.579E-02	1.353E-01	3.153E-01
		MID	0.000E+00	0.000E+00	0.000E+00	0.0	0.000E+00	0.000E+00	0.000E+00	0.000E+00
28	0	Z1	1.337E+00	4.418E+00	1.552E-01	87.1234	4.426E+00	1.329E+00	1.549E+00	3.934E+00
		Z2	-1.337E+00	-4.418E+00	-1.552E-01	-2.8766	-1.329E+00	-4.426E+00	1.549E+00	3.934E+00
		MID	0.000E+00	0.000E+00	0.000E+00	0.0	0.000E+00	0.000E+00	0.000E+00	0.000E+00
29	0	Z1	1.355E+00	4.346E+00	9.750E-02	88.1349	4.350E+00	1.352E+00	1.499E+00	3.856E+00
		Z2	-1.355E+00	-4.346E+00	-9.750E-02	-1.8651	-1.352E+00	-4.350E+00	1.499E+00	3.856E+00
		MID	0.000E+00	0.000E+00	0.000E+00	0.0	0.000E+00	0.000E+00	0.000E+00	0.000E+00
30	0	Z1	1.033E+00	3.427E+00	2.550E-02	89.3900	3.428E+00	1.033E+00	1.197E+00	3.045E+00
		Z2	-1.033E+00	-3.427E+00	-2.550E-02	-0.6100	-1.033E+00	-3.428E+00	1.197E+00	3.045E+00
		MID	0.000E+00	0.000E+00	0.000E+00	0.0	0.000E+00	0.000E+00	0.000E+00	0.000E+00
31	0	Z1	8.017E-01	3.686E+00	9.782E-02	88.0600	3.689E+00	7.984E-01	1.446E+00	3.362E+00
		Z2	-8.017E-01	-3.686E+00	-9.782E-02	-1.9400	-7.984E-01	-3.689E+00	1.446E+00	3.362E+00
		MID	0.000E+00	0.000E+00	0.000E+00	0.0	0.000E+00	0.000E+00	0.000E+00	0.000E+00
32	0	Z1	3.465E-01	3.054E+00	-4.098E-03	-89.9133	3.054E+00	3.465E-01	1.354E+00	2.897E+00
		Z2	-3.465E-01	-3.054E+00	4.098E-03	0.0867	-3.465E-01	-3.054E+00	1.354E+00	2.897E+00
		MID	0.000E+00	0.000E+00	0.000E+00	0.0	0.000E+00	0.000E+00	0.000E+00	0.000E+00
33	0	Z1	3.678E-02	2.571E+00	-1.116E-01	-87.4843	2.576E+00	3.188E-02	1.272E+00	2.560E+00
		Z2	-3.678E-02	-2.571E+00	1.116E-01	2.5157	-3.188E-02	-2.576E+00	1.272E+00	2.560E+00
		MID	0.000E+00	0.000E+00	0.000E+00	0.0	0.000E+00	0.000E+00	0.000E+00	0.000E+00
34	0	Z1	1.238E-01	3.215E+00	-1.582E-01	-87.0781	3.223E+00	1.157E-01	1.554E+00	3.167E+00
		Z2	-1.238E-01	-3.215E+00	1.582E-01	2.9219	-1.157E-01	-3.223E+00	1.554E+00	3.167E+00
		MID	0.000E+00	0.000E+00	0.000E+00	0.0	0.000E+00	0.000E+00	0.000E+00	0.000E+00
35	0	Z1	1.885E-01	3.601E+00	-2.073E-01	-86.5855	3.613E+00	1.760E-01	1.719E+00	3.528E+00
		Z2	-1.885E-01	-3.601E+00	2.073E-01	3.4645	-1.760E-01	-3.613E+00	1.719E+00	3.528E+00
		MID	0.000E+00	0.000E+00	0.000E+00	0.0	0.000E+00	0.000E+00	0.000E+00	0.000E+00
36	0	Z1	-3.192E-02	2.718E+00	-2.394E-01	-85.0617	2.739E+00	-5.261E-02	1.396E+00	2.766E+00
		Z2	3.192E-02	-2.718E+00	2.394E-01	4.9383	-5.261E-02	-2.739E+00	1.396E+00	2.766E+00
		MID	0.000E+00	0.000E+00	0.000E+00	0.0	0.000E+00	0.000E+00	0.000E+00	0.000E+00
37	0	Z1	-1.806E-01	1.973E+00	-2.131E-01	-84.4037	1.994E+00	-2.015E-01	1.098E+00	2.102E+00
		Z2	1.806E-01	-1.973E+00	2.131E-01	5.5962	-2.015E-01	-1.994E+00	1.098E+00	2.102E+00
		MID	0.000E+00	0.000E+00	0.000E+00	0.0	0.000E+00	0.000E+00	0.000E+00	0.000E+00
38	0	Z1	3.333E-02	2.543E+00	-1.772E-01	-85.9809	2.555E+00	2.088E-02	1.267E+00	2.545E+00
		Z2	-3.333E-02	-2.543E+00	1.772E-01	0.0	-2.088E-02	-2.555E+00	1.267E+00	2.545E+00
		MID	0.000E+00	0.000E+00	0.000E+00	0.0	0.000E+00	0.000E+00	0.000E+00	0.000E+00

WINFEM NASTRAN OUTPUT SUBCASE = 1 SUBCASE 1

S T R E S S E S A T G R I D P O I N T S - - S U R F A C E 1

GRID ID	ELEMENT ID	SURFACE X-AXIS X			NORMAL(Z-AXIS) Z			REFERENCE COORDINATE SYSTEM FOR SURFACE DEFINITION CID			VON MISES	
		FIBER	NORMAL-X	NORMAL-Y	SHEAR-XY	FIBER	NORMAL-X	NORMAL-Y	SHEAR-XY	MAX		
39	0	Z1	1.155E-01	2.519E+00	-1.896E-01	-85.5178	2.534E+00	1.006E-01	1.217E+00	1.217E+00	2.485E+00	
		Z2	-1.155E-01	-2.519E+00	1.896E-01	4.4822	-1.006E-01	-2.534E+00	-2.534E+00	1.217E+00	1.217E+00	2.485E+00
		MID	0.000E+00	0.000E+00	0.000E+00	0.0	0.000E+00	0.000E+00	0.000E+00	0.000E+00	0.000E+00	0.000E+00
40	0	Z1	-1.475E-01	1.006E+00	-1.855E-01	-81.0867	1.035E+00	-1.768E-01	6.059E-01	6.059E-01	1.134E+00	
		Z2	1.475E-01	-1.006E+00	1.855E-01	8.9132	-1.766E-01	-1.035E+00	1.766E-01	6.059E-01	6.059E-01	1.134E+00
		MID	0.000E+00	0.000E+00	0.000E+00	0.0	0.000E+00	0.000E+00	0.000E+00	0.000E+00	0.000E+00	0.000E+00
41	0	Z1	8.954E-01	3.583E+00	-4.036E-02	-89.1398	3.583E+00	8.948E-01	1.344E+00	1.344E+00	3.230E+00	
		Z2	-8.954E-01	-3.583E+00	4.036E-02	0.8602	-8.948E-01	-3.583E+00	-3.583E+00	1.344E+00	1.344E+00	3.230E+00
		MID	0.000E+00	0.000E+00	0.000E+00	0.0	0.000E+00	0.000E+00	0.000E+00	0.000E+00	0.000E+00	0.000E+00
42	0	Z1	4.561E-01	2.973E+00	-1.219E-01	-87.2340	2.979E+00	4.502E-01	1.264E+00	1.264E+00	2.781E+00	
		Z2	-4.561E-01	-2.973E+00	1.219E-01	2.7660	-4.502E-01	-2.979E+00	-2.979E+00	1.264E+00	1.264E+00	2.781E+00
		MID	0.000E+00	0.000E+00	0.000E+00	0.0	0.000E+00	0.000E+00	0.000E+00	0.000E+00	0.000E+00	0.000E+00
43	0	Z1	9.195E-02	2.539E+00	-1.458E-01	-86.6020	2.547E+00	8.329E-02	1.232E+00	1.232E+00	2.507E+00	
		Z2	-9.195E-02	-2.539E+00	1.458E-01	3.3980	-8.329E-02	-2.547E+00	-2.547E+00	1.232E+00	1.232E+00	2.507E+00
		MID	0.000E+00	0.000E+00	0.000E+00	0.0	0.000E+00	0.000E+00	0.000E+00	0.000E+00	0.000E+00	0.000E+00
44	0	Z1	1.508E-01	3.180E+00	-1.252E-01	-87.6372	3.185E+00	1.454E-01	1.520E+00	1.520E+00	3.115E+00	
		Z2	-1.508E-01	-3.180E+00	1.252E-01	2.3628	-1.454E-01	-3.185E+00	-3.185E+00	1.520E+00	1.520E+00	3.115E+00
		MID	0.000E+00	0.000E+00	0.000E+00	0.0	0.000E+00	0.000E+00	0.000E+00	0.000E+00	0.000E+00	0.000E+00
45	0	Z1	2.172E-01	3.592E+00	-1.047E-01	-88.2239	3.595E+00	2.140E-01	1.690E+00	1.690E+00	3.493E+00	
		Z2	-2.172E-01	-3.592E+00	1.047E-01	1.7761	-2.140E-01	-3.595E+00	-3.595E+00	1.690E+00	1.690E+00	3.493E+00
		MID	0.000E+00	0.000E+00	0.000E+00	0.0	0.000E+00	0.000E+00	0.000E+00	0.000E+00	0.000E+00	0.000E+00
46	0	Z1	-3.713E-02	2.766E+00	-1.102E-01	-87.7520	2.770E+00	-4.145E-02	1.406E+00	1.406E+00	2.791E+00	
		Z2	3.713E-02	-2.766E+00	1.102E-01	2.2479	4.145E-02	-2.770E+00	-2.770E+00	1.406E+00	1.406E+00	2.791E+00
		MID	0.000E+00	0.000E+00	0.000E+00	0.0	0.000E+00	0.000E+00	0.000E+00	0.000E+00	0.000E+00	0.000E+00
47	0	Z1	-2.304E-01	2.014E+00	-1.041E-01	-87.3515	2.019E+00	-2.353E-01	1.127E+00	1.127E+00	2.147E+00	
		Z2	2.304E-01	-2.014E+00	1.041E-01	2.6485	2.353E-01	-2.019E+00	-2.019E+00	1.127E+00	1.127E+00	2.147E+00
		MID	0.000E+00	0.000E+00	0.000E+00	0.0	0.000E+00	0.000E+00	0.000E+00	0.000E+00	0.000E+00	0.000E+00
48	0	Z1	-5.416E-03	2.535E+00	-5.060E-02	-88.8595	2.536E+00	-6.423E-03	1.271E+00	1.271E+00	2.539E+00	
		Z2	5.416E-03	-2.535E+00	5.060E-02	1.1405	6.423E-03	-2.536E+00	-2.536E+00	1.271E+00	1.271E+00	2.539E+00
		MID	0.000E+00	0.000E+00	0.000E+00	0.0	0.000E+00	0.000E+00	0.000E+00	0.000E+00	0.000E+00	0.000E+00
49	0	Z1	1.090E-01	2.545E+00	-2.293E-02	-89.4608	2.545E+00	1.088E-01	1.218E+00	1.218E+00	2.493E+00	
		Z2	-1.090E-01	-2.545E+00	2.293E-02	0.5392	-1.088E-01	-2.545E+00	-2.545E+00	1.218E+00	1.218E+00	2.493E+00
		MID	0.000E+00	0.000E+00	0.000E+00	0.0	0.000E+00	0.000E+00	0.000E+00	0.000E+00	0.000E+00	0.000E+00
50	0	Z1	-1.801E-01	1.072E+00	-4.794E-02	-87.8109	1.074E+00	-1.819E-01	6.280E-01	6.280E-01	1.176E+00	
		Z2	1.801E-01	-1.072E+00	4.794E-02	2.1890	1.819E-01	-1.074E+00	-1.074E+00	6.280E-01	6.280E-01	1.176E+00
		MID	0.000E+00	0.000E+00	0.000E+00	0.0	0.000E+00	0.000E+00	0.000E+00	0.000E+00	0.000E+00	0.000E+00

WTFE00 "NASTRAN" OUTPUT
 .NFEM NASTRAN OUTPUT
 SUBCASE =

SUBCASE 1

STRESSES AT GRID POINTS -- SURFACE 1		REFERENCE COORDINATE SYSTEM FOR SURFACE DEFINITION CID 0									
GRID ID	ELEMENT ID	SURFACE X-AXIS X STRESSES IN ELEMENT SYSTEM		PRINCIPAL STRESSES		MAX SHEAR	VON MISES				
		NORMAL-X	NORMAL-Y	ANGLE	MAJOR			MINOR			
51	0	Z1	6.716E-01	3.255E+00	-1.811E-01	-86.0103	3.268E+00	6.589E-01	1.304E+00	1.304E+00	2.993E+00
		Z2	-6.716E-01	-3.255E+00	1.811E-01	3.9897	-6.589E-01	-3.268E+00	1.304E+00	1.304E+00	2.993E+00
		MID	0.000E+00	0.000E+00	0.000E+00	0.0	0.000E+00	0.000E+00	0.000E+00	0.000E+00	0.000E+00
52	0	Z1	3.335E-01	2.973E+00	-2.449E-01	-84.7432	2.995E+00	3.110E-01	1.342E+00	1.342E+00	2.853E+00
		Z2	-3.335E-01	-2.973E+00	2.449E-01	5.2568	-3.110E-01	-2.995E+00	1.342E+00	1.342E+00	2.853E+00
		MID	0.000E+00	0.000E+00	0.000E+00	0.0	0.000E+00	0.000E+00	0.000E+00	0.000E+00	0.000E+00
53	0	Z1	4.813E-02	2.550E+00	-1.872E-01	-85.7432	2.564E+00	3.419E-02	1.265E+00	1.265E+00	2.547E+00
		Z2	-4.813E-02	-2.550E+00	1.872E-01	4.2568	-3.419E-02	-2.564E+00	1.265E+00	1.265E+00	2.547E+00
		MID	0.000E+00	0.000E+00	0.000E+00	0.0	0.000E+00	0.000E+00	0.000E+00	0.000E+00	0.000E+00
54	0	Z1	1.169E-01	3.162E+00	-1.027E-01	-88.0705	3.165E+00	1.134E-01	1.528E+00	1.528E+00	3.110E+00
		Z2	-1.169E-01	-3.162E+00	1.027E-01	1.9295	-1.134E-01	-3.165E+00	1.528E+00	1.528E+00	3.110E+00
		MID	0.000E+00	0.000E+00	0.000E+00	0.0	0.000E+00	0.000E+00	0.000E+00	0.000E+00	0.000E+00
55	0	Z1	1.739E-01	3.616E+00	-2.079E-02	-89.6540	3.617E+00	1.738E-01	1.721E+00	1.721E+00	3.533E+00
		Z2	-1.739E-01	-3.616E+00	2.079E-02	0.3460	-1.738E-01	-3.617E+00	1.721E+00	1.721E+00	3.533E+00
		MID	0.000E+00	0.000E+00	0.000E+00	0.0	0.000E+00	0.000E+00	0.000E+00	0.000E+00	0.000E+00
56	0	Z1	-4.444E-02	2.834E+00	1.551E-02	89.6912	2.834E+00	-4.453E-02	1.439E+00	1.439E+00	2.856E+00
		Z2	4.444E-02	-2.834E+00	-1.551E-02	-0.3088	4.453E-02	-2.834E+00	1.439E+00	1.439E+00	2.856E+00
		MID	0.000E+00	0.000E+00	0.000E+00	0.0	0.000E+00	0.000E+00	0.000E+00	0.000E+00	0.000E+00
57	0	Z1	-1.999E-01	2.050E+00	1.658E-02	89.5779	2.050E+00	-2.000E-01	1.125E+00	1.125E+00	2.157E+00
		Z2	1.999E-01	-2.050E+00	-1.658E-02	-0.4221	2.000E-01	-2.050E+00	1.125E+00	1.125E+00	2.157E+00
		MID	0.000E+00	0.000E+00	0.000E+00	0.0	0.000E+00	0.000E+00	0.000E+00	0.000E+00	0.000E+00
58	0	Z1	8.174E-03	2.540E+00	7.624E-02	88.2765	2.542E+00	5.881E-03	1.268E+00	1.268E+00	2.539E+00
		Z2	-8.174E-03	-2.540E+00	-7.624E-02	-1.7235	-5.881E-03	-2.542E+00	1.268E+00	1.268E+00	2.539E+00
		MID	0.000E+00	0.000E+00	0.000E+00	0.0	0.000E+00	0.000E+00	0.000E+00	0.000E+00	0.000E+00
59	0	Z1	1.008E-01	2.590E+00	1.353E-01	86.8984	2.597E+00	9.343E-02	1.252E+00	1.252E+00	2.552E+00
		Z2	-1.008E-01	-2.590E+00	-1.353E-01	-3.1016	-9.343E-02	-2.597E+00	1.252E+00	1.252E+00	2.552E+00
		MID	0.000E+00	0.000E+00	0.000E+00	0.0	0.000E+00	0.000E+00	0.000E+00	0.000E+00	0.000E+00
60	0	Z1	-1.611E-01	1.134E+00	9.552E-02	85.8046	1.141E+00	-1.681E-01	6.546E-01	6.546E-01	1.234E+00
		Z2	1.611E-01	-1.134E+00	-9.552E-02	-4.1954	1.681E-01	-1.141E+00	6.546E-01	6.546E-01	1.234E+00
		MID	0.000E+00	0.000E+00	0.000E+00	0.0	0.000E+00	0.000E+00	0.000E+00	0.000E+00	0.000E+00

ELEMENT ID.	FIBRE DISTANCE	STRESSES IN ELEMENT COORD SYSTEM		SHEAR-XY	ANGLE	PRINCIPAL STRESSES (ZERO SHEAR)		VON MISES
		NORMAL-X	NORMAL-Y			MAJOR	MINOR	
17	-2.300000E-02	2.979532E-01	4.113494E+00	-2.080021E-01	-86.8888	4.124800E+00	2.866476E-01	3.989207E+00
	2.300000E-02	-2.979532E-01	-4.113494E+00	2.080021E-01	3.1112	-2.866476E-01	-4.124800E+00	3.989207E+00
18	-2.300000E-02	3.673856E-01	4.039130E+00	-1.332266E-01	-87.9241	4.043981E+00	3.625550E-01	3.875423E+00
	2.300000E-02	-3.673856E-01	-4.039130E+00	1.332266E-01	2.0759	-3.625550E-01	-4.043981E+00	3.875423E+00
19	-2.300000E-02	3.605648E-01	4.015341E+00	-5.327843E-02	-89.1650	4.016117E+00	3.597863E-01	3.848856E+00
	2.300000E-02	-3.605648E-01	-4.015341E+00	5.327843E-02	0.8350	-3.597863E-01	-4.016117E+00	3.848856E+00
20	-2.300000E-02	2.663415E-01	3.986241E+00	-1.948646E-02	-89.6999	3.986343E+00	2.662394E-01	3.860116E+00
	2.300000E-02	-2.663415E-01	-3.986241E+00	1.948646E-02	0.3001	-2.662394E-01	-3.986343E+00	3.860116E+00
21	-2.300000E-02	1.485958E-02	3.115174E+00	-3.198974E-01	-84.1699	3.147838E+00	-1.780400E-02	3.156777E+00
	2.300000E-02	-1.485958E-02	-3.115174E+00	3.198974E-01	5.8301	1.780400E-02	-3.147838E+00	3.156777E+00
22	-2.300000E-02	7.398248E-02	3.134958E+00	-1.681842E-01	-86.8645	3.144172E+00	6.476939E-02	3.112292E+00
	2.300000E-02	-7.398248E-02	-3.134958E+00	1.681842E-01	3.1355	-6.476939E-02	-3.144172E+00	3.112292E+00
23	-2.300000E-02	6.696254E-02	3.177151E+00	-6.417173E-02	-88.8185	3.178473E+00	6.563908E-02	3.146168E+00
	2.300000E-02	-6.696254E-02	-3.177151E+00	6.417173E-02	1.1815	-6.563908E-02	-3.178473E+00	3.146168E+00
24	-2.300000E-02	1.793356E-03	3.287268E+00	5.376816E-02	89.0627	3.288148E+00	9.136531E-04	3.287691E+00
	2.300000E-02	-1.793356E-03	-3.287268E+00	-5.376816E-02	-0.9373	-9.136531E-04	-3.288148E+00	3.287691E+00
25	-2.300000E-02	7.429665E-02	2.275505E+00	-3.086718E-01	-82.6399	2.315376E+00	-1.141675E-01	2.374519E+00
	2.300000E-02	-7.429665E-02	-2.275505E+00	3.086718E-01	7.3601	1.141675E-01	-2.315376E+00	2.374519E+00
26	-2.300000E-02	-1.422799E-01	2.347034E+00	-1.608126E-01	-86.3190	2.357380E+00	-1.526256E-01	2.437280E+00
	2.300000E-02	1.422799E-01	-2.347034E+00	1.608126E-01	3.6810	1.526256E-01	-2.357380E+00	2.437280E+00
27	-2.300000E-02	-1.472253E-01	2.402821E+00	-4.761279E-02	-88.9307	2.403708E+00	-1.481139E-01	2.481084E+00
	2.300000E-02	1.472253E-01	-2.402821E+00	4.761279E-02	1.0693	1.481139E-01	-2.403708E+00	2.481084E+00
28	-2.300000E-02	-9.934419E-02	2.468912E+00	1.200851E-01	87.3267	2.472519E+00	-1.049512E-01	2.526630E+00
	2.300000E-02	9.934419E-02	-2.468912E+00	-1.200851E-01	-2.6733	1.049512E-01	-2.472519E+00	2.526630E+00
29	-2.300000E-02	-1.960796E-01	1.623987E+00	-2.273515E-01	-82.9865	1.651958E+00	-2.240491E-01	1.774621E+00
	2.300000E-02	1.960796E-01	-1.623987E+00	2.273515E-01	7.0135	2.240491E-01	-1.651958E+00	1.774621E+00
30	-2.300000E-02	-3.098902E-01	1.645374E+00	-1.554177E-01	-85.4835	1.657651E+00	-3.221667E-01	1.840010E+00
	2.300000E-02	3.098902E-01	-1.645374E+00	1.554177E-01	4.5165	3.221667E-01	-1.657651E+00	1.840010E+00
31	-2.300000E-02	-3.223254E-01	1.662590E+00	-5.239899E-02	-88.4889	1.663973E+00	-3.237077E-01	1.847223E+00
	2.300000E-02	3.223254E-01	-1.662590E+00	5.239899E-02	1.5111	3.237077E-01	-1.663973E+00	1.847223E+00
32	-2.300000E-02	-2.305142E-01	1.668878E+00	4.624113E-02	88.6048	1.668004E+00	-2.316405E-01	1.795069E+00
	2.300000E-02	2.305142E-01	-1.668878E+00	-4.624113E-02	-1.3952	2.316405E-01	-1.668004E+00	1.795069E+00

PROCEEDING PAGE BLANK NOT FILMED

SUBCASE 1

WINFEM NASTRAN OUTPUT

ELEMENT ID.	FIBRE DISTANCE	STRESSES IN QUADRILATERAL ELEMENTS (QUAD4)		PRINCIPAL STRESSES (ZERO SHEAR)		VON MISES		
		NORMAL-X	NORMAL-Y	MAJOR	MINOR			
33	-2.300000E-02 2.300000E-02	3.285409E-01 -3.285409E-01	3.482395E+00 -3.482395E+00	-2.391807E-01 2.391807E-01	-85.6877 4.3123	3.500431E+00 -3.500431E+00	3.105052E-01 -3.105052E-01	3.355968E+00 3.355968E+00
34	-2.300000E-02 2.300000E-02	3.108945E-01 -3.108945E-01	3.419175E+00 -3.419175E+00	-8.677983E-02 8.677983E-02	-88.4020 1.5980	3.421597E+00 -3.421597E+00	3.084736E-01 -3.084736E-01	3.278262E+00 3.278262E+00
35	-2.300000E-02 2.300000E-02	2.998165E-01 -2.998165E-01	3.413251E+00 -3.413251E+00	9.218085E-02 -9.218085E-02	88.3058 -1.6944	3.415978E+00 -2.970897E-01	2.970897E-01 -3.415978E+00	3.277548E+00 3.277548E+00
36	-2.300000E-02 2.300000E-02	2.858822E-01 -2.858822E-01	3.416528E+00 -3.416528E+00	2.190431E-01 -2.190431E-01	86.0170 -3.9830	3.431779E+00 -2.706307E-01	2.706307E-01 -3.431779E+00	3.304785E+00 3.304785E+00
37	-2.300000E-02 2.300000E-02	-9.296155E-02 9.296155E-02	1.538758E+00 -1.538758E+00	-3.105443E-01 3.105443E-01	-79.5807 10.4193	1.595861E+00 1.500651E-01	-1.500651E-01 -1.595861E+00	1.675941E+00 1.675941E+00
38	-2.300000E-02 2.300000E-02	-8.438581E-02 8.438581E-02	1.636045E+00 -1.636045E+00	-1.218535E-01 1.218535E-01	-85.9687 4.0313	1.644632E+00 9.297347E-02	-9.297347E-02 -1.644632E+00	1.693034E+00 1.693034E+00
39	-2.300000E-02 2.300000E-02	-9.005648E-02 9.005648E-02	1.712047E+00 -1.712047E+00	2.482191E-02 -2.482191E-02	89.2110 -0.7890	1.712389E+00 9.039831E-02	-9.039831E-02 -1.712389E+00	1.759331E+00 1.759331E+00
40	-2.300000E-02 2.300000E-02	-9.251648E-02 9.251648E-02	1.818872E+00 -1.818872E+00	2.050107E-01 -2.050107E-01	83.9463 -6.0537	1.840614E+00 1.142581E-01	-1.142581E-01 -1.840614E+00	1.900322E+00 1.900322E+00
41	-2.300000E-02 2.300000E-02	-1.454785E-01 1.454785E-01	3.988787E-01 -3.988787E-01	-2.067387E-01 2.067387E-01	-71.3904 18.6096	4.684926E-01 2.150924E-01	-2.150924E-01 -4.684926E-01	6.054083E-01 6.054083E-01
42	-2.300000E-02 2.300000E-02	-2.672830E-01 2.672830E-01	4.503005E-01 -4.503005E-01	-1.026778E-01 1.026778E-01	-82.0151 7.9849	4.647034E-01 2.816859E-01	-2.816859E-01 -4.647034E-01	6.528373E-01 6.528373E-01
43	-2.300000E-02 2.300000E-02	-2.787562E-01 2.787562E-01	4.904491E-01 -4.904491E-01	7.874046E-03 -7.874046E-03	89.4136 -0.5864	4.905298E-01 2.788368E-01	-2.788368E-01 -4.905298E-01	6.746460E-01 6.746460E-01
44	-2.300000E-02 2.300000E-02	-1.830198E-01 1.830198E-01	5.147663E-01 -5.147663E-01	1.443647E-01 -1.443647E-01	78.7608 -11.2394	5.434544E-01 2.117079E-01	-2.117079E-01 -5.434544E-01	6.746973E-01 6.746973E-01

WINFEM NASTRAN OUTPUT

DECEMBER 11, 1993 MSC/NASIRAN 1/30/94 PAGE 34

G R I D P O I N T F O R C E B A L A N C E

POINT-ID ELEMENT-ID SOURCE T1 T2 T3 R1 R2 R3

1	1	F-OF-SPC	0.0	0.0	-3.547325E-01	-2.092920E+01	1.131013E+01	0.0
1	1	QUAD4	0.0	0.0	3.547325E-01	2.092920E+01	-1.131013E+01	0.0
1	1	*TOTALS*	0.0	0.0	0.0	-7.105427E-15	-3.907985E-14	0.0
2	2	APP-LOAD	0.0	0.0	1.450000E-01	0.0	0.0	0.0
2	2	QUAD4	0.0	0.0	-1.450000E-01	5.967671E-12	2.248868E-12	0.0
2	2	*TOTALS*	0.0	0.0	-3.652190E-12	5.967671E-12	2.248868E-12	0.0
3	3	F-OF-SPC	0.0	0.0	5.586644E-01	-9.528893E+00	-8.691465E+00	0.0
3	3	QUAD4	0.0	0.0	-5.586644E-01	9.528893E+00	8.691465E+00	0.0
3	3	*TOTALS*	0.0	0.0	0.0	4.862777E-14	-5.684342E-14	0.0
4	4	APP-LOAD	0.0	0.0	1.450000E-01	0.0	0.0	0.0
4	4	QUAD4	0.0	0.0	-1.449999E-01	-4.646949E-12	1.371347E-12	0.0
4	4	*TOTALS*	0.0	0.0	3.790745E-12	-4.646949E-12	1.371347E-12	0.0
5	5	APP-LOAD	0.0	0.0	1.450000E-01	0.0	0.0	0.0
5	5	QUAD4	0.0	0.0	-2.841415E-01	-2.033755E-01	-2.071603E-01	0.0
5	5	QUAD4	0.0	0.0	1.391415E-01	2.033755E-01	2.071603E-01	0.0
5	5	*TOTALS*	0.0	0.0	5.069722E-12	9.566126E-12	-2.042810E-12	0.0
6	6	APP-LOAD	0.0	0.0	1.450000E-01	0.0	0.0	0.0
6	6	QUAD4	0.0	0.0	-4.270937E-01	-1.055639E+00	-3.362633E-01	0.0
6	6	QUAD4	0.0	0.0	2.820938E-01	1.055639E+00	3.362633E-01	0.0
6	6	*TOTALS*	0.0	0.0	-1.831868E-13	6.487699E-12	-7.496226E-13	0.0
7	7	APP-LOAD	0.0	0.0	1.450000E-01	0.0	0.0	0.0
7	7	QUAD4	0.0	0.0	-5.762565E-01	-2.313122E+00	1.529788E-01	0.0
7	7	QUAD4	0.0	0.0	4.312565E-01	2.313122E+00	-1.529788E-01	0.0
7	7	*TOTALS*	0.0	0.0	1.758593E-12	1.434342E-11	5.069056E-12	0.0
8	8	APP-LOAD	0.0	0.0	1.450000E-01	0.0	0.0	0.0
8	8	QUAD4	0.0	0.0	-7.199568E-01	-3.229188E+00	-8.100601E-01	0.0
8	8	QUAD4	0.0	0.0	5.749568E-01	3.229188E+00	8.100601E-01	0.0
8	8	*TOTALS*	0.0	0.0	3.282707E-12	1.937561E-11	-3.165468E-12	0.0
9	9	APP-LOAD	0.0	0.0	1.450000E-01	0.0	0.0	0.0
9	9	QUAD4	0.0	0.0	-8.556296E-01	-5.129704E+00	-1.187954E+00	0.0
9	9	QUAD4	0.0	0.0	7.106296E-01	5.129704E+00	1.187954E+00	0.0
9	9	*TOTALS*	0.0	0.0	4.296785E-12	1.758371E-11	-2.437162E-12	0.0
10	10	APP-LOAD	0.0	0.0	1.450000E-01	0.0	0.0	0.0
10	10	QUAD4	0.0	0.0	-9.282596E-01	-7.711790E+00	-1.238106E+00	0.0
10	10	QUAD4	0.0	0.0	7.832596E-01	7.711790E+00	1.238106E+00	0.0
10	10	*TOTALS*	0.0	0.0	2.760903E-12	1.536926E-11	-2.015943E-12	0.0
11	11	APP-LOAD	0.0	0.0	1.450000E-01	0.0	0.0	0.0
11	11	QUAD4	0.0	0.0	-9.697331E-01	-1.063636E+01	5.287400E-02	0.0
11	11	QUAD4	0.0	0.0	8.247331E-01	1.063636E+01	-5.287400E-02	0.0
11	11	*TOTALS*	0.0	0.0	6.327161E-12	8.168133E-12	-6.382450E-12	0.0

SUBCASE 1

GRID POINT FORCE BALANCE

POINT-ID	ELEMENT-ID	SOURCE	T1	T2	T3	R1	R2	R3
12		APP-LOAD	0.0	0.0	1.45000E-01	0.0	0.0	0.0
12	9	QUAD4	0.0	0.0	-8.53890E-01	-1.31417E+01	-1.56758E+00	0.0
12	13	QUAD4	0.0	0.0	7.08890E-01	1.31417E+01	1.56758E+00	0.0
12		*TOTALS*	0.0	0.0	6.07514E-12	4.11359E-12	-3.05533E-13	0.0
13		APP-LOAD	0.0	0.0	1.45000E-01	0.0	0.0	0.0
13	5	QUAD4	0.0	0.0	-7.16139E-01	-1.70146E+01	-1.38068E+00	0.0
13	9	QUAD4	0.0	0.0	5.71139E-01	1.70146E+01	1.38068E+00	0.0
13		*TOTALS*	0.0	0.0	2.47624E-12	9.13047E-13	4.05009E-13	0.0
14		APP-LOAD	0.0	0.0	1.45000E-01	0.0	0.0	0.0
14	1	QUAD4	0.0	0.0	-5.00879E-01	-2.35888E+01	-1.63798E+00	0.0
14	5	QUAD4	0.0	0.0	3.55878E-01	2.35888E+01	-1.63798E+00	0.0
14		*TOTALS*	0.0	0.0	5.50670E-13	3.94351E-13	-4.22772E-13	0.0
15		APP-LOAD	0.0	0.0	1.45000E-01	0.0	0.0	0.0
15	4	QUAD4	0.0	0.0	2.02231E-01	-1.88989E+01	-4.26035E+00	0.0
15	8	QUAD4	0.0	0.0	-3.47231E-01	1.88989E+01	4.26035E+00	0.0
15		*TOTALS*	0.0	0.0	-3.55271E-13	-3.23296E-13	-1.04094E-12	0.0
16		APP-LOAD	0.0	0.0	1.45000E-01	0.0	0.0	0.0
16	8	QUAD4	0.0	0.0	-2.26561E-01	-1.63819E+01	-1.58549E+00	0.0
16	12	QUAD4	0.0	0.0	8.15611E-02	1.63819E+01	1.58549E+00	0.0
16		*TOTALS*	0.0	0.0	1.15463E-12	-7.92285E-13	4.72510E-13	0.0
17		APP-LOAD	0.0	0.0	1.45000E-01	0.0	0.0	0.0
17	12	QUAD4	0.0	0.0	-5.33971E-01	-1.32893E+01	-8.65954E-01	0.0
17	16	QUAD4	0.0	0.0	3.88971E-01	1.32893E+01	8.65954E-01	0.0
17		*TOTALS*	0.0	0.0	-2.64672E-12	-2.33058E-12	-3.14059E-12	0.0
18		APP-LOAD	0.0	0.0	1.45000E-01	0.0	0.0	0.0
18	16	QUAD4	0.0	0.0	-6.66776E-01	-9.05372E+00	-1.71939E+00	0.0
18	20	QUAD4	0.0	0.0	5.21776E-01	9.05372E+00	1.71939E+00	0.0
18		*TOTALS*	0.0	0.0	-1.11199E-12	-2.29860E-12	4.58655E-12	0.0
19		APP-LOAD	0.0	0.0	1.45000E-01	0.0	0.0	0.0
19	20	QUAD4	0.0	0.0	-7.62886E-01	-8.10088E+00	-3.85102E-01	0.0
19	24	QUAD4	0.0	0.0	6.17886E-01	8.10088E+00	3.85102E-01	0.0
19		*TOTALS*	0.0	0.0	-3.25783E-12	-5.68789E-12	-5.75539E-12	0.0
20		APP-LOAD	0.0	0.0	1.45000E-01	0.0	0.0	0.0
20	24	QUAD4	0.0	0.0	-7.96285E-01	-5.75674E+00	-4.09414E-02	0.0
20	28	QUAD4	0.0	0.0	6.51285E-01	5.75674E+00	4.09414E-02	0.0
20		*TOTALS*	0.0	0.0	-3.11573E-12	-1.34932E-11	-4.14601E-12	0.0
21		APP-LOAD	0.0	0.0	1.45000E-01	0.0	0.0	0.0
21	28	QUAD4	0.0	0.0	-6.84308E-01	-3.77166E+00	-1.21024E-01	0.0
21	32	QUAD4	0.0	0.0	5.39308E-01	3.77166E+00	1.21024E-01	0.0
21		*TOTALS*	0.0	0.0	4.63984E-12	-1.55964E-11	1.13686E-12	0.0

POINT-ID	ELEMENT-ID	SOURCE	T1	T2	T3	R1	R2	R3
22	32	APP-LOAD	0.0	0.0	1.450000E-01	0.0	0.0	0.0
22	32	QUAD4	0.0	0.0	-3.983885E-01	-1.886166E+00	-3.726369E-01	0.0
22	36	QUAD4	0.0	0.0	2.533885E-01	1.886166E+00	3.726369E-01	0.0
22		*TOTALS*	0.0	0.0	5.730527E-12	-6.580958E-12	-1.893596E-12	0.0
23	36	APP-LOAD	0.0	0.0	1.450000E-01	0.0	0.0	0.0
23	36	QUAD4	0.0	0.0	-4.107967E-01	-1.347902E+00	5.405211E-02	0.0
23	40	QUAD4	0.0	0.0	2.657967E-01	1.347902E+00	-5.405211E-02	0.0
23		*TOTALS*	0.0	0.0	-4.085621E-13	-6.090239E-12	-3.261391E-12	0.0
24	40	APP-LOAD	0.0	0.0	1.450000E-01	0.0	0.0	0.0
24	40	QUAD4	0.0	0.0	-3.545870E-01	-4.058046E-01	8.041102E-02	0.0
24	44	QUAD4	0.0	0.0	2.095870E-01	4.058046E-01	-8.041102E-02	0.0
24		*TOTALS*	0.0	0.0	1.698197E-12	-7.730261E-12	-4.192202E-13	0.0
25	43	APP-LOAD	0.0	0.0	1.450000E-01	0.0	0.0	0.0
25	43	QUAD4	0.0	0.0	-1.137034E-01	7.211924E-02	-1.179002E-01	0.0
25	44	QUAD4	0.0	0.0	3.129658E-02	-7.211924E-02	1.179002E-01	0.0
25		*TOTALS*	0.0	0.0	4.973799E-14	1.465050E-12	6.838974E-12	0.0
26	42	APP-LOAD	0.0	0.0	1.450000E-01	0.0	0.0	0.0
26	42	QUAD4	0.0	0.0	-7.879877E-02	9.084159E-02	-1.733377E-01	0.0
26	43	QUAD4	0.0	0.0	6.620115E-02	-9.084159E-02	1.733377E-01	0.0
26		*TOTALS*	0.0	0.0	-7.212009E-13	-4.070078E-13	4.146017E-12	0.0
27	41	APP-LOAD	0.0	0.0	1.450000E-01	0.0	0.0	0.0
27	41	QUAD4	0.0	0.0	-4.129180E-02	6.626219E-02	-1.253899E-01	0.0
27	42	QUAD4	0.0	0.0	1.037081E-01	-6.626219E-02	1.253899E-01	0.0
27		*TOTALS*	0.0	0.0	5.613288E-13	-1.738831E-12	4.650502E-12	0.0
28	1	F-OFF-SPC	0.0	0.0	-3.364391E+00	-5.994963E+01	3.713194E+00	0.0
28	2	QUAD4	0.0	0.0	1.752451E+00	2.978267E+01	-1.680724E+00	0.0
28	2	QUAD4	0.0	0.0	1.611939E+00	3.016696E+01	-5.393919E+00	0.0
28		*TOTALS*	0.0	0.0	-1.310063E-14	7.105427E-15	-2.149392E-13	0.0
29	2	F-OFF-SPC	0.0	0.0	-2.649501E+00	-5.363058E+01	-4.649229E+00	0.0
29	3	QUAD4	0.0	0.0	6.400302E-01	2.359975E+01	7.744589E+00	0.0
29	3	QUAD4	0.0	0.0	1.809470E+00	3.003084E+01	-3.095359E+00	0.0
29		*TOTALS*	0.0	0.0	-5.773160E-15	5.684342E-14	-1.352252E-13	0.0
30	3	F-OFF-SPC	0.0	0.0	-2.165038E+00	-4.518658E+01	-9.814965E+00	0.0
30	4	QUAD4	0.0	0.0	2.559456E-01	1.836028E+01	8.183112E+00	0.0
30	4	QUAD4	0.0	0.0	1.909092E+00	2.682629E+01	-1.631853E+00	0.0
30		*TOTALS*	0.0	0.0	-7.016610E-14	6.039613E-14	-9.636736E-14	0.0
31	1	APP-LOAD	0.0	0.0	1.450000E-01	0.0	0.0	0.0
31	2	QUAD4	0.0	0.0	-1.606304E+00	-1.878912E+01	9.013713E+00	0.0
31	2	QUAD4	0.0	0.0	-1.405725E+00	-1.964749E+01	-7.368034E+00	0.0
31	5	QUAD4	0.0	0.0	1.511719E+00	1.816751E+01	3.584524E+00	0.0

FEM RAN OUT
W...FEM NASTRAN OUTPUT

SUBCASE 1

GRID POINT FORCE BALANCE

POINT-ID	ELEMENT-ID	SOURCE	T1	T2	T3	R1	R2	R3
31	6	QUAD4	0.0	0.0	1.355310E+00	2.026910E+01	-5.230203E+00	0.0
31		*TOTALS*	0.0	0.0	1.953993E-13	5.364598E-13	-6.261658E-14	0.0
32		APP-LOAD	0.0	0.0	1.450000E-01	0.0	0.0	0.0
32	5	QUAD4	0.0	0.0	-1.151459E+00	-1.735721E+01	1.236070E+00	0.0
32	6	QUAD4	0.0	0.0	-1.200343E+00	-1.585064E+01	-2.362542E+00	0.0
32	9	QUAD4	0.0	0.0	1.104706E+00	1.603975E+01	2.022169E+00	0.0
32	10	QUAD4	0.0	0.0	1.102097E+00	1.716809E+01	-8.956973E-01	0.0
32		*TOTALS*	0.0	0.0	2.815082E-12	1.868727E-12	-4.729550E-13	0.0
33		APP-LOAD	0.0	0.0	1.450000E-01	0.0	0.0	0.0
33	9	QUAD4	0.0	0.0	-8.219547E-01	-1.328473E+01	-5.049565E-01	0.0
33	10	QUAD4	0.0	0.0	-1.045683E+00	-1.259247E+01	-1.491426E+00	0.0
33	13	QUAD4	0.0	0.0	7.376720E-01	1.321798E+01	1.077378E+00	0.0
33	14	QUAD4	0.0	0.0	9.849660E-01	1.265922E+01	9.190040E-01	0.0
33		*TOTALS*	0.0	0.0	-9.476864E-13	7.729817E-12	-4.600986E-12	0.0
34		APP-LOAD	0.0	0.0	1.450000E-01	0.0	0.0	0.0
34	13	QUAD4	0.0	0.0	-4.768293E-01	-1.000363E+01	-1.593703E+00	0.0
34	14	QUAD4	0.0	0.0	-1.003344E+00	-1.067146E+01	-1.809010E-02	0.0
34	17	QUAD4	0.0	0.0	5.121641E-01	9.988397E+00	1.670793E+00	0.0
34	18	QUAD4	0.0	0.0	8.230094E-01	1.068669E+01	-5.899853E-02	0.0
34		*TOTALS*	0.0	0.0	-1.127654E-11	9.598100E-12	-6.554313E-12	0.0
35		APP-LOAD	0.0	0.0	1.450000E-01	0.0	0.0	0.0
35	17	QUAD4	0.0	0.0	-4.086377E-01	-7.625549E+00	8.471179E-02	0.0
35	18	QUAD4	0.0	0.0	-7.778202E-01	-7.044700E+00	-1.613313E+00	0.0
35	21	QUAD4	0.0	0.0	3.497629E-01	7.229667E+00	1.070107E+00	0.0
35	22	QUAD4	0.0	0.0	6.916568E-01	7.440583E+00	4.584935E-01	0.0
35		*TOTALS*	0.0	0.0	1.199130E-11	-8.130829E-12	-7.826628E-12	0.0
36		APP-LOAD	0.0	0.0	1.450000E-01	0.0	0.0	0.0
36	21	QUAD4	0.0	0.0	-2.773929E-01	-5.331786E+00	-8.135614E-01	0.0
36	22	QUAD4	0.0	0.0	-6.510009E-01	-5.227432E+00	-7.411713E-01	0.0
36	25	QUAD4	0.0	0.0	2.300861E-01	5.346663E+00	5.604473E-01	0.0
36	26	QUAD4	0.0	0.0	5.533077E-01	5.212555E+00	9.942854E-01	0.0
36		*TOTALS*	0.0	0.0	7.724932E-12	-1.055356E-11	-7.183587E-12	0.0
37		APP-LOAD	0.0	0.0	1.450000E-01	0.0	0.0	0.0
37	25	QUAD4	0.0	0.0	-2.207589E-01	-3.526649E+00	-8.589798E-01	0.0
37	26	QUAD4	0.0	0.0	-5.357060E-01	-3.538169E+00	-1.890659E-01	0.0
37	29	QUAD4	0.0	0.0	1.631902E-01	3.914519E+00	-7.354778E-02	0.0
37	30	QUAD4	0.0	0.0	4.482747E-01	3.150298E+00	1.121593E+00	0.0
37		*TOTALS*	0.0	0.0	1.997336E-11	-1.799805E-11	-1.065814E-14	0.0
38		APP-LOAD	0.0	0.0	1.450000E-01	0.0	0.0	0.0
38	29	QUAD4	0.0	0.0	-1.618906E-01	-1.911955E+00	-8.489614E-01	0.0
38	30	QUAD4	0.0	0.0	-4.974885E-01	-2.516264E+00	5.359875E-01	0.0
38	33	QUAD4	0.0	0.0	1.316301E-01	2.073442E+00	3.564165E-01	0.0
38	34	QUAD4	0.0	0.0	3.827491E-01	2.354778E+00	-4.344262E-02	0.0

GRID POINT FORCE BALANCE

POINT-ID	ELEMENT-ID	SOURCE	T1	T2	T3	R1	R2	R3
38		*TOTALS*	0.0	0.0	2.664935E-11	-2.076184E-11	6.463496E-12	0.0
39		APP-LOAD	0.0	0.0	1.450000E-01	0.0	0.0	0.0
39	33	QUAD4	0.0	0.0	-1.357928E-01	-1.104706E+00	1.524861E-01	0.0
39	34	QUAD4	0.0	0.0	-3.204221E-01	-8.618148E-01	-4.015348E-01	0.0
39	37	QUAD4	0.0	0.0	8.976507E-02	9.899691E-01	7.207453E-02	0.0
39	38	QUAD4	0.0	0.0	2.214499E-01	9.765519E-01	1.769740E-01	0.0
39		*TOTALS*	0.0	0.0	-1.355360E-12	2.279510E-12	1.101341E-12	0.0
40		APP-LOAD	0.0	0.0	1.450000E-01	0.0	0.0	0.0
40	37	QUAD4	0.0	0.0	-8.771735E-02	-3.718998E-01	-1.761507E-01	0.0
40	38	QUAD4	0.0	0.0	-1.834553E-01	-3.378754E-01	-6.251711E-02	0.0
40	41	QUAD4	0.0	0.0	4.715026E-02	4.671437E-01	-5.935043E-02	0.0
40	42	QUAD4	0.0	0.0	7.902253E-02	2.426316E-01	2.980183E-01	0.0
40		*TOTALS*	0.0	0.0	1.152500E-11	2.693401E-13	-2.625455E-12	0.0
41		APP-LOAD	0.0	0.0	1.450000E-01	0.0	0.0	0.0
41	2	QUAD4	0.0	0.0	-1.046245E+00	-2.442168E+01	4.884541E+00	0.0
41	3	QUAD4	0.0	0.0	-1.501542E+00	-1.659015E+01	-7.273601E+00	0.0
41	6	QUAD4	0.0	0.0	5.459668E-01	1.952768E+01	4.206126E+00	0.0
41	7	QUAD4	0.0	0.0	1.856820E+00	2.148416E+01	-1.817067E+00	0.0
41		*TOTALS*	0.0	0.0	1.036948E-13	9.876544E-13	-7.933654E-13	0.0
42		APP-LOAD	0.0	0.0	1.450000E-01	0.0	0.0	0.0
42	6	QUAD4	0.0	0.0	-7.009337E-01	-1.642848E+01	3.316503E+00	0.0
42	7	QUAD4	0.0	0.0	-1.152811E+00	-1.407513E+01	-4.747624E+00	0.0
42	10	QUAD4	0.0	0.0	5.129544E-01	1.498937E+01	2.759335E+00	0.0
42	11	QUAD4	0.0	0.0	1.493342E+00	1.551425E+01	-1.328213E+00	0.0
42		*TOTALS*	0.0	0.0	3.842704E-12	2.423617E-12	-4.090062E-13	0.0
43		APP-LOAD	0.0	0.0	1.450000E-01	0.0	0.0	0.0
43	10	QUAD4	0.0	0.0	-5.693685E-01	-1.317747E+01	-1.040308E-01	0.0
43	11	QUAD4	0.0	0.0	-1.152811E+00	-1.260937E+01	-1.588579E+00	0.0
43	14	QUAD4	0.0	0.0	4.403898E-01	1.323627E+01	7.481492E-01	0.0
43	15	QUAD4	0.0	0.0	1.136790E+00	1.255057E+01	9.444615E-01	0.0
43		*TOTALS*	0.0	0.0	1.257883E-12	8.757439E-12	-7.367218E-12	0.0
44		APP-LOAD	0.0	0.0	1.450000E-01	0.0	0.0	0.0
44	14	QUAD4	0.0	0.0	-4.220116E-01	-9.588175E+00	-1.159542E+00	0.0
44	15	QUAD4	0.0	0.0	-9.520109E-01	-1.030345E+01	-3.030158E-01	0.0
44	18	QUAD4	0.0	0.0	4.502762E-01	9.423122E+00	1.806864E+00	0.0
44	19	QUAD4	0.0	0.0	7.787464E-01	1.046850E+01	-3.443062E-01	0.0
44		*TOTALS*	0.0	0.0	-7.535306E-12	9.427348E-12	2.128075E-12	0.0
45		APP-LOAD	0.0	0.0	1.450000E-01	0.0	0.0	0.0
45	18	QUAD4	0.0	0.0	-4.955035E-01	-8.029274E+00	1.050472E-01	0.0
45	19	QUAD4	0.0	0.0	-6.258985E-01	-6.987775E+00	-1.366362E+00	0.0
45	22	QUAD4	0.0	0.0	3.811743E-01	7.407646E+00	8.367658E-01	0.0
45	23	QUAD4	0.0	0.0	5.952278E-01	7.609404E+00	4.245489E-01	0.0
45		*TOTALS*	0.0	0.0	9.176659E-12	-1.326850E-11	-1.222489E-11	0.0

WINFEM NASTRAN OUTPUT
FEM NASTRAN OUTPUT

GRID POINT FORCE BALANCE

POINT-ID	ELEMENT-ID	SOURCE	T1	T2	T3	R1	R2	R3
46		APP-LOAD	0.0	0.0	0.0	0.0	0.0	0.0
46	22	QUAD4	0.0	0.0	-4.218302E-01	0.0	0.0	0.0
46	23	QUAD4	0.0	0.0	-4.863201E-01	-5.378828E+00	-3.508754E-01	0.0
46	26	QUAD4	0.0	0.0	3.392345E-01	5.155451E+00	-6.619812E-01	0.0
46	27	QUAD4	0.0	0.0	4.259158E-01	5.393163E+00	2.354881E-01	0.0
46		*TOTALS*	0.0	0.0	1.877254E-11	-8.606227E-12	1.705303E-13	0.0
47		APP-LOAD	0.0	0.0	0.0	0.0	0.0	0.0
47	26	QUAD4	0.0	0.0	-3.568361E-01	-3.537543E+00	-8.119581E-01	0.0
47	27	QUAD4	0.0	0.0	-3.863052E-01	-3.736813E+00	5.372421E-02	0.0
47	30	QUAD4	0.0	0.0	2.742003E-01	3.985279E+00	-4.297503E-01	0.0
47	31	QUAD4	0.0	0.0	3.239411E-01	3.289076E+00	1.187984E+00	0.0
47		*TOTALS*	0.0	0.0	1.697487E-11	-1.948020E-11	4.369838E-13	0.0
48		APP-LOAD	0.0	0.0	0.0	0.0	0.0	0.0
48	30	QUAD4	0.0	0.0	-2.249865E-01	-1.762650E+00	-8.895936E-01	0.0
48	31	QUAD4	0.0	0.0	-3.990613E-01	-2.433758E+00	6.359425E-01	0.0
48	34	QUAD4	0.0	0.0	1.636724E-01	1.928622E+00	3.519821E-01	0.0
48	35	QUAD4	0.0	0.0	3.153754E-01	2.267786E+00	-1.183310E-01	0.0
48		*TOTALS*	0.0	0.0	2.626788E-11	-1.379719E-11	3.677059E-12	0.0
49		APP-LOAD	0.0	0.0	0.0	0.0	0.0	0.0
49	34	QUAD4	0.0	0.0	-2.259994E-01	-1.260488E+00	1.013995E-01	0.0
49	35	QUAD4	0.0	0.0	-2.114392E-01	-9.156260E-01	-3.163712E-01	0.0
49	38	QUAD4	0.0	0.0	1.400653E-01	1.124888E+00	1.421128E-02	0.0
49	39	QUAD4	0.0	0.0	1.523735E-01	1.051225E+00	2.007604E-01	0.0
49		*TOTALS*	0.0	0.0	-2.209788E-12	6.365131E-12	2.053469E-12	0.0
50		APP-LOAD	0.0	0.0	0.0	0.0	0.0	0.0
50	38	QUAD4	0.0	0.0	-1.780598E-01	-3.341309E-01	-9.923953E-02	0.0
50	39	QUAD4	0.0	0.0	-9.810108E-02	-3.486169E-01	-5.375290E-02	0.0
50	42	QUAD4	0.0	0.0	1.034844E-01	4.546016E-01	-1.356757E-01	0.0
50	43	QUAD4	0.0	0.0	2.767657E-02	2.281463E-01	2.886682E-01	0.0
50		*TOTALS*	0.0	0.0	7.389644E-13	5.601297E-12	-4.106937E-12	0.0
51		APP-LOAD	0.0	0.0	0.0	0.0	0.0	0.0
51	3	QUAD4	0.0	0.0	-5.638738E-01	-2.363223E+01	1.867935E+00	0.0
51	4	QUAD4	0.0	0.0	-1.552659E+00	-1.211528E+01	-6.791834E+00	0.0
51	7	QUAD4	0.0	0.0	-3.383034E-02	1.704961E+01	5.526526E+00	0.0
51	8	QUAD4	0.0	0.0	2.005363E+00	1.869791E+01	-6.026282E-01	0.0
51		*TOTALS*	0.0	0.0	8.415491E-13	1.374900E-12	-6.110668E-13	0.0
52		APP-LOAD	0.0	0.0	0.0	0.0	0.0	0.0
52	7	QUAD4	0.0	0.0	-3.726273E-01	-1.725053E+01	2.139672E-01	0.0
52	8	QUAD4	0.0	0.0	-1.431571E+00	-1.465873E+01	-3.341761E+00	0.0
52	11	QUAD4	0.0	0.0	1.147938E-01	1.609222E+01	2.466125E+00	0.0
52	12	QUAD4	0.0	0.0	1.544404E+00	1.581704E+01	6.616681E-01	0.0
52		*TOTALS*	0.0	0.0	1.502798E-12	2.110312E-12	-7.460699E-14	0.0
53		APP-LOAD	0.0	0.0	0.0	0.0	0.0	0.0

SUBCASE 1

W. J. EM NASTRAN OUTPUT

SUBCASE 1

GRID POINT FORCE BALANCE

POINT-ID	ELEMENT-ID	SOURCE	T1	T2	T3	R1	R2	R3
53	11	QUAD4	0.0	0.0	-4.553248E-01	-1.263692E+01	-9.217501E-02	0.0
53	12	QUAD4	0.0	0.0	-1.091993E+00	-1.247886E+01	-1.982635E+00	0.0
53	15	QUAD4	0.0	0.0	3.062597E-01	1.304383E+01	8.453632E-01	0.0
53	16	QUAD4	0.0	0.0	1.096059E+00	1.207196E+01	1.229448E+00	0.0
53		*TOTALS*	0.0	0.0	-4.920508E-12	5.190515E-12	-6.856737E-12	0.0
54		APP-LOAD						
54	15	QUAD4	0.0	0.0	1.450000E-01	0.0	0.0	0.0
54	16	QUAD4	0.0	0.0	-4.910390E-01	-9.585126E+00	-1.425379E+00	0.0
54	19	QUAD4	0.0	0.0	-8.182548E-01	-1.043581E+01	-2.725097E-01	0.0
54	20	QUAD4	0.0	0.0	4.580454E-01	9.418978E+00	1.574976E+00	0.0
54		*TOTALS*	0.0	0.0	7.062485E-01	1.060196E+01	1.229123E-01	0.0
54			0.0	0.0	-8.252954E-12	7.928991E-12	6.746603E-12	0.0
55		APP-LOAD						
55	19	QUAD4	0.0	0.0	1.450000E-01	0.0	0.0	0.0
55	20	QUAD4	0.0	0.0	-6.108933E-01	-8.008197E+00	2.882280E-01	0.0
55	23	QUAD4	0.0	0.0	-4.651377E-01	-6.697969E+00	-1.312350E+00	0.0
55	24	QUAD4	0.0	0.0	4.613383E-01	7.344657E+00	7.943302E-01	0.0
55		*TOTALS*	0.0	0.0	4.696926E-01	7.361509E+00	2.297924E-01	0.0
55			0.0	0.0	1.526246E-11	-1.148903E-11	-1.577405E-11	0.0
56		APP-LOAD						
56	23	QUAD4	0.0	0.0	1.450000E-01	0.0	0.0	0.0
56	24	QUAD4	0.0	0.0	-5.682481E-01	-5.620953E+00	-3.072945E-01	0.0
56	27	QUAD4	0.0	0.0	-2.912940E-01	-5.405364E+00	-3.326860E-01	0.0
56	28	QUAD4	0.0	0.0	4.581242E-01	5.640488E+00	7.065684E-02	0.0
56		*TOTALS*	0.0	0.0	2.564159E-01	5.385829E+00	5.693237E-01	0.0
56			0.0	0.0	2.216183E-11	-1.428191E-11	-1.027445E-11	0.0
57		APP-LOAD						
57	27	QUAD4	0.0	0.0	1.450000E-01	0.0	0.0	0.0
57	28	QUAD4	0.0	0.0	-4.977348E-01	-3.548410E+00	-5.107444E-01	0.0
57	31	QUAD4	0.0	0.0	-2.233929E-01	-3.780954E+00	-2.142265E-02	0.0
57	32	QUAD4	0.0	0.0	3.952339E-01	3.885690E+00	4.133779E-01	0.0
57		*TOTALS*	0.0	0.0	1.808937E-01	3.443675E+00	9.026997E-01	0.0
57			0.0	0.0	2.458833E-11	-2.043166E-11	8.490986E-13	0.0
58		APP-LOAD						
58	31	QUAD4	0.0	0.0	1.450000E-01	0.0	0.0	0.0
58	32	QUAD4	0.0	0.0	-3.201138E-01	-1.897393E+00	-7.925326E-01	0.0
58	35	QUAD4	0.0	0.0	-3.218137E-01	-2.481495E+00	5.825108E-01	0.0
58	36	QUAD4	0.0	0.0	2.197123E-01	1.995842E+00	2.912477E-01	0.0
58		*TOTALS*	0.0	0.0	2.772153E-01	2.383046E+00	-8.122587E-02	0.0
58			0.0	0.0	2.998490E-11	-1.993805E-11	-4.146017E-12	0.0
59		APP-LOAD						
59	35	QUAD4	0.0	0.0	1.450000E-01	0.0	0.0	0.0
59	36	QUAD4	0.0	0.0	-3.236484E-01	-1.231730E+00	1.814110E-01	0.0
59	39	QUAD4	0.0	0.0	-1.198071E-01	-8.227709E-01	-3.126292E-01	0.0
59	40	QUAD4	0.0	0.0	2.044072E-01	1.112578E+00	3.695750E-02	0.0
59		*TOTALS*	0.0	0.0	9.404844E-02	9.419212E-01	9.426069E-02	0.0
59			0.0	0.0	-8.327561E-12	2.583267E-12	-1.843858E-12	0.0
60		APP-LOAD						
60	39	QUAD4	0.0	0.0	1.450000E-01	0.0	0.0	0.0
60			0.0	0.0	-2.586793E-01	-4.044740E-01	-9.624594E-02	0.0

SUBCASE 1

GRID POINT FORCE BALANCE

POINT-ID	ELEMENT-ID	SOURCE	T1	T2	T3	R1	R2	R3
60	40	QUAD4	0.0	0.0	-5.258238E-03	-4.611875E-01	-1.260503E-02	0.0
60	43	QUAD4	0.0	0.0	1.522280E-01	5.020963E-01	-1.508442E-01	0.0
60	44	QUAD4	0.0	0.0	-3.329043E-02	3.635651E-01	2.594952E-01	0.0
60		*TOTALS*	0.0	0.0	-9.357848E-12	7.840839E-12	-1.888711E-12	0.0

RECORD NT = 83
DBC FILE CREATED- PROCESSED TO NORMAL END OF JOB

**APPENDIX D2: STRENGTH / WEIGHT
FACTOR**

Using the equations 6.1 and 6.2 in the chapter 6.3. (section 6.3.3.1), PVC factor (Strength/Weight) is calculated:

$$\text{Factor (Strength/Weight)} = \sigma_u / \rho$$

$$\text{Area of the wing} = 565.57 \text{ in}^2$$

$$\text{Strip load} = 1 \text{ lb}$$

$$F S = 1.5 \text{ unmanned aircraft}$$

$$\rho \text{ (density of PVC)} = 3 \text{ lb/ft}^3 = 0.00173611 \text{ lb/in}^3$$

Then

$$\text{Factor for PVC} = (1 \text{ lb} * 1.5) / (565.57 \text{ in}^2 * 0.00173611 \text{ lb/in}^3)$$

$$\text{Factor for PVC} = 1.52 \text{ in}$$

The Factor of composite PVC and Kevlar is obtained as the following:

$$\text{Density of PVC} = 0.0017366 \text{ lb/in}^3$$

$$\text{Density of Kevlar} = 0.052 \text{ lb/in}^3$$

$$\text{Ratio of Density} = \rho_{\text{Kevlar}} / \rho_{\text{PVC}}$$

$$\text{Ratio of Density} = 0.052 / 0.00173611 = 29.952$$

Therefore:

$$\text{Factor (Strength/Weight)} = \sigma_u / \rho_{\text{den comp}}$$

$$\text{Factor (Strength/Weight)} = (1.5 * 1.04516) / (565.57 * 0.00173611)$$

$$\text{Factor (Strength/Weight)} = 1.60 \text{ in}$$

**APPENDIX D3 : CALCULATING
WING SHEARS AND MOMENT FOR
ONE UNIT LOAD CONDITION**

Calculation of the wing shear V_z and the wing moments M_x and M_y due to the total unit load, distributed on a half wing load of 565.57 lbs, acting upward in Z direction and applied at aerodynamic centers of the wing sections goes through the following steps:

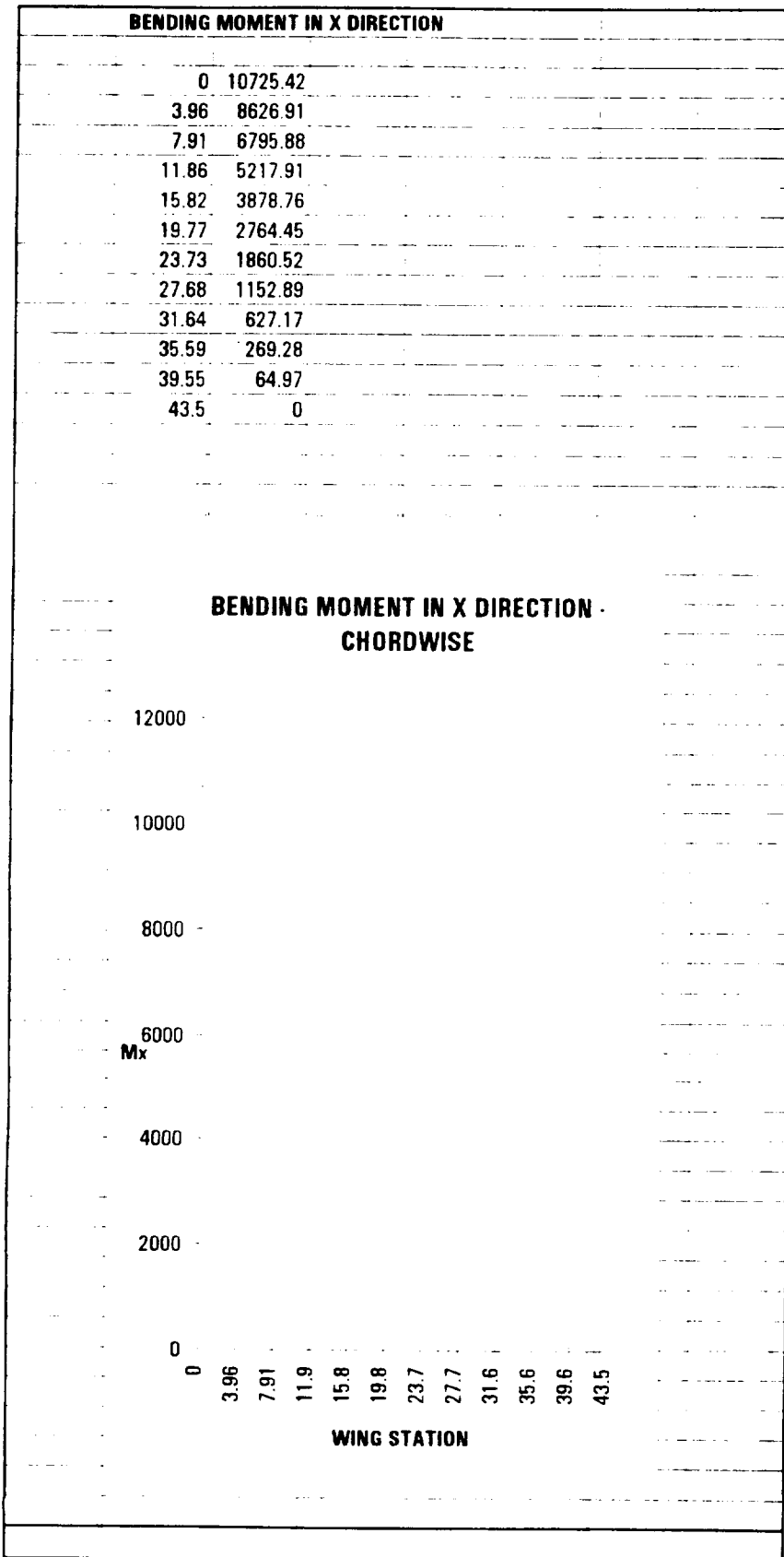
- Step 1 : The distance from the wing root section, called station y (Column 1)
- Step 2 : The wing chord length of each section (Column 2)
- Step 3 : Ratio of Lift coefficient is assumed to be unity (Column 3)
- Step 4 : The wing running load per inch of span at each station point. The area of a half wing (565.57 square inches) was treated as a total unit load; then, the running load per inch at any station equals the wing chord length at that station.
(Column 4)
- Step 5 : Average running load (Column 5)
- Step 6 : The distance between stations (Column 6)
- Step 7 : Strip load (Column 7)
- Step 8 : The location of the strip load which is at the centroid of a trapezoidal distributed load whose end values are given in column 4. The centroid locations are determined by Table A3.4 of Chapter 3. (Column 8)
- Step 9 : Shears (Column 9)
- Step 10 : The product of shear and delta y (Column 10)
- Step 11 : The product of strip load and arm to the centroid (Column 11)
- Step 12 : The value of moment (Column 12)
- Step 13 : The distance from aerodynamic center to the y reference axis (Column 13)
- Step 14 : The strip load distance from y axis (Column 14)
- Step 15 : Bending moment for each strip load on the y axis (Column 15)
- Step 16 : The bending moment at the various stations equals to the summation of the strip moments as one progresses from station 43.5 to zero.

(Ref: 5)

SHEAR XIS

CALCULATION OF WING SHEAR V _Z AND WING MOMENTS M _X AND M _Y DUE TO TOTAL UNIT DISTRIBUTED HALF WING LOAD OF 565.75 LBS. ACTING UPWARD IN Z DIRECTION AND APPLIED AT AERODYNAMIC CENTERS OF WING SECTIONS															
STATION - Y - DISTANCE FROM WING ROOT SECTION	CHORD LENGTH	CIRCULAR RATIO ASSUMED UNITY	RUNNING LOAD PER MCH OF WING	AVERAGE RUNNING LOAD	Y - DISTANCE BETWEEN STATIONS	STRIP LOAD P _Z (col.5)	d - ARM TO CENTROID OF STRIP LOAD	SHEAR V _Z = P _Z	V _Z Y = (col.9)(col.6)	P _Z d = (col.7)(col.8)	M _X = col.12 previous + col.11 + col.10	X DISTANCE FROM AERODYNAMIC CENTER TO FROM Y AXIS	X _{ave} OR STRIP LOAD AERODYNAMIC DISTANCE CENTER TO FROM Y AXIS	P _Z X _{ave} = (col.7)(col.14)	M _Y = P _Z X _{ave} - SUMMATION OF Col.15.
1	2	3	4	5	6	7	8	9	10	11	12	13	14	15	16
43.50	8.00	1.00	8.00	8.45	3.96	33.44	1.94	0.00	0.00	0.00	0.00	1.20	1.27	42.40	0.00
38.55	8.91	1.00	8.91	9.36	3.96	37.03	1.95	33.44	0.00	64.97	64.97	1.34	1.40	42.40	42.40
35.59	9.82		9.82	10.27	3.96	40.63	1.95	70.47	132.25	72.07	289.28	1.47	1.54	52.01	94.42
31.64	10.73	1.00	10.73	11.18	3.96	44.22	1.95	111.10	278.71	79.18	627.17	1.61	1.68	62.80	157.02
27.68	11.64	1.00	11.64	12.09	3.96	47.82	1.95	155.32	439.39	86.32	1,152.89	1.75	1.81	74.17	231.19
23.73	12.55	1.00	12.55	13.00	3.96	51.42	1.96	203.14	614.29	93.34	1,860.52	1.88	1.95	88.72	317.91
19.77	13.46	1.00	13.46	13.91	3.96	55.01	1.96	254.55	803.41	100.52	2,764.45	2.02	2.09	100.26	418.17
15.82	14.36	1.00	14.36	14.82	3.96	58.61	1.96	309.57	1,006.76	107.55	3,878.76	2.15	2.22	114.78	532.95
11.86	15.27	1.00	15.27	15.73	3.96	62.20	1.96	368.17	1,224.33	114.81	5,217.91	2.29	2.36	130.27	683.22
7.91	16.18	1.00	16.18	16.64	3.96	65.80	1.96	430.38	1,456.12	121.85	6,795.88	2.43	2.50	146.74	809.96
3.96	17.09	1.00	17.09	17.55	3.96	69.39	1.96	496.17	1,702.13	128.90	8,626.91	2.56	2.63	164.20	974.16
0.00	18.00	1.00	18.00	17.55	3.96	69.39	1.96	565.57	1,962.36	136.15	10,725.42	2.70	2.83	182.53	1,158.79

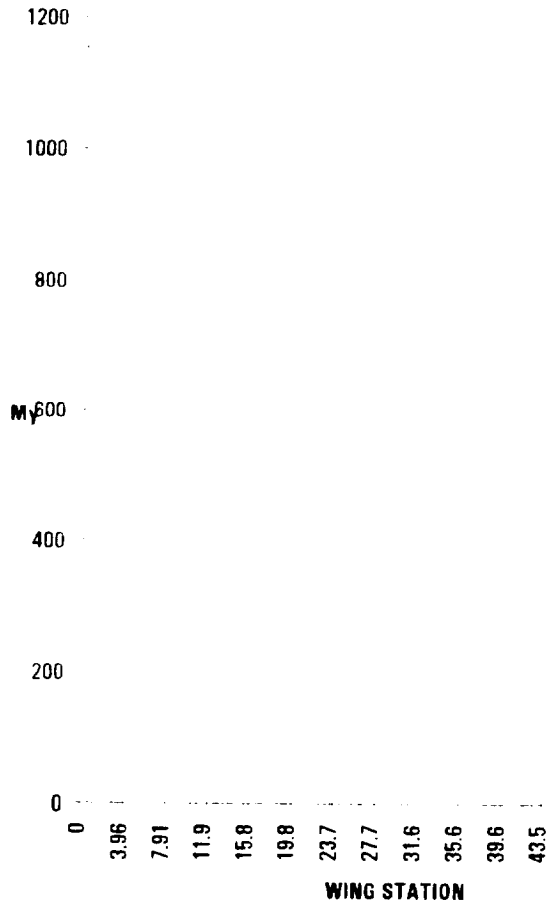
SUM - 565.57 CHECKS TOTAL LIMIT LOAD ASSUMED ON HALF WING

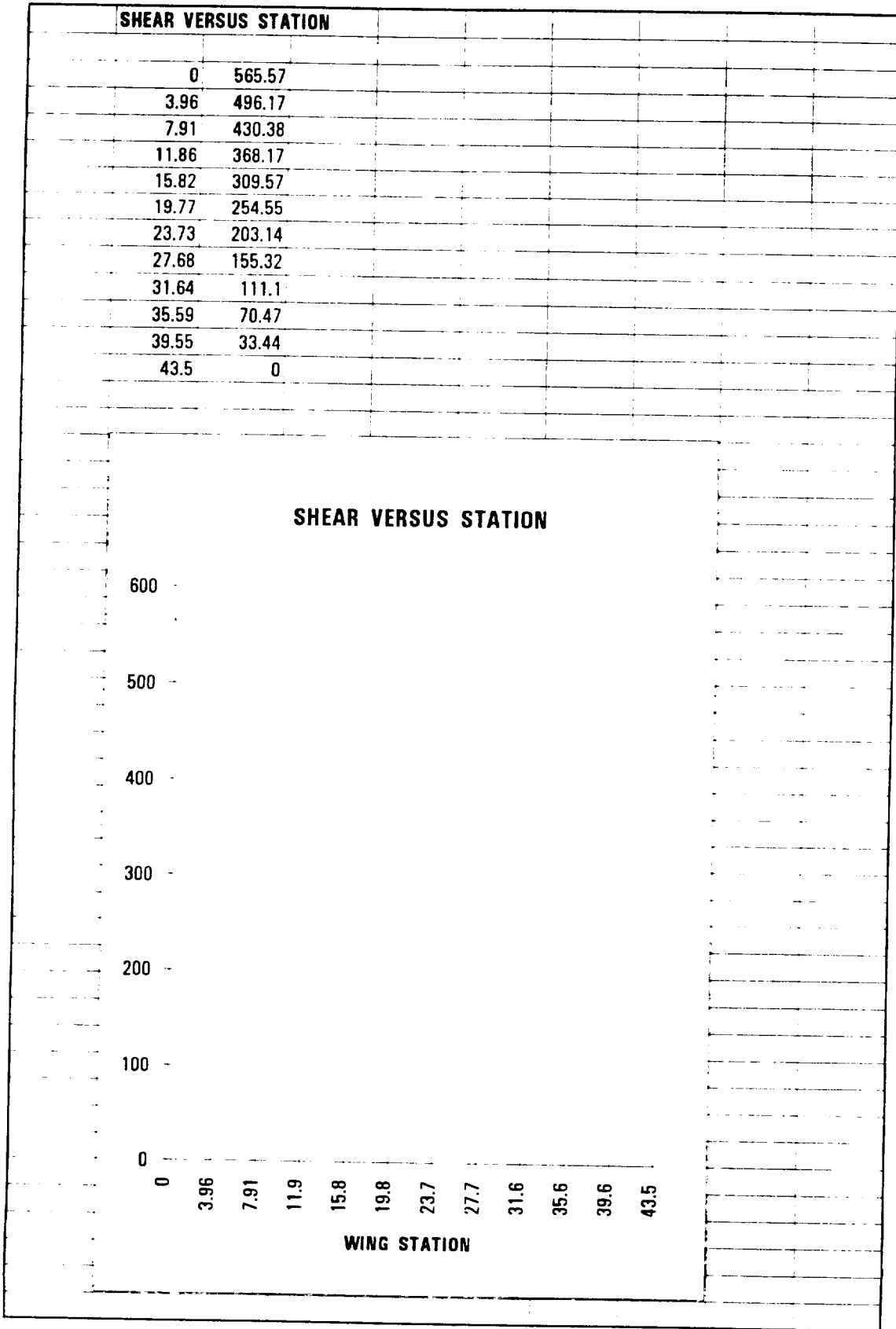


BENDING MOMENT IN Y DIRECTION

0	1156.79
3.96	974.16
7.91	809.96
11.86	663.22
15.82	532.95
19.77	418.17
23.73	317.91
27.68	231.19
31.64	157.02
35.59	94.42
39.55	42.4
43.5	0

**BENDING MOMENT IN Y DIRECTION
SPANWISE**





**APPENDIX D4 :
SECTION PROPERTIES
OF
THE COMPOSITE MATERIALS**

The product EI of each wing section (E329, E327, E326, E326, E325) is calculated through the following steps:

- Step 1 : The geometry of each section is known.
- Step 2 : The reference points of coordinates system is chosen.
- Step 3 : The cross section area is divided into available partitions and numbered from 1 to 12 or 13 (which depend on each cross section area) . (Column 1)
- Step 4 : The dimensions of each partition are measured in z and y directions, called Δz and Δy (Columns 2 and 3)
- Step 5 : The area of each partition is calculated, and after that areas of all partitions are summed up (Column 4)
- Step 6 : The centroid Z_{cg} and Y_{cg} for each partition is calculated . (Columns 5 and 6)
- Step 7 : The product of area and the distance from the centroid in z and y directions are found, and after that they are summed up (Columns 7 and 8)
- Step 8 : The product of area and square of Z_{cg} and square Y_{cg} are calculated , and summed up (Columns 9 and 10)
- Step 9 : The Inertia at the centroid of each partition are found in the z and y direction and summed up . (Columns 11 and 12)
- Step 10 : The product of area and Z_{cg} and Y_{cg} are calculated, and summed up. (Column 13)
- Step 11 : Torsional constant is defined as:

- For a rectangular section:

$$J_c = (1 + 12)ZY \times (Y^2 + Z^2)$$

- For a quarter of an ellipse section:

$$J_o = (1 \div 16)YZ \times (Y^2 + Z^2)$$

- For a rectangular section:

$$J_o = (K^4 \sqrt{3}) / 80$$

where

$$K = \sqrt{Y^2 + Z^2}$$

(Column 14)

(Reference Engineering Mechanics Statics, by R C Hibbeler, section Centroid and Center Gravity, page 457)

Step 12 : Z(BAR) and Y(BAR) are the centroid components of an object in Y and z directions, and determined by the centroid equations:

$$\bar{Z} = \frac{\sum AZ}{\sum A}$$
$$\bar{Y} = \frac{\sum AY}{\sum A}$$

(Reference Engineering Mechanics Statics, by R C Hibbeler, section Centroid and Center Gravity, page 420)

Step 13 : I_{zz} , I_{yy} and I_{zy} are calculated by the equations

$$I_{zz} = \sum AZ^2 + \sum I_{zz} - \bar{Z}^2 A$$
$$I_{yy} = \sum AY^2 + \sum I_{yy} - \bar{Y}^2 A$$
$$I_{zy} = \sum AYZ - \bar{A}\bar{Y}\bar{Z}$$

Step 14 : The product of flexural rigidity is defined as

$$EI_{zz} = E_{(PVCave)} \times I_{zz}$$

Step 15 : The product of torsional stiffness is

$$JG = G_{(PVCave)} \times J_o$$

Step 16 : The torsional stiffness applied at the centroid is given by the equation

$$J_c = J_o - A\bar{Y}\bar{Z}$$

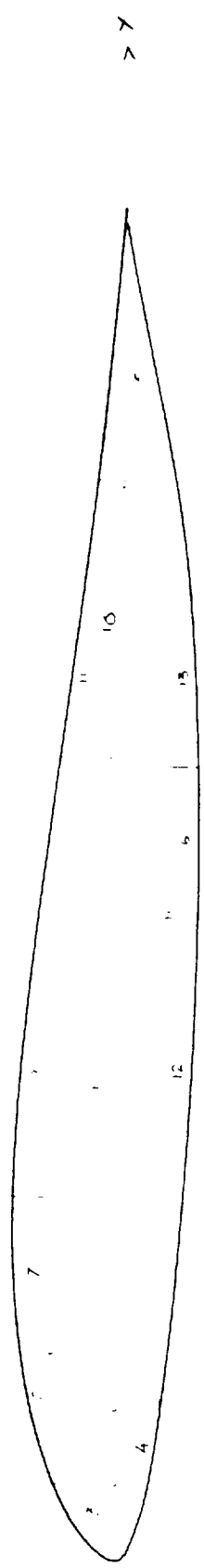
The whole procedure is shown in the tables 1,2,3,4,and 5 for each section E325, E326, E327, E328 and E329.

(Reference Introduction to Aerospace Structural Analysis, by David h. Allen and Walter E. Haisler, section of Determination of Modulus Weighted Section Properties 4.3.2.3, page177)

Finally, the graph represents the flexural rigidity and the torsional stiffness versus the stations of the wing.

z
^

E325

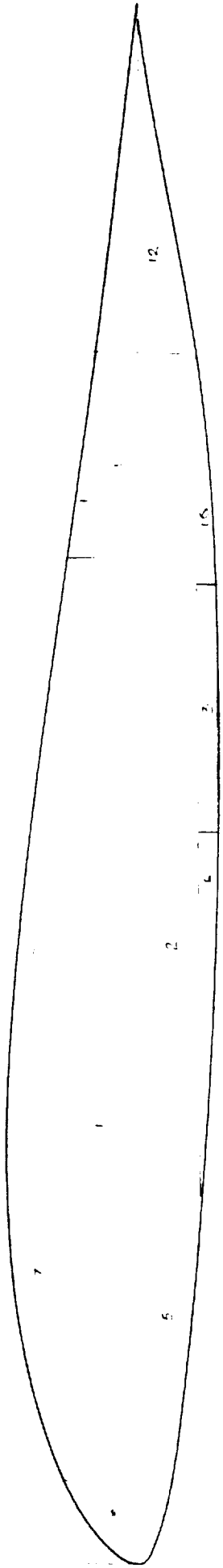


TIP WING SECTION

CORE ONLY

SECTION E-325														
1	2	3	4	5	6	7	8	9	10	11	12	13	14	15
ELE	DEL. Z	DEL. Y	AREA	Zcg	Ycg	AZ	AY	AZ ²	AY ²	Ioz	Ioy	AZY	Jo	Jc
1	0.36	4.41	1.59	0.18	2.27	0.286	3.61	0.052	8.19	2.573	0.0171	0.649	2.59E+00	1.94E+00
2	0.261	6.02	1.57	0.13	3.83	-2.04	6.01	0.027	23.02	4.74	0.01	-0.78	4.75E+00	5.53E+00
3	0.36	0.43	0.103	0.13	0.26	0.0134	0.027	0.0017	0.007	0.0013	0.008	0.003	9.56E-03	6.56E-03
4	0.261	0.85	0.15	-0.097	0.53	-0.0146	0.08	0.0014	0.042	0.073	0.006	-0.007	3.44E-02	4.14E-02
5	0.37	1.2	0.222	-0.03	7.14	-0.0067	1.59	0.0002	11.35	0.0133	0.013	-0.047	5.33E-02	1.00E-01
6	0.227	1.6	0.363	-0.357	4.39	-0.13	1.59	0.0464	7	0.077	0.0016	0.57	7.90E-02	6.49E-01
7	0.283	1.22	0.346	-0.53	2.2	0.183	0.76	0.097	1.67	0.043	0.0023	0.4	4.51E-02	3.55E-01
8	0.283	1.17	0.331	0.45	0.78	0.15	0.26	0.022	0.32	0.025	0.011	0.117	4.00E-02	7.70E-02
9	0.283	2.02	0.29	0.45	3.33	0.13	0.965	0.059	3.22	0.13	0.0013	0.434	3.75E-01	5.92E-02
10	0.1	2.01	0.201	0.05	5.8	0.01	1.17	0.0005	6.8	0.063	0.0002	0.058	6.78E-02	9.84E-03
11	0.26	2.01	0.262	0.18	5.3	0.047	1.39	0.0085	7.37	0.07	0.0028	0.25	3.68E-01	1.18E-01
12	0.226	2.79	0.322	-0.34	2.7	-0.109	0.87	0.037	2.35	0.136	0.004	-0.28	1.32E+00	1.60E+00
13	0.204	1.62	0.17	-0.31	5.76	-0.053	0.98	0.016	5.64	0.02	0.0004	-0.3	1.57E-01	4.57E-01
SUM			5.913			0.254	19.6	0.37	77.05	7.94	1.142	-0.85	9.89E+00	9.96E+00
			Z(BAR) = SUM(AZ) / SUM(A)			Izz = SUM(AZ ²) / SUM(AZ) - (Z(BAR)) ² * A								
			Z(BAR) = 0.254 / 5.913 = 0.043 inches			Izz = 0.37 + 7.94 / (0.043 ² * 5.91)								
			Y(BAR) = SUM(AY) / SUM(A)			Iyy = SUM(AY ²) + SUM(Ioy) - (Y(BAR)) ² * A								
			Y(BAR) = 19.6 / 5.913 = 3.32 inches			Iyy = 77.05 + 1.142 - (3.32 ² * 5.91)								
			PVC (Klogecell)			Iyy = 13.05 inches ⁴								
			E(pvc av) = (5700 + 4500) / 2 = 5100 psi			Izy = AZY - A * Z(BAR) * Y(BAR)								
			Etzz = 5100 * 8.28 = 42279 lb/in ²			Izy = -0.085 * 5.91 * 0.043 * 3.32								
						Izy = -0.914 inches ⁴								
						JG = 9.96 * 2700 = 26892 lb/in ²								

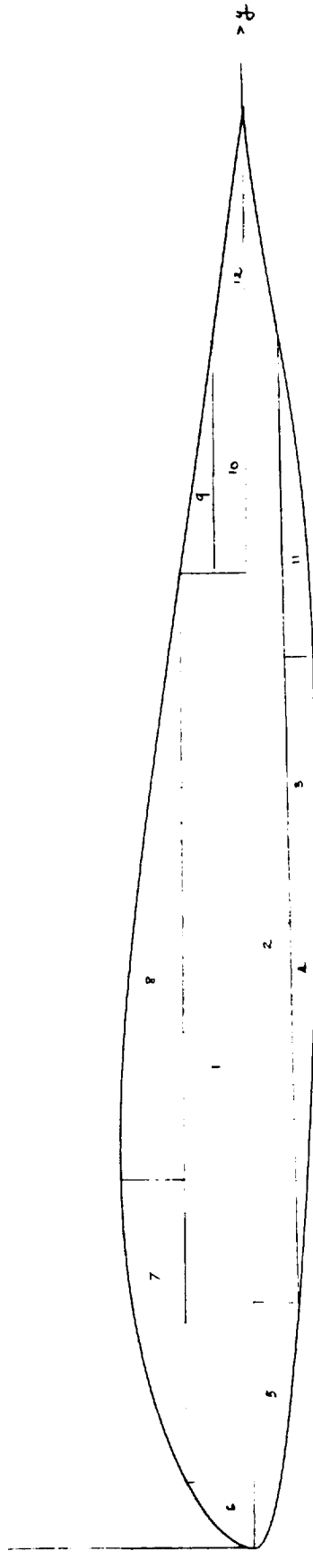
E326



SEMISPAN SECTION

CORE ONLY

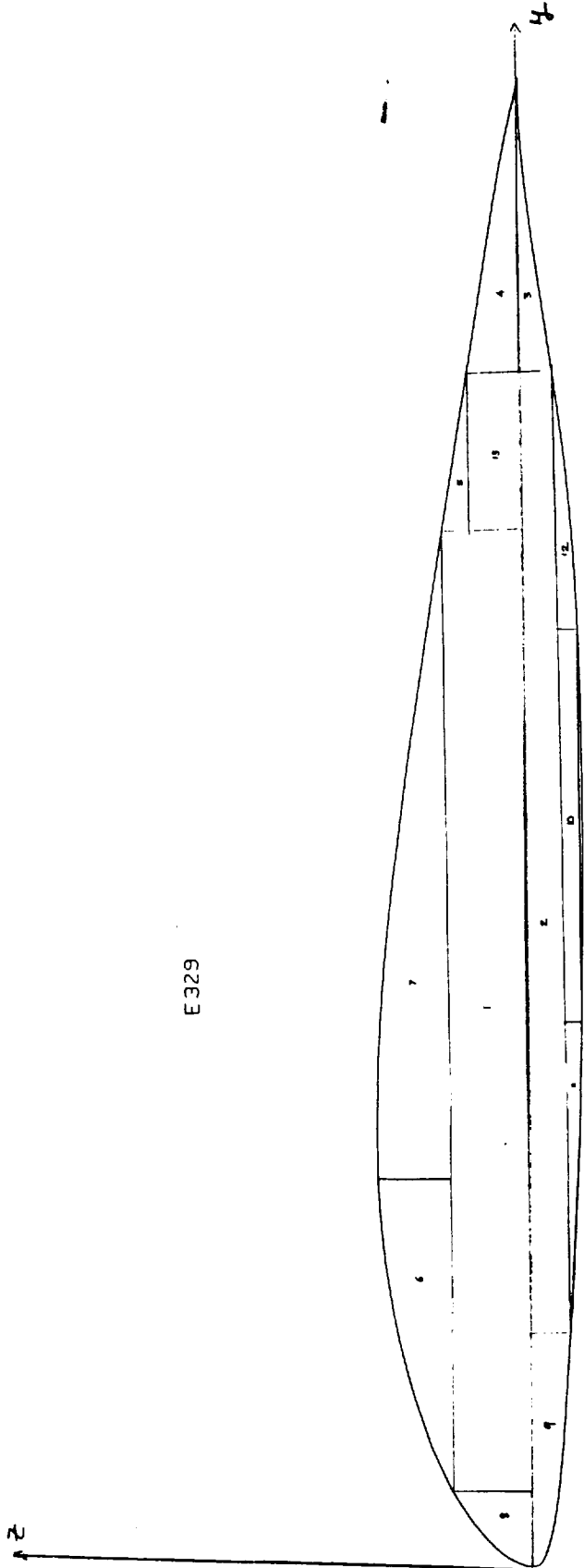
E327



MIDSPAN SECTION

CORE ONLY

1	2	3	4	5	6	7	8	9	10	11	12	13	14	15
ELE	DELT.Z	DELT.Y	AREA	Z cg	Y cg	AZ	AY	AZ^2	AY^2	Ioz	Ioy	AZY	Jc	Jc
			SECTION E-327											
1	0.62	7.48	4.64	0.31	4.42	1.44	0.445	20.5	90.65	21.62	0.15	6.36	2.18E+01	1.54E+01
2	0.4	10.2	4.1	-0.2	6.4	-0.82	0.163	26.24	167.94	35.37	0.055	-5.25	3.54E+01	4.07E+01
3	0.4	4.7	1.64	-0.6	6.83	-0.92	-0.59	11.2	76.5	2.3	0.022	-6.72	3.49E+00	1.02E+01
4	0.376	3.43	1.29	-0.135	2.3	-0.75	0.024	2.97	6.82	0.42	0.005	-0.4	3.08E+00	3.48E+00
5	0.4	1.37	0.37	-0.15	0.82	-0.056	0.0083	0.303	0.25	0.041	0.004	-0.046	2.19E-01	2.65E-01
6	0.62	0.7	0.28	0.23	0.42	0.064	0.015	0.12	0.05	0.0084	0.008	0.027	7.45E-02	4.75E-02
7	0.49	2.73	0.9	0.184	1.64	0.166	0.03	1.47	2.42	0.456	0.013	0.27	1.25E+00	9.85E-01
8	0.49	4.78	1.5	0.24	4.88	0.36	0.086	7.32	35.72	1.5	0.016	1.75	1.17E+01	9.94E+00
9	0.42	3.88	0.71	0.13	9.49	0.092	0.012	6.73	63.94	0.45	0.007	0.88	5.06E+00	4.18E+00
10	0.2	3.38	0.676	0.1	9.88	0.068	0.0068	6.78	65.98	0.64	0.0023	0.67	6.46E-01	-2.42E-02
11	0.37	2.73	0.65	-0.55	9.76	-0.36	0.2	6.33	61.8	0.24	0.004	-3.48	1.26E+00	4.74E+00
12	0.6	1.91	0.57	-0.087	12.09	-0.05	0.0043	6.9	83.3	1.116	0.012	-0.6	2.94E-01	8.94E-01
SUM			17.33			-0.25	1.58	96.86	655.37	63.16	0.298	-6.54	8.43E+01	9.08E+01
			ZIBAR) = SUM(AZ) / SUM(A)											
			ZIBAR) - 0.25 / 17.33 - 0.0144 inches											
			YIBAR) = SUM(AY) / SUM(A)											
			YIBAR) - 96.86 / 17.33 - 5.59 inches											
			PVC (Kiegcell)											
			E(pvc av) - (5700 + 4500) / 2 - 5100 psi											
			E(Izz - 5100 * 64.74 - 330174) / bin^2											
			JG - 90.8 * 2700 - 245160											



E329

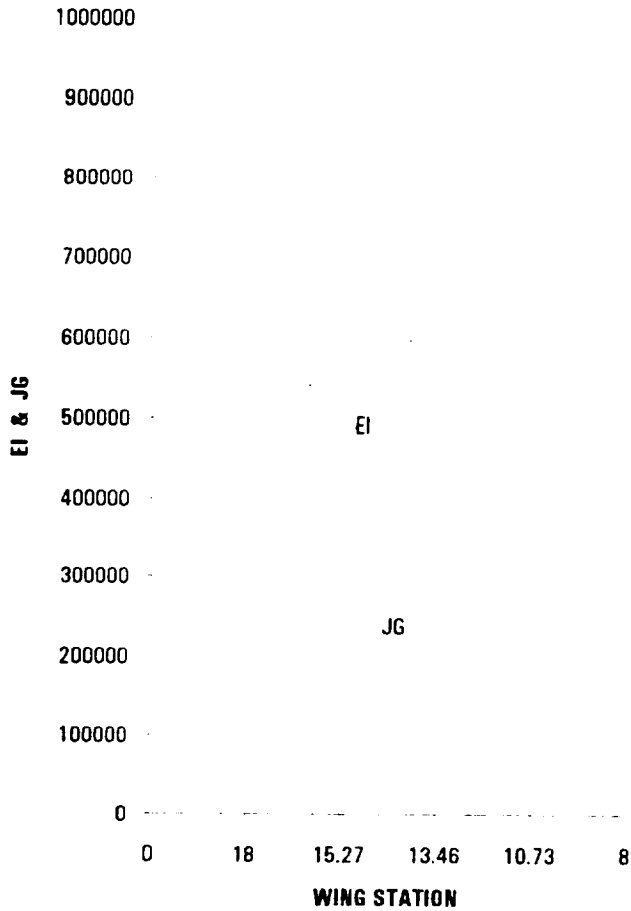
ROOT WING SECTION - - CORE ONLY

ELE	3		4	5		6		7		8		9		10		11		12		13		14		15	
	DELT.Z	DELT.Y		AREA	Zcg	Ycg	AZ	AY	AZ ²	AY ²	AZ ²	AY ²	loz	loy	AZY	Jc	Jc	AZY	Jc	loy	AZY	Jc	Jc	AZY	Jc
1	0.826	10.03	8.28	0.41	6.93	3.4	49.1	1.39	291.16	69.45	0.47	20.13	6.99E+01	4.98E+01											
2	0.66	11.84	7.81	-0.33	8.63	2.58	67.4	0.85	581.66	91.29	0.284	22.24	9.16E+01	1.14E+02											
3	0.7	3.45	1.21	-0.26	15.6	-0.31	18.87	0.081	294.46	0.8	0.033	-4.9	3.43E+00	8.33E+00											
4	0.35	3.45	0.6	0.14	15.26	0.085	9.16	0.012	139.72	0.4	0.004	1.28	3.30E+00	2.02E+00											
5	0.99	3.66	0.9	0.53	11.91	0.48	10.72	0.25	127.66	0.67	0.012	5.68	4.17E+00	1.51E+00											
6	0.65	3.66	1.28	0.31	3.31	0.49	5.23	0.152	17.31	1.45	0.04	1.62	3.96E+00	2.34E+00											
7	0.65	6.36	2.6	1.06	6.4	2.75	16.64	2.92	106.5	7.64	0.07	17.63	3.72E+01	1.95E+01											
8	0.79	0.9	0.45	0.26	5.6	1.2	0.25	0.03	0.14	0.026	0.017	0.066	2.00E+01	1.34E+01											
9	0.66	2.78	1.21	-0.3	1.79	-0.36	2.16	0.11	3.87	0.63	0.03	-0.65	2.94E+00	3.59E+00											
10	0.33	4.55	1.5	-0.87	8.66	-1.31	13	1.14	112.5	2.62	0.014	-11.3	9.85E+00	2.11E+01											
11	0.3	3.66	0.55	-0.79	5.4	-0.43	2.97	0.34	6.03	0.41	0.0027	2.35	4.14E+00	6.49E+00											
12	0.35	3.62	0.7	-0.85	12.03	-0.59	8.42	0.5	101.3	0.4	0.004	7.15	3.78E+00	1.09E+01											
13	0.35	3.62	1.23	0.17	12.75	-0.21	15.68	0.036	199.95	1.34	0.012	2.67	1.40E+00	1.27E+00											
SUM			28.62		1.956		219.6	7.81	1992.26	177.12	0.99	0.486	2.36E+02	2.35E+02											
	$Z(\text{BAR}) = \text{SUM}(AZ) / \text{SUM}(A)$ $Z(\text{BAR}) = 1.956 / 28.62 = 0.068 \text{ inches}$																								
	$Y(\text{BAR}) = \text{SUM}(AY) / \text{SUM}(A)$ $Y(\text{BAR}) = 219.6 / 28.62 = 7.67 \text{ inches}$																								
	PVC (Kigeceff)																								
	$E(\text{pvc av}) = (5700 + 4500) / 2 = 5100 \text{ psi}$																								
	$E(\text{zz}) = 5100 * 184.8 = 942480 \text{ bin}^2$																								
	JG - 235 * 2700 = 634500 lb.in²																								

EI AND JG VERSUS WING STATION

WING STATION	EI		JG
	in	lb in ²	lb in ²
		EI	JG
0			
329	18	9.42E+05	634500
328	15.27	5.12E+05	337500
327	13.46	3.30E+05	245160
326	10.73	1.50E+05	106650
325	8	4.23E+04	26892

EI AND JG VERSUS WING STATION



VERTICAL STATIC DEFLECTION OF ENTIRE WING							
WING BOX IS MADE OF PVC AND KEVLAR							
WING STRUCTURE: PVC CORE + 1 PLY OF KEVLAR							
KEVLAR 49 WRAPPING AROUND (90 DEG. OR 0 DEG. PLY ORIENTATION)							
SECTION E 325 PROPERTIES							
ELEM.	A	E	AE	Z cent.	AEZcent.	AEZct. ²	EIoz
1	0.37	4.40E+06	1.63E+06	0.34	5.54E+05	1.88E+05	7.23E+01
2	5.81	5100	2.96E+04	0.043	1.27E+03	5.48E+01	4.35E+04
3	0.35	4.40E+06	1.54E+06	0.31	4.77E+05	1.48E+05	7.23E+01
SUM	6.53		3.20E+06		7.74E+04	3.36E+05	4.36E+04
Z (BAR) cg = SUM (AEZct.) / SUM (AE)							
Z (BAR) cg = 2.42E-02 inches							
EI (composite) = SUM (AEZct. ²) + SUM (EI _o) - SUM (AEZct. * Z (BAR) cg)							
EI (composite) = 3.78E+05 lb in ²							

VERTICAL STATIC DEFLECTION OF ENTIRE WING						
WING BOX IS MADE OF PVC AND KEVLAR						
WING STRUCTURE: PVC CORE + 1 PLY OF KEVLAR						
KEVLAR 49 WRAPPING AROUND (90 DEG. OR 0 DEG. PLY ORIENTATION)						
SECTION E 329 PROPERTIES						
ELM.	A	E	AE	Z cent.	AEZcent.	AEZet. * Z
1	0.83	4.40E+06	3.65E+06	0.91	3.32E+06	3.02E+06
2	28.62	5100	1.46E+05	0.068	9.93E+03	6.75E+02
3	0.82	4.40E+06	3.61E+06	-0.49	-1.77E+06	8.66E+05
SUM	30.27		7.41E+06		1.57E+06	3.89E+06
Z (BAR) cg = SUM (AEZet.) / SUM (AE)						
Z (BAR) cg = 2.11E-01 inches						
EI (composite) = SUM (AEZet. * Z) + SUM (EIa) - SUM (AEZet. * Z (BAR) cg)						
EI (composite) = 4.46E+06 lb in ²						

VERTICAL STATIC DEFLECTION OF ENTIRE WING									
WING BOX IS MADE OF PVC AND KEVLAR									
WING STRUCTURE: PVC CORE + 1 PLY OF KEVLAR									
KEVLAR 49 WRAPPING AROUND 190 DEG. OR 0 DEG. PLY ORIENTATION)									
SECTION E 328 PROPERTIES									
ELEM.	A	E	AE	Z cent.	AEZcent.	AEZct.^2	EIoz		
1	0.7	4.40E+06	3.08E+06	0.78	2.40E+06	1.87E+06	1.34E+02		
2	21.31	5100	1.09E+05	0.0041	4.46E+02	1.83E+00	4.75E+05		
3	0.7	4.40E+06	3.08E+06	0.56	1.72E+06	9.66E+05	1.34E+02		
SUM	22.71		6.27E+06		6.78E+05	2.84E+06	4.75E+05		
Z (BAR) cg = SUM (AEZct.) / SUM (AE)									
Z (BAR) cg = 1.08E-01 inches									
EI (composite) = SUM (AEZct.^2) + SUM (EIo) - SUM (AEZct. * Z (BAR) cg)									
EI (composite) = 3.24E+06 lb in^2									

VERTICAL STATIC DEFLECTION OF ENTIRE WING						
WING BOX IS MADE OF PVC AND KEVLAR						
WING STRUCTURE: PVC CORE + 1 PLY OF KEVLAR						
KEVLAR 49 WRAPPING AROUND (90 DEG. OR 0 DEG. PLY ORIENTATION)						
SECTION E 327 PROPERTIES						
ELEM.	A	E	AE	Z cent.	AEZcent.	AEZct. * Z
1	0.627	4.40E+06	2.76E+06	0.67	1.85E+06	1.24E+06
2	11.83	5100	6.03E+04	-0.0144	-8.69E+02	1.25E+01
3	0.627	4.40E+06	2.76E+06	-0.47	-1.30E+06	6.09E+05
SUM	13.084		5.58E+06		5.51E+05	1.85E+06
Z (BAR) cg = SUM (AEZct.) / SUM (AE)						
Z (BAR) cg = 9.88E-02 inches						
EI (composite) = SUM (AEZct. * Z) + SUM (EIe) - SUM (AEZct. * Z (BAR) cg)						
EI (composite) = 2.12E+06 lb in ²						

VERTICAL STATIC DEFLECTION OF ENTIRE WING							
WING BOX IS MADE OF PVC AND KEVLAR							
WING STRUCTURE: PVC CORE + 1 PLY OF KEVLAR							
KEVLAR 49 WRAPPING AROUND (90 DEG. OR 0 DEG. PLY ORIENTATION)							
SECTION E 326 PROPERTIES							
ELEM.	A	E	AE	Z cent.	AEZcent.	AEZct. * 2	EIoz
1	0.53	4.40E+06	2.33E+06	0.56	1.31E+06	7.31E+05	9.87E+01
2	11.83	5100	6.03E+04	0.051	3.08E+03	1.57E+02	1.53E+05
3	0.54	4.40E+06	2.38E+06	-0.4	-9.50E+05	3.80E+05	9.87E+01
...							
SUM	12.9		4.77E+06		3.59E+05	1.11E+06	1.53E+05
Z (BAR) cg = SUM (AEZct.) / SUM (AE)							
Z (BAR) cg = 7.52E-02 inches							
EI (composite) = SUM (AEZct. * 2) + SUM (EIo) - SUM (AEZct. * Z (BAR) cg)							
EI (composite) = 1.24E+06 lb in ²							

**APPENDIX D5 : THE RESULTS
FOR CHECKING DEFLECTION FOR
PCV CORE
AND
FOR COMPOSITES--PVC & KEVLAR**

The procedures for calculating the vertical static deflection for the PVC wing core are going through the eight steps.

Step 1 : The wing station for each airfoil section is determined. (Column 1)

Step 2 : The change in distance along the spanwise.(Column 2)

Step 3 : The bending moments are taken from the Column 16, Table of Calculation of wing shear and wing moments, Appendix C. (Column 3)

Step 4 : The flexural rigidity is imported from Tables E325, E326, E327, E328, E329, Appendix D. (Column 4)

Step 5 : The ratios of the bending moments and the product of flexural rigidity are calculated. (Column 5)

Step 6 : The area of each section is calculated. (Column 6)

Step 7 : The deflection of each section is determined. (Column 7)

Step 8: The total is deflection for the whole wing is the sum of the deflections from the root to the tip.

Similarly, the deflection for the wing, made of PVC and Kevlar, is calculated. After that, a graph shows the deflection versus the wing stations

WING VERTICAL STATIC DEFLECTION						
WING BOX IS MADE OF PVC ONLY						
1	2	3	4	5	6	7
WING STATION	x	M	EI	M/EI	AREA	DEFLECTION
0.0 - 7.91	39.54	974.16	942480	0.001033613	0.008175882	0.323274368
7.91 - 15.82	31.64	663.22	512193	0.001294863	0.01024237	0.324068586
15.82 - 23.73	23.73	418.17	330174	0.001266514	0.010018126	0.237730128
23.73 - 31.64	15.82	231.19	150195	0.001539266	0.012144806	0.192130827
31.64 - 43.5	5.93	42.4	42279	0.001002862	0.011893943	0.07053108
				TOTAL DEFLECTION		1.147735008

VERTICAL STATIC DEFLECTION OF ENTIRE WING AT STATIC CONDITION

WING BOX IS MADE OF PVC AND KEVLAR

WING STRUCTURE: PVC CORE + 1 PLY OF KEVLAR
 KEVLAR 49 WRAPPING AROUND (90 DEG. OR 0 DEG. PLY ORIENTATION)

STATION	x	EI	M	M / EI	AREA	DEFLECTION
0 - 7.91	39.54	4.46E+06	133.27	2.98812E-05	0.00023636	0.009345675
7.91 - 15.82	31.64	3.24E+06	84.03	2.59352E-05	0.000205147	0.006490861
15.82 - 23.73	23.73	2.12E+06	47.65	2.24764E-05	0.000177788	0.00421892
23.73 - 31.64	15.82	1.24E+06	22.71	1.83145E-05	0.000144868	0.002291809
31.64 - 43.5	5.93	3.78E+05	6.76	1.78836E-05	0.000212099	0.00125775
TOTAL DEFL.						0.023605015

FIND MOMENT

	1	2	3	4	5
	MOMENT				
X		(1) + (2)	(3) / 2	(4) / 4.4	
0	709.65	709.65	354.825		
7.91	463.15	1172.80	586.40	133.27	
15.82	276.34	739.49	369.74	84.03	
23.73	143.00	419.34	209.67	47.65	
31.64	56.88	199.88	99.94	22.71	
43.5	2.62	59.50	29.75	6.76	